UNIVERSITA' VITA-SALUTE SAN RAFFAELE

CORSO DI DOTTORATO DI RICERCA
INTERNAZIONALE IN MEDICINA MOLECOLARE

Curriculum in Fisiopatologia Cellulare e Molecolare

SOURCES OF NF-κB DYNAMIC HETEROGENEITY: FROM QUASI-IDENTICAL CELLS TO PARACRINE INFLAMMATORY SIGNALING

DoS: Prof. Marco E. Bianchi

Second Supervisor: Prof. Felix Naef

Tesi di DOTTORATO di RICERCA di Cise Kizilirmak

Matr. 014325

Ciclo di Dottorato XXXIV

SSD BIO/11

Anno Academico 2020/2021

RELEASE OF PHD THESIS

La sottoscritta / *I, the undersigned*: Cise Kizilirmak

Matricola / *Registration Number*: 014325

Nata / *Born in*: Duzce, Turkey

Il/*on*: 25.05.1992

autore della tesi di Dottorato di ricerca dal titolo / author of the PhD thesis titled:

SOURCES OF NF-κB DYNAMIC HETEROGENEITY: FROM QUASI-IDENTICAL CELLS TO PARACRINE INFLAMMATORY SIGNALING

■ AUTORIZZA la Consultazione della tesi / AUTHORIZE the public release of the thesis

Data /Date .....20.04.2022..... Firma /Signature .....

DECLARATION

This thesis has been composed by myself and has not been used in any previous application for a degree. Throughout the text I use both 'I' and 'We' interchangeably.

All the results presented here were obtained by myself, except for:

1) Immunohistochemistry experiments for liver tissue sections (Results, Figure 5.21) were performed by Amleto Fiocchi, Mouse Histopathology Unit, San Raffaele Scientific Institute, Milan, Italy.

2) Bioinformatic analysis on RNA-seq data was performed by:

- Prof Samuel Zambrano (Results, Figure 5.11, 5.13, 5.14, 5.15, 5.17), Division of Genetics and Cell Biology, San Raffaele Scientific Institute, Milan, Italy.
- Dr Emanuele Monteleone (Results, Figure 5.9, 5.10, 5,12), Division of Genetics and Cell Biology, San Raffaele Scientific Institute, Milan, Italy.
- Dr Jose M. Garcia Manteiga (Results, Figure 5.9, 5.10, 5.11, 5.13) Center for Translational genomics and BioInformatics, San Raffaele Scientific Institute, Milan, Italy.

3) Mathematical modeling (Results, Figure 5.18) was performed by Prof Samuel Zambrano, Division of Genetics and Cell Biology, San Raffaele Scientific Institute, Milan, Italy.

4) Cell cycle analysis (Results, Figure 5.7) was performed by Dr Francesca Brambilla, Division of Genetics and Cell Biology, San Raffaele Scientific Institute, Milan, Italy.

Part of the results presented in this thesis is published in BioRxiv preprint server. Full text is available at: https://doi.org/10.1101/2021.12.07.471485.

Kizilirmak C, Monteleone E, García-Manteiga JM, Brambilla F, Agresti A, Bianchi ME & Zambrano S (2021) Small transcriptional differences lead to distinct NF-κB dynamics in quasi-identical cells.

All sources of information are acknowledged by means of reference.

ACKNOWLEDGEMENTS

I would like to acknowledge Prof Manolis Pasparakis for sharing with us the immortalized mouse embryonic fibroblast population from a single embryo and Prof Roberto Sitia for suggesting the idea of single cell cloning experiment. I thank Dr Dario Bonanomi for the agarose beads, Dr Emilie Venereau for damaged liver tissue samples and Dr Federica Moalli for hepatocellular carcinoma carrying liver tissue sections.

I would like to thank my director of studies Prof Marco Bianchi for giving me this opportunity to work in Chromatin Dynamics Unit and sharing his guidance and experience with me in last 4 years. I am extremely thankful to my supervisor Prof Samuel Zambrano for his guidance, full support, and enthusiasm. This project would not have been possible without his endless supply of great ideas. Thank you for being a great mentor and encouraging me to give impressive presentations like yours. I do my best to inherit this from you and I hope to carry this successfully throughout my career. I would like to thank to my second supervisor Prof Felix Naef for his encouraging and detailed feedbacks that helped improving this thesis work every year. Thanks to current and previous members of Chromatin Dynamics, In vivo Transcription and Tissue Regeneration & Homeostasis Units who contributed to this project during long lab meeting discussions. I thank especially to Dr Alessandra Agresti for her contribution to my thesis work and sharing her expertise with me.

Thanks to Franci for making me feel like I am not alone. Your mental support, career advice and our long scientific discussions meant so much to me. Your thesis, labbook, protocols will always stay as 'golden standard' for me.

Thanks to my Power Rangers: Elena and Luca and our extended family with Setfano and Thomas for always being by my side. It would be so difficult without you, our after-work beers, 'caffe' pausas, aperitivos, burrito wars and many mores. Thanks to Kaalindi for making our house 'a home' and thank you all for being my family in Italy.

Thanks to my partner Matias for his endless support during this journey, for reminding me to take one day at a time and being the best motivational speaker ever when things were overwhelming. You and Moomin guys made my days in Italy so much fun even though favorite activity of one of them is being a sleeping machine.

Thanks to my family and friends for supporting and comforting me when I need the most. Lastly a special thanks goes to my sister for giving me the best advice of my life at a moment when I didn't feel the best: *Bırak Eve Git.*

ABSTRACT

Nuclear factor kappa B (NF-κB) is a master transcription factor in the cell's response to inflammatory stimuli as it controls the expression of key chemokines and cytokines. NF-κB itself is activated by many of these molecules, largely mediated by its nuclear localization dynamics. NF-κB dynamics is fundamental for proper target gene expression, however it can also be highly heterogeneous in different cell types and even within homogeneous populations. The source of such dynamic variability is unclear. On the other hand, in a tissue, paracrine signaling implies that cells receive different NF-κB activating signals depending on their position relative to the sources. The resulting NF-κB dynamic response might be also heterogeneous and yet might carry spatiotemporal information, but this has not been properly characterized.

To gain insights on the source of heterogeneity of NF-κB dynamics we isolated multiple clonal populations of a homogenous GFP-NF-κB fibroblast population and found that each has a robustly distinct NF-κB nuclear localization dynamics upon stimulation with tumor necrosis factor alpha (TNF-α). We focused on three clonal populations displaying oscillatory, persistent, and weak responses to TNF-α and found that they have small but significant differences in the expression of genes belonging to the NF-κB regulatory circuit. To characterize the heterogeneous NF-κB dynamics that might arise in paracrine inflammatory signaling, we developed in vitro sender receiver models where we can image the dynamics of NF-κB receiving signals from two senders: RAW 264.7 cells and an engineered version of our GFP-NF-κB fibroblasts that secrete TNF-α instantaneously upon induction. We found that single cells use spatiotemporal NF-κB activation to encode location and strength of the danger signals, even with a certain degree of heterogeneity. Furthermore, this spatiotemporal dynamics is shaped by a desensitization effect due to the basal secretion of cytokines by the senders, which results in a moderate spatially-dependent population level response to strong cytokine secretion.

Overall, our results show that part of populational heterogeneity on NF-κB activation might emerge in tissue as a result of the interaction of many layers: first, due to small variations in the expression levels of genes of the NF-κB regulatory circuit between cells and second, depending on the spatiotemporal context. Our study has provided additional insights on how inflammation develops through heterogeneous dynamics of NF-κB in space and time and will potentially contribute to shed light on how complex immune responses are coordinated in healthy and pathological conditions.

TABLE OF CONTENTS

1. ACRONYMS AND ABBREVIATIONS

NF-κB	Nuclear factor kappa-light-chain-enhancer of activated B cells
TNF-α	Tumor necrosis factor alpha
TFs	Transcription factors
IκB	Nuclear factor kappa-light-polypeptide gene enhancer in B cells inhibitor
PRRs	Pattern recognition receptors
TAD	Transactivating domain
LPS	Lipopolysaccharide
GFP	Green fluorescent protein
RFP	Red fluorescent protein
IL-1β	Interleukin 1 beta
MEFs	Mouse embryonic fibroblasts
HCC	Hepatocellular carcinoma
APAP	Acetaminophen
NCI	Nuclear to cytosolic intensity
AUC	Area under curve
ASOs	Antisense oligonucleotides
SBP	Streptavidin binding protein
SNPs	Single nucleotide polymorphism

2. LIST OF FIGURES AND TABLES

3. INTRODUCTION

3.1 A dynamical view of the function of transcription factors

Cells adapt to environmental cues by precisely mediating their transcriptional responses (Milo & Phillips, 2016). External and internal stimuli activate key proteins: transcription factors (TFs), that bind regulatory regions of DNA to modulate the transcription of target genes (Adcock & Caramori, 2009). TFs act as molecular switches that lead to a specific transcriptional output given a certain input (Seshasayee *et al*, 2006). As an example, in 2006 it was shown that by switching on the expression of only four transcription factors (Oct4, Sox2, c-Myc, Klf4) it is possible to induce pluripotency in somatic cells (Takahashi & Yamanaka, 2006).

Many TFs are kept sequestered in subcellular localizations to regulate their activity (Whiteside & Goodbourn, 1993). In this way, instant cellular responses can be achieved upon stimuli that releases them, without the need of *de novo* protein synthesis. Activation of the TFs typically is accompanied by the dynamic process of their nuclear accumulation. Remarkably, many TFs do not behave like simple "on-off" switches, and live cell imaging has allowed to show that this process can be oscillatory at single-cell level (Levine *et al*, 2013). After the discovery of core circadian clock genes, oscillations were first shown for circadian rhythms in response to day/night cycle (Lowrey & Takahashi, 2004). Later, oscillations were discovered for a wide variety of TFs such as p53 (Purvis *et al*, 2012), extracellular signal regulated kinases (Erk) (Shankaran *et al*, 2009), and nuclear factor of activated T-cells (NFAT) (Yissachar *et al*, 2013).

As a result, the emerging view is that such TFs dynamics is not merely a by-product of the regulatory mechanisms, but that it has a functional role in gene expression (Purvis & Lahav, 2013) and impacts a wide array of cellular processes, e.g., determining cell fate (as for p53, (Purvis *et al*, 2012)), the response to mechanical cues (as for YAP/TAZ, (Franklin *et al*, 2020)) or the speed of the segmentation clock during embryo development (as for Hes7, (Matsuda *et al*, 2020)), to cite a few. Somewhat paradoxically, in spite of the central role of TF dynamics, single-cell live cell imaging shows consistently a high degree of heterogeneity in TF dynamics within homogeneous cell populations; however, this is compatible with the cell's ability to process inputs into transcriptional outputs (Selimkhanov *et al*, 2014). The precise origin and role of TF dynamic heterogeneity, and how it is reconciled with its ability to provide specific response to stimuli, are far from being completely understood.

A paradigmatic example of the dynamic nature of TF activation is the nuclear factor kappa B (NF-κB): the central player of this PhD project and a key player in innate and adaptive immune responses (Hayden & Ghosh, 2008; Natoli & Ostuni, 2019).

3.2 The transcription factor NF-κB

NF-κB was first discovered as a DNA binding protein in activated B cells as its name suggests (Sen & Baltimore, 1986). Its function in the maturation and development of the B cells has been shown soon after is the discovery. Later on, NF-κB was found to be expressed in almost all cell types and shown to be a central regulator of the immune and inflammatory responses (Zhang *et al*, 2017b).

Inflammation is a protective immune response to harm, such as infections or tissue damage. This evolutionary conserved process (Hagai *et al*, 2018) includes the activation of host cells that sense damage signals through proper receptors and the timely and accurate recruitment of immune cells. Since the NF-κB signaling pathway responds to diverse stimuli through receptors including pattern recognition receptors (PRRs) and B and T cell receptors, it makes NF-κB an important player in both innate and adaptive immune system. NF-κB signaling can be identified as a master regulator of inflammation as it gets activated by a wide variety of damage signals and mediates the induction of expression of pro-inflammatory genes (Liu *et al*, 2017). The cells of the innate immunity contain PRRs to detect harmful stimulations through pathogen associated molecular patterns (PAMPs) or damage-associated molecular patterns (DAMPs) and activate the NF-κB signaling cascade (Newton & Dixit, 2012). The activation regulates the inflammation by production and secretion of the inflammatory cytokines but also depending on the activated immune cell type it can also regulate different cellular mechanisms such as dendritic cell maturation (Rescigno *et al*, 1998), neutrophil recruitment (Lawrence, 2009) or M1 polarization of the macrophages (Wang *et al*, 2014). T cells are also able to activate the NF-κB signaling through their receptor upon antigen presentation and this leads to activation and the differentiation of inflammatory T cells (Oh & Ghosh, 2013).

Many knock-out studies showed that NF-κB plays an important role in many different cellular processes (Figure 3.1). This includes regulating the proliferation (Chen *et al*, 2000), apoptosis (Beg *et al*, 1995; Rudolph *et al*, 2000), growth, differentiation, and morphogenesis of a variety of tissues (Bushdid *et al*, 1998; Hu *et al*, 1999; Klement *et al*, 1996; Li *et al*, 1999). Unsurprisingly, when deregulated, NF-

κB is found to be linked with inflammatory diseases and also various types of cancer (Ben-Neriah & Karin, 2011).

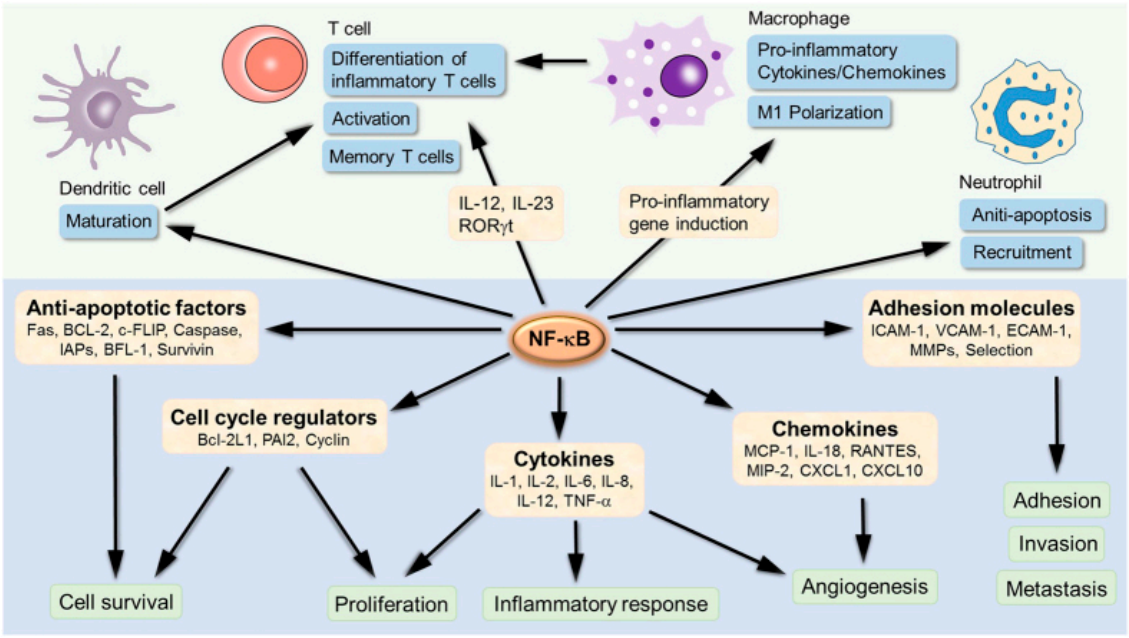

Figure 3.1. The biological role of NF-κB in various cellular processes. NF-κB regulates the expression of many target genes including cytokines and chemokines and has been found to play an important role for many biological processes including inflammatory response, proliferation, cell survival as shown in the figure. Figure taken from Liu *et al* 2017 is licensed under CC BY 4.0 (To view a copy of this license visit: http://creativecommons.org/licenses/by/4.0)

3.3 NF-κB signaling pathway

The NF-κB signaling pathway responds to diverse stimuli through different receptors including TNF receptor superfamily members, cytokine receptors, PRRs and B and T cell receptors. Upon ligand binding to such receptors two major signaling pathways could activate NF-κB: canonical (also known as classical) and non-canonical (Hayden & Ghosh, 2008).

The NF-κB family consist of 5 members: p65 (RelA), c-Rel and RelB proteins that contain the transactivating domain (TAD) and p52, p50 subunits (Hayden & Ghosh, 2008). The last two subunits are produced from their precursors known as p100 and p105 respectively. In the inactive state, NF-κB dimers are kept in the cytosol. In the canonical signaling pathway this is achieved by the IκB inhibitors that binds to the dimers whereas in the non-canonical pathway this is done by the precursors p100 and p105 that possess IκB like function (Sun, 2017) (Figure 3.2).

The canonical activation of NF-κB involves dimers including the monomer p65 and starts with the ligand binding of the external signals, such as tumor necrosis alpha (TNF-α) or interleukin 1 beta (IL-1β) to their receptors. This then activates the TGF beta activated kinase 1 (TAK1) to phosphorylate the IκB inhibitors complex known as IKK (IKKα, IKKβ, IKKγ) and consequently lead to the phosphorylation of the IκBs. Upon phosphorylation, IκBα undergoes the ubiquitylation which eventually leads to its proteasomal degradation and allows the nuclear transportation of NF-κB (Sun, 2017). On the other hand, the non-canonical pathway uses NF-κB inducing kinase (NIK) as a first activating protein in the cascade. This then leads to phosphorylation of IKKα and eventually proteasomal degradation of the IκB-like precursors to release NF-κB (Sun, 2017) (Figure 3.2).

Once in nucleus NF-κB regulates the expression of many target genes. Canonical activation of NF-κB occurs fast and transiently whereas non-canonical pathway activation is slow but persistent (Sun, 2017). NF-κB heterodimers containing monomers with the TAD domain are responsible for gene activation whereas homodimers lacking TAD can act as a gene repressor (Hayden & Ghosh, 2008). Dimers containing the p65 monomer were found to have the strongest transcription activation potential in the canonical NF-κB signaling pathway (Schmitz & Baeuerle, 1991) therefore p65 will be referred as NF-κB in the following sections and the canonical NF-κB pathway will be the main focus of this thesis.

NF-κB also controls the gene expression of its own IκB inhibitors hence making its dynamics tightly controlled by a negative feedback mechanism (A.Hoffmann *et al*, 2002). With the new synthesis of the inhibitors, nuclear to cytosol translocation of NF-κB occurs. Another negative feedback mechanism in NF-κB signaling is through an ubiquitin editing enzyme, A20 (TNFAIP3), which is shown to be activated by phosphorylation via IKK complex to inhibit NF-κB activation (Hutti *et al*, 2007). Together with IκB they play a crucial role in the signal termination of the NF-κB activation. Biochemical experiments showed that the negative feedback mechanisms of the NF-κB system could lead to oscillations in its nuclear concentration. This was eventually confirmed by live cell imaging which then became a powerful tool in the field.

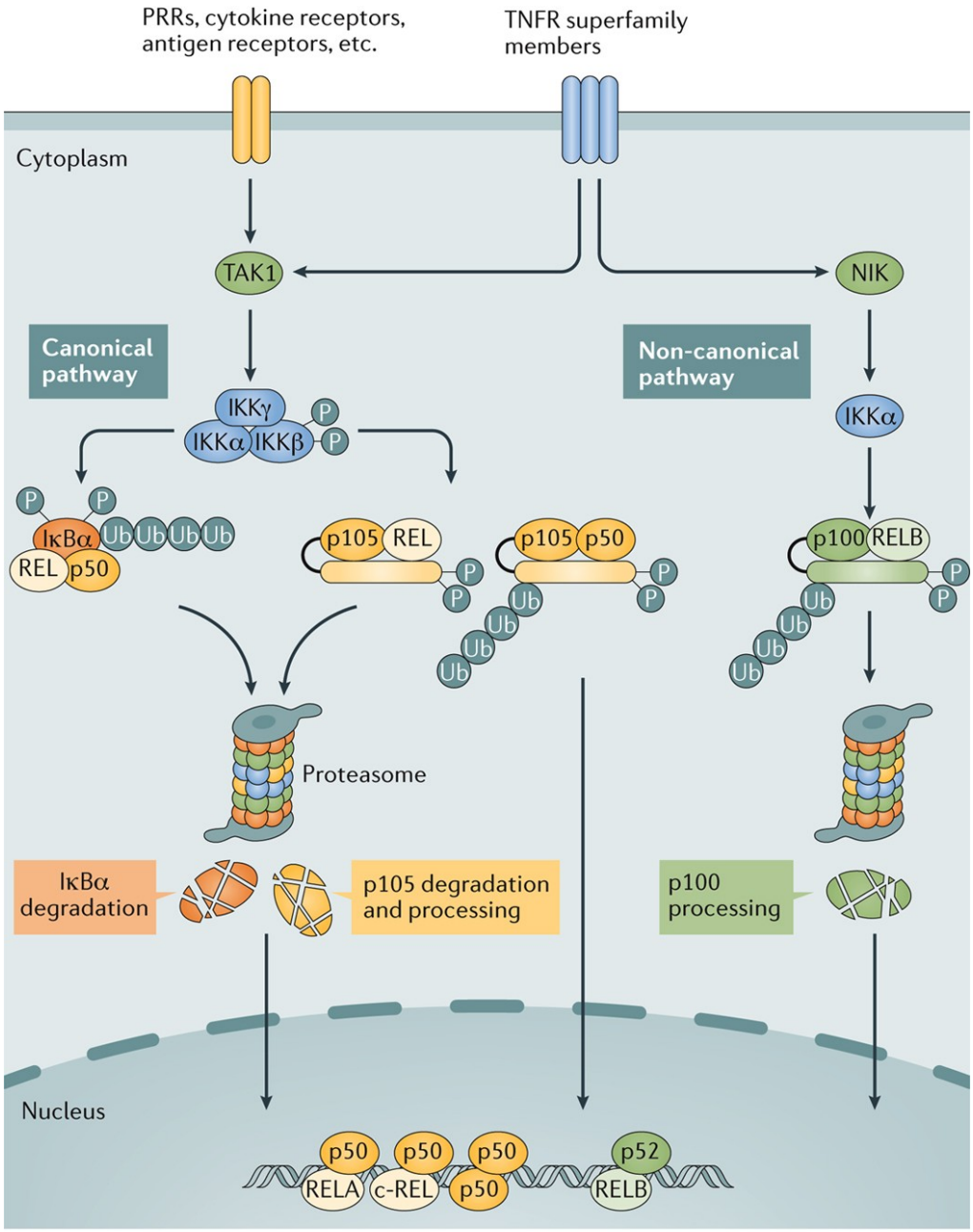

Figure 3.2. The canonical and non-canonical NF-κB pathways. Upon NF-κB activation through different receptors one of the 2 signaling pathways is activated. The canonical pathway uses kinase TAK1 whereas the non-canonical pathway uses NIK as first activator protein of their cascade. This leads to phosphorylation of the IκB kinase (IKK) which eventually results in the ubiquitylation and proteasomal degradation of the inhibitor IκBα for canonical, p100 for non-canonical pathway. In both cases NF-κB dimers are released and translocate to the nucleus to regulate their target genes. Figure is taken from Sun, 2017 by permission from Springer Nature: Nature Reviews Immunology, The non-canonical NF-κB pathway in immunity and inflammation by Shao-Cong Sun (2017).

3.4 Key approaches of live cell imaging-based research of NF-κB:

3.4.1 Fluorescent tagging and imaging of NF-κB in single living cells

NF-κB was visualized for the first time in single cells by transient transfection with fluorescently tagged NF-κB (Carlotti *et al*, 1999), and oscillations were first visualized in single living cancer cell lines (HeLA and SK-N-AS) that are stably transfected with fluorescently tagged NF-κB in 2004 (Nelson *et al*, 2004). Although oscillations were observed with suspicion at the beginning due to ectopic overexpression (Barken *et al*, 2005), they are widely accepted now (Ashall *et al*, 2009; Paszek *et al*, 2009; Turner *et al*, 2010). Oscillations have been confirmed in a variety of alternative systems, e.g., 3T3 cells where the endogenous gene has been knocked-out and is reconstituted by a fusion protein under the control of the endogenous promoter (Lee *et al*, 2009) or cells derived from knocked-in NF-κB mice (De Lorenzi *et al*, 2009). The dynamics of fluorescently tagged NF-κB can be observed in standard confocal and widefield microscopes equipped with adequate temperature and CO_2 control; nowadays data on NF-κB nuclear localization dynamics are commonly extracted automatically from time lapse recordings using software such as MATLAB and taking advantage of nuclear dyes/markers allowing to segment the nuclei (Zambrano *et al*, 2016) (Lee *et al*, 2009).

3.4.2 Mathematical modelling

A second key ingredient has been mathematical models, that have proved to be a valuable tool in the analysis of the NF-κB system in concomitance with live cell imaging. These models reproduce the time evolution of the copy number/concentration of biochemical species in different biochemical compartments upon stimuli. For example, for the NF-κB signaling this biochemical species include its complex with the inhibitor IκBs and the target mRNA levels which are all synthesized and/or degraded by certain rates. Hence, the global temporal evolution of the system of biochemical molecules that form the NF-κB system is described by a set of ordinary differential equations that is typically integrated using appropriate software (Lipniacki *et al*, 2004). Mathematical models allow to formulate hypothesis and produce predictions that are subsequently tested experimentally.

3.5 Insights on NF-κB regulation by live cell imaging

By using the single-cell live imaging methodologies sketched above for the study of NF-κB, researchers have been able to provide a deeper characterization on how NF-κB responds to stimuli. This also provided important insights on how the activation

of NF-κB is regulated by the interaction of ligands with receptors, by transducers and by downstream feedbacks. Here we provide some notable examples.

In 2009, thanks to the live cell imaging, it was shown that pulses of TNF-α (in the range between 60 and 200 minutes) followed by washouts led to nuclear localizations of NF-κB whose frequency matched that of the periodic stimulation. Interestingly, by measuring the amplitude of those nuclear localization peaks it was found that the amplitude of the second and third peaks were lower for higher frequency, indicating that the system has a refractory time for reactivation. Using mathematical modelling, the key role of the interplay between A20 and the two negative feedbacks IκBα and IκBε in this context was revealed (Ashall *et al*, 2009). More recently it was shown that if a pulse of IL-1β followed that of TNF-α, it resulted in a stronger nuclear activation showing that the refractoriness of the system is cytokine-specific, and somehow encodes specifically for previous cytokine exposures (Adamson *et al*, 2016). In fact, recently a mechanism was described where A20 and IκBα provide an activation memory for previous exposure by adjusting the receptor abundance and kinase cycling and this allows cells to respond only to differences in the concentrations of environmental cytokines (Son *et al*, 2021b).

It is also known that small portion of NF-κB shows dynamic shuffling between cytosol and nucleus not only upon stimulus but also in the basal conditions without any external signals. In 2021, by combining computer vision, live cell imaging and modelling it was revealed that the levels of IκBα and its ratio to NF-κB determine the responsiveness of cells to TNF-α (Patel *et al*, 2021). Finally, live cell imaging also allowed Sung and collaborators to unveil a novel positive feedback on NF-κB (Sung *et al*, 2014): LPS stimulated macrophage-like cells induce a positive feedback loop on p65 expression to overcome the existing negative feedback mechanisms. This was suggested as a new mechanism for immune cells to establish a threshold for proper immune response to the danger signals.

Overall, these works reveal how live cell imaging is a powerful tool to understand the NF-κB.

3.6 Insights on the transcriptional control exerted by NF-κB through live cell imaging

Live cell imaging combined with transcriptional information of the population has also contributed to improve our understanding on how NF-κB dynamics controls gene

expression. The very first observations of the oscillatory nature of NF-κB in single living cells (Nelson *et al*, 2004) already showed that target genes could be expressed with different kinetics in populations of oscillating cells. This was then further tested by (Sung *et al*, 2009), and the gene expression dynamics was classified as early (peaking at about 1hour), intermediate (at about 2-3 hours) and late (4 hours or later). Interestingly, perturbation of this dynamics using drugs completely disrupted the gene expression dynamics. Using a similar setting, it was shown that NF-κB activation is binary, but its dynamics are different when given different doses of TNF-α. Lower doses of the stimulus led to lower percentage of the activated cells and target gene expression correlated well with this fraction of activated cells (Tay *et al*, 2010). A similar correlation was also found using a luciferase NF-κB reporter even when cells were stimulated with extremely low doses of TNF-α (Turner *et al*, 2010).

Additional key insight on NF-κB control of gene expression was provided by the previously cited pioneering work by (Ashall *et al*, 2009). Pulsed TNF-α stimulation (consisting of carefully applied short pulses of TNF-α followed by washouts of different lengths), led to different dynamics of NF-κB, as discussed, and resulting in different gene expression levels in a target-specific way. This provided an additional and intriguing link between NF-κB dynamical features and its target gene expression.

Microfluidic devices allow a more careful manipulation of the cell's environment. By using them, it was proved that periodic sawtooth-like TNF-α profiles that are able to entrain the sustained cell oscillations –e.g., synchronize to the external periodic input- led to higher expression levels of the target genes (Kellogg & Tay, 2015). Similarly, using microfluidics systems coupled with population-level microarray gene expression data, it was found that periodic stimuli can synchronize NF-κB dynamics to different oscillatory frequencies. As a result, different patterns of gene expression (ranging from oscillatory to non-oscillatory) did emerge in the population of damped oscillatory mouse embryonic fibroblasts (Zambrano *et al*, 2016) that were enriched for genes involved in different cell functions.

Studies that rely on population-level transcriptional measurements have the advantage of well-established protocol and analytical pipelines. However, since the dynamics of NF-κB is extremely heterogeneous at single-cell level, extracting quantitative links between both remain challenging. Indeed, direct observation of transcription and imaging of single living cells provide a way to circumvent this difficulty, but this still has its limitations. As an alternative way to gain insights on the connection between NF-κB dynamics in single cells is through single-cell expression assays. Indeed, the fluorescent tagging of IκBα showed how NF-κB and

IκBα oscillate out of phase (Nelson *et al*, 2004). In a different study, by using a dual reporter system for NF-κB and NF-κB driven gene expression via TNF-α reporter in immune like cells it was found that maximum nuclear occupancy is correlated with the reporter expression (Sung *et al*, 2014). Later on, a study using a fluorescent reporter under the control of a promoter with NF-κB binding sites showed that TNF-α induced transcription bursts that are ultimately driven by fold-change in NF-κB nuclear localization (Wong *et al*, 2018).

Overall, many studies pointed to an important role of NF-κB activation dynamics in determining target gene expression.

3.7 Heterogeneity of NF-κB in response to stimuli

As mentioned before, NF-κB signaling shows a dynamic nuclear localization response upon activation, which is crucial for many cellular decisions and for gene expression. However, a very first evident observation derived from single-cell live cell imaging measurements is that its dynamics are widely heterogeneous. This heterogeneity includes cells that do oscillate and others that do not even respond within homogenous cell populations (Zambrano *et al*, 2014). Studies using various cell types reported that NF-κB dynamics can be qualitatively very different. It was first shown that continuous exposure of TNF-α results in oscillations with a period of 100 minutes in SK-N-AS cells (Nelson *et al*, 2004). Similarly, also for 3T3 cells sustained oscillations every 90 minutes were reported (Kellogg & Tay, 2015). On the other hand, MEF cells have been shown to be damped oscillators with typically less than three oscillatory peaks upon TNF-α treatment (Zambrano *et al*, 2016) while a persistent nuclear localization upon stimulus were reported for 3T3 upon LPS (Lee *et al*, 2009) and HeLa cells upon TNF-α (Lee *et al*, 2014). Moreover, later on it was found that when given LPS, RAW 264.7 cells have persistent nuclear activation (Sung *et al*, 2014). Another example of distinct NF-κB dynamic response was nicely shown by (Bartfeld *et al*, 2010) on three different cell lines expressing the same NF-κB-GFP reporter: depending on stimulus type and concentration clonal populations of each cell line showed oscillatory or non-oscillatory phenotypes (Figure 3.3). These hinted that NF-κB dynamics are not only cell type specific but also sensitive to different types of stimuli. In fact, recently it has been shown that macrophages and 3T3 cells discriminate between different pathogen derived stimulations and cytokines by relying on different features of their NF-κB activation (Adelaja *et al*, 2021; Martin *et al*, 2020).

When comparing the fraction of cells that were activated within a population it was found that low doses of TNF-α activated fewer cells in comparison to higher concentrations (Turner *et al*, 2010). This showed that stimulus concentration contributes to the dynamical heterogeneity within the population. Thanks to the usage of the microfluidics system, how the duration time of the stimulus changes the NF-κB dynamics was also investigated. It was reported that long and weak stimulation led to NF-κB activation of fewer cells in comparison to a short but strong pulse of stimulus (Kellogg *et al*, 2015). Overall, both papers concluded that NF-κB dynamics uses a switch-like mechanism by having an activation threshold for activation of a population's proper gene expression and avoiding out-of-context inflammatory responses. However, recently it was proposed that activation threshold varied between single cells of a population (Zhang *et al*, 2017a).

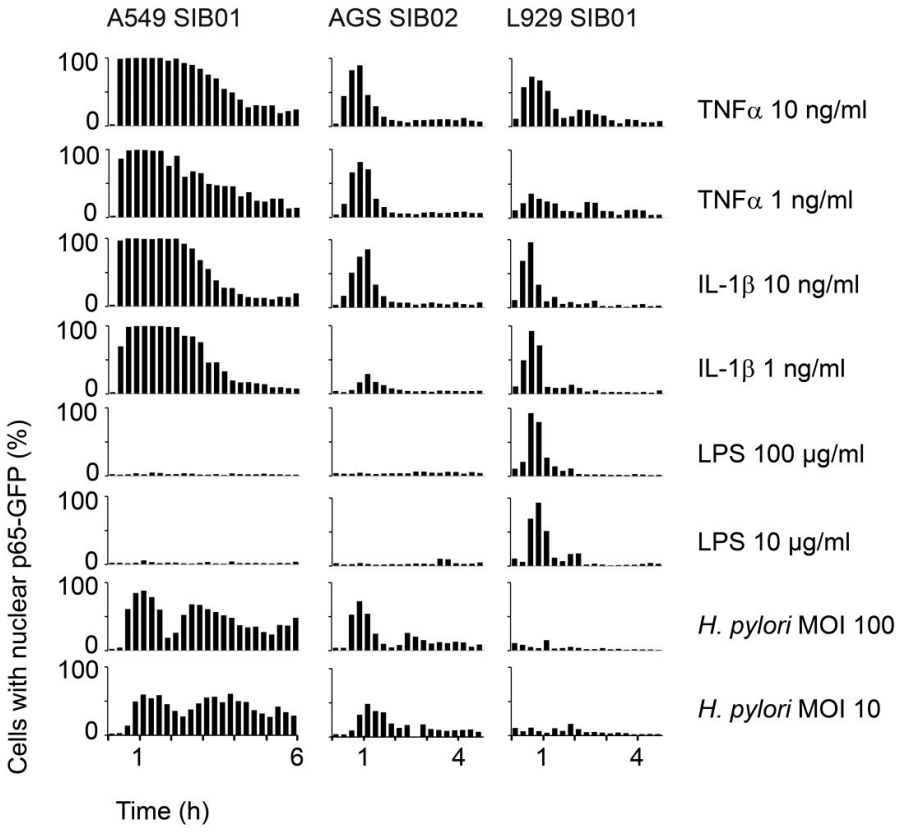

Figure 3.3. Stimulus specific NF-κB oscillation heterogeneity. 3 cell lines: a human alveolar epithelial cell line (A549 SIB01), a human gastric epithelial cell line (AGS SIB02) and a mouse fibroblast cell line (L929 SIB01) were treated with the indicated stimulus and concentration over a period of 6 hours. Percentage of activated cells is indicated on the graph. Figure is taken from Bartfeld *et al*, 2016, licensed under CC BY 2.0 (To view a copy of this license visit: http://creativecommons.org/licenses/by/2.0)

In a study that combined live cell imaging with mathematical modeling it was reported that the timing between the two maxima of the nuclear localization peak (also known as period) stays invariant. At population level this feature was conserved even when given various stimuli and concentrations. However, at single cell level the period was found to be variable between the different cells. Hence it was concluded that the heterogeneity of the single cell dynamics contributes to the populational robustness (Hughey *et al*, 2015).

Some studies were conducted to understand the source of the NF-κB dynamics heterogeneity. It was then found that the dual negative IκB feedback (IκBα and IκBε) of the system induces the heterogeneity to keep populational robustness for fluctuating environmental damage signals (Paszek *et al*, 2010). More recently, researchers built a synthetic NF-κB signaling in yeast cells. Using this system, the dynamics are shown to be modulated by 3 simple features: the amount of NF-κB protein, synthesis, and degradation rates of the inhibitor IκBα (Zhang *et al*, 2017c). Hence, it was suggested that having small and cell-dependent variations contribute to the heterogeneity.

Overall, what became clear in the field is that NF-κB heterogeneity in response to a stimulus is not meaningless but instead functional, and that studying the origin of such heterogeneity can be informative on how dynamic TFs generate robust and meaningful responses upon activation.

3.8 NF-κB dynamics in space and time

Inflammation can be considered as a hallmark of multicellularity as it involves a variety of different cells that need to work in a coordinated way (Netea *et al*, 2017). Once activated, cells use cytokines to communicate information about the infections or tissue damage to the neighboring cells. Timely and accurate recruitment of immune cells through a proper spatial distribution of cytokines around the damage site is essential to clear and repair the damaged area, as improperly resolved inflammation can lead to sepsis and systemic failure (Singer *et al*, 2016).

In physiological conditions the activation of NF-κB could potentially propagate to the neighboring cells through cytokine secretion. Mathematical models suggest that activation of NF-κB in a point in a tissue could result in a wave-like propagation of the activation and of cytokines in the tissue (Yde *et al*, 2011; Gangstad *et al*, 2013). However, the propagation of NF-κB activation in a tissue has never been observed experimentally and many important questions are still far from having a complete

answer: How far and how long do signals propagate in the tissue? How is this propagation limited? What is the role played by each cell type and cell-to-cell dynamical heterogeneity? Which intrinsic cell regulatory mechanisms are necessary for each cell to work adequately in its context? How are immune cells guided by this complex spatiotemporal signaling?

Several in vitro studies have shown cell-to-cell communication through cytokine production. A very first study pointed out autocrine signaling by showing persistent NF-κB activation upon LPS stimulation which is achieved by a secondary activation due to the cell's own TNF-α production (Covert *et al*, 2005). Next, paracrine activation of NF-κB was also reported by co-culturing LPS responsive and unresponsive (TLR4 receptor depleted) cell types. Upon LPS stimulation NF-κB activation was observed in LPS responsive cells and this was later followed by the activation of LPS unresponsive cells, which was attributed to paracrine TNF-α secretion (Lee *et al*, 2009). Another similar study conducted by Kasper and collaborators also showed nicely how an activated cell can generate activation zones in a layer of cells through cell-to-cell communication (Kasper *et al*, 2010). In this in vitro system a pathogen was used to activate NF-κB, which led to activation of non-infected bystander cells (Figure 3.4).

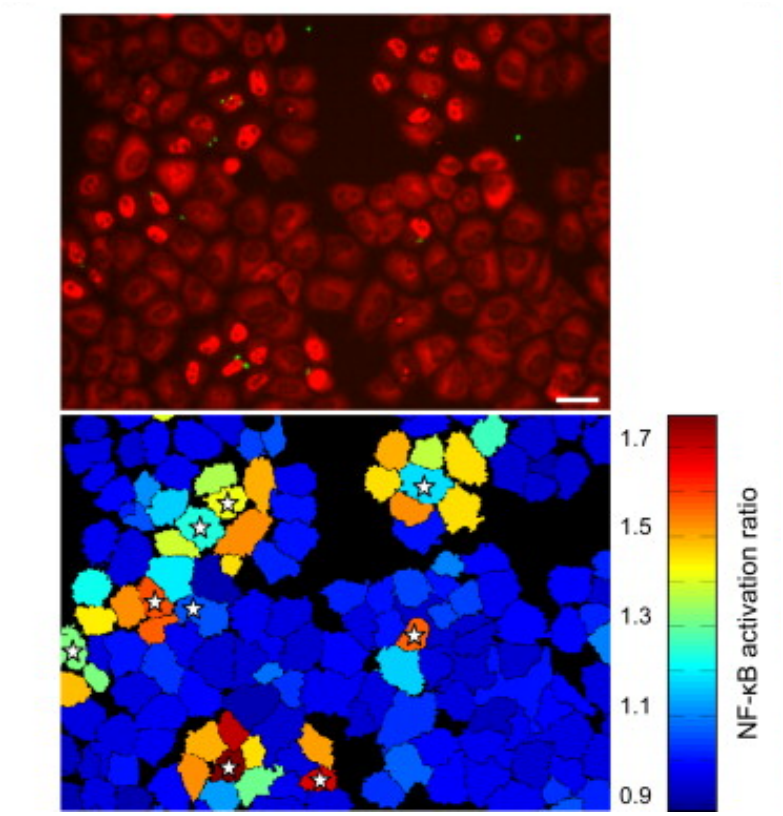

Figure 3.4. NF-κB activation zones upon pathogen infection. Immunofluorescence staining of NF-κB after 1 hour infection with the pathogen *Shigella flexneri* (green dots) (top). False color representation of the NF-κB activation ratio (bottom). Stars indicate the infected cells. Figure is taken from Kasper *et al,* 2010 by permission from Elsevier: Immunity, Cell-Cell Propagation of NF-κB Transcription Factor and MAP Kinase Activation Amplifies Innate Immunity against Bacterial Infection by Christoph Alexander Kasper, Isabel Sorg, Christoph Schmutz, Therese Tschon, Harry Wischnewski, Man Lyang Kim, Cécile Arrieumerlou (2010).

Cell-to-cell communication between different cell types has been considered in other studies. By combining live cell imaging and mathematical modelling it was shown that competitive uptake of TNF-α defines the cytokine gradients and predicts the signal propagation of immune cell activation (Bagnall *et al*, 2018). In another study a microfluidics device was designed to co-culture cell types without cell-to-cell contact. This revealed that NF-κB activation in macrophages results in the secretion of NF-κB–activating stimuli that propagate the signal from immune cells to the fibroblasts (Frank & Tay, 2015). Very recently, the same microfluidic device was used to characterize NF-κB dynamics based on the distance of cells from the cytokine source, and a wave-like propagation of NF-κB was imaged for the first time (Son *et al*, 2021a).

Taken together, the evidence suggests that NF-κB activation dynamics can be heterogeneous at a tissue level. This is in line with what is observed in complex

inflammatory contexts, such as a tumor like hepatocellular carcinoma (HCC), where NF-κB can be found activated in only a fraction of cells within a liver tumor mass (Pikarsky *et al*, 2004), (Figure 3.5).

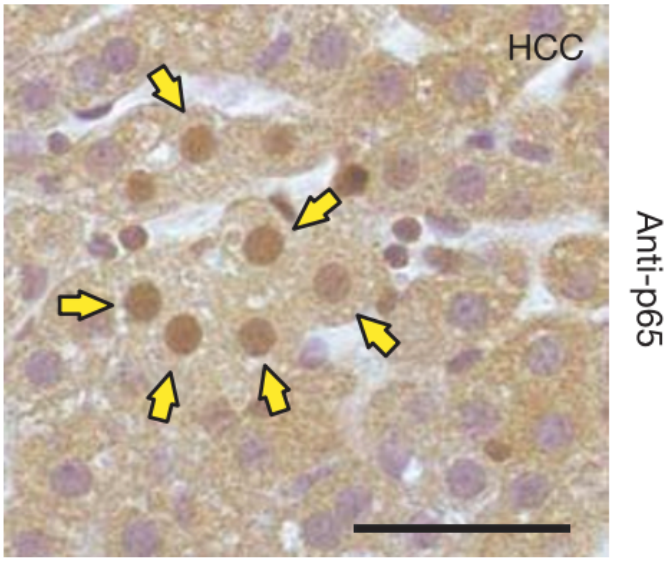

Figure 3.5. Heterogeneity of NF-κB activation in tissue. Immunohistochemistry against p65 protein in a liver tissue section of hepatocellular carcinoma (HCC) carrying mice. Yellow arrows show activated NF-κB in the nuclei whereas cytosolic staining can be observed in the surrounding cells. Scale bar is 50 μm. Figure is taken from Pikarsky *et al,* 2004 by permission from Springer Nature: Nature, NF-κB functions as a tumour promoter in inflammation-associated cancer by Eli Pikarsky et al (2004).

Although the heterogeneity in the tissue hints towards cell-to-cell inflammatory communication leading to NF-κB activation in the tissue, a static immunohistochemical image on a fixed tissue does not provide many insights on the role of NF-κB dynamics in this context. Some studies suggest that cell-to-cell communication through cytokines can be very dynamic. Recently, by co-culturing interleukin-2 consuming and producing immune cells it was shown that diffusion-consumption kinetics apply to cytokine propagation in vitro. This was further tested in vivo, which revealed cytokine niches within the tissue that can expand or shrink depending on the number of interleukin-2 consuming cells (Oyler-Yaniv *et al*, 2017). However, the general principles modulating the dynamic activation of the NF-κB pathway in cell co-cultures in a context of paracrine inflammatory cell-to-cell communication have not been thoroughly investigated.

4. AIM OF THE WORK

NF-κB nuclear localization dynamics are fundamental for a wide range of cellular processes to achieve proper target gene expression upon activation yet are highly heterogeneous. In this work, we aimed to gain insights on the origin of the heterogeneity of the dynamics of NF-κB and to understand the role of such dynamics in the context of inflammatory cell-to-cell communication.

First, we want to characterize the origin of the heterogeneous NF-κB dynamics in a homogeneous population. To do so, we will focus on a population of mouse embryonic fibroblasts knock-in for GFP-NF-κB deriving from a single embryo, and hence quasi-identical. By single cell cloning of our population, we will be able to evaluate if clones respond differently to simple stimuli. Furthermore, we will be able to better dissect the source of the heterogeneity between the clones taking advantage of their biological homogeneity. In particular, we aim to study whether clones behaving differently do display differences at a transcriptomic level in the NF-κB regulatory circuit. Mathematical models and interference of the regulatory circuit will allow us to evaluate if transcriptional differences between cells can lead to different NF-κB dynamic responses.

Second, we want to study the potential heterogeneity of NF-κB dynamics in the inflammatory cell-to-cell communication. First, we will use immunohistochemistry to understand if NF-κB activation status is indeed spatially inhomogeneous within a tissue in different settings. To gain further insights on this in vitro, we will setup a system where we can observe the spatial NF-κB activation heterogeneity. We will do so through co-cultures of naturally (immune-like) or inducible (engineered MEFs) signal sending cells co-cultured with our model GFP-p65 knock-in MEFs in different conditions, which will provide us clues about the general principles guiding spatiotemporal NF-κB dynamic responses in cell-to-cell communication in inflammation.

We think that our study could lead to novel insights on the complexity of NF-κB responses in space and time and on the multiple sources of cell-to-cell heterogeneity, while providing clues on how cells within a population are able to articulate a robust and informative response to danger signals in space and time. This might yield important insights on how inflammation and the immune response are coordinated in health and disease.

5. RESULTS

The results presented in the following chapter of this thesis (5.1) are published in BioRxiv preprint server (Kizilirmak *et al,* 2021).

5.1 The heterogeneity of NF-κB dynamics

To study NF-κB nuclear localization dynamics in single cells, we used GFP-NF-κB tagged MEFs. The cells were derived from a single embryo of homozygous knock-in GFP-NF-κB mice (hence referred as quasi-identical) and used for live cell imaging. The setup for the live cell imaging includes an incubator where we stably maintain our cells in 5% CO_2 at 37°C and we take time lapse images every six minutes. Our imaging shows that when there is no inflammatory stimulation, NF-κB is found in the cytosol of the cells (Figure 5.1A). Upon TNF-α stimulation, NF-κB translocates to the nucleus (Figure 5.1A).

To analyze single cell dynamics of NF-κB we calculate the average nuclear to cytosolic fluorescent intensity ratio using MATLAB scripts that were previously developed in our laboratory (Zambrano *et al*, 2016). Briefly, these scripts allow us to track our cells between frames using an optimized algorithm based on the Hungarian linker method (Careccia, 2019) and to create nuclear masks to calculate average nuclear signal of NF-κB using Hoechst staining (Figure 5.1B). To estimate the average cytosolic NF-κB intensity, it creates a ring of width size 0.5 times the nuclear radius around each nucleus and calculates the average intensity within this area excluding the background signal (Figure 5.1B). Using these scripts, we quantify NF-κB dynamics in hundreds of cells during hours for each of our live cell imaging experiments.

Our results show that NF-κB translocation to the nucleus starts after addition of TNF-α, and it reaches the nuclear localization peak around 30 minutes post stimulus (Figure 5.1C). Interestingly, as previously reported (Zambrano *et al*, 2014), each cell exhibits their unique NF-κB dynamic signal showing a great heterogeneity in the population's overall TNF-α response (Figure 5.1C). We find cells that display oscillatory peaks of nuclear localization while some others display a non-oscillatory dynamics, a kind of dynamics also referred to as persistent activation, similar to the one reported for macrophages (Cheng *et al*, 2021). Moreover, we also find differences in the strength of the cell's response to TNF-α as assessed by their maximum NCI value. Therefore, to better represent the heterogenous NF-κB dynamics across our population we introduced the dynamic heatmaps where such differences are visually captured (Figure 5.1D).

Although such variety in the NF-κB response has been previously reported for different cell types (Lee *et al*, 2014 non oscillatory nuclear localization for HeLa cells; Kellogg & Tay, 2015 sustained oscillation for 3T3 cells) the source of the heterogeneity is still unknown. Thus, we took advantage of our very homogenous population of MEFs exhibiting yet heterogenous dynamics to understand the origin of the different NF-κB dynamics.

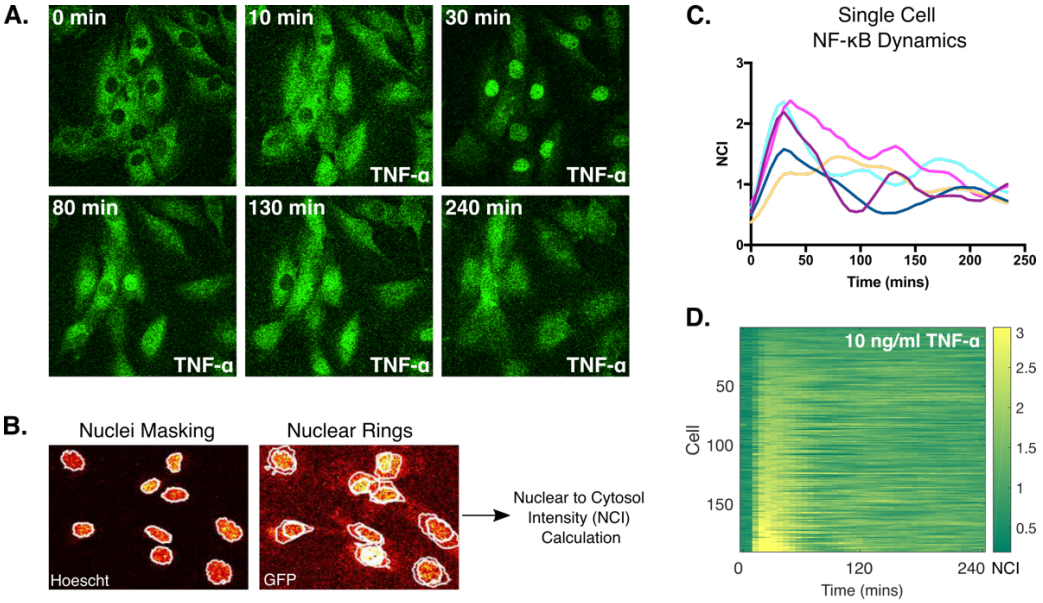

Figure 5.1. Live cell imaging shows MEFs have heterogeneous NF-κB dynamics upon TNF-α stimulation. A*. Representative images of the heterogeneous response of our MEFs to 10 ng/ml TNF-α stimulation.* ***B.*** *An example of quantification process by the automated MATLAB scripts. Hoechst channel was used to track the cells over time and to generate nuclear masks to identify the nuclear GFP signal. Nuclear rings were used for the estimation of the cytosolic GFP signal and nuclear to cytosolic intensity (NCI) ratio was then calculated for each cell****. C.*** *Single cell NF-κB dynamics upon TNF-α in randomly chosen six different cells of the population.* ***D.*** *Dynamic heatmap represents the NF-κB dynamics of hundreds of cells sorted by their maximum NCI value.*

5.1.1 Clonal populations of fibroblasts derived from a single embryo display distinct NF-κB dynamics upon TNF-α

To investigate the origin of the dynamical heterogeneity of NF-κB, starting from our general population of MEFs (that we refer to as the "pool" in what follows) we generated clonal populations by single cell cloning (Figure 5.2A). Overall, we generated 17 clonal populations of which 8 were imaged upon stimulation with 10 ng/ml TNF-α (Figure 5.2B). We found that NF-κB dynamics of each clonal population upon TNF-α was markedly different, even if a certain degree of intra-clonal heterogeneity was observed (Figure 5.2B).

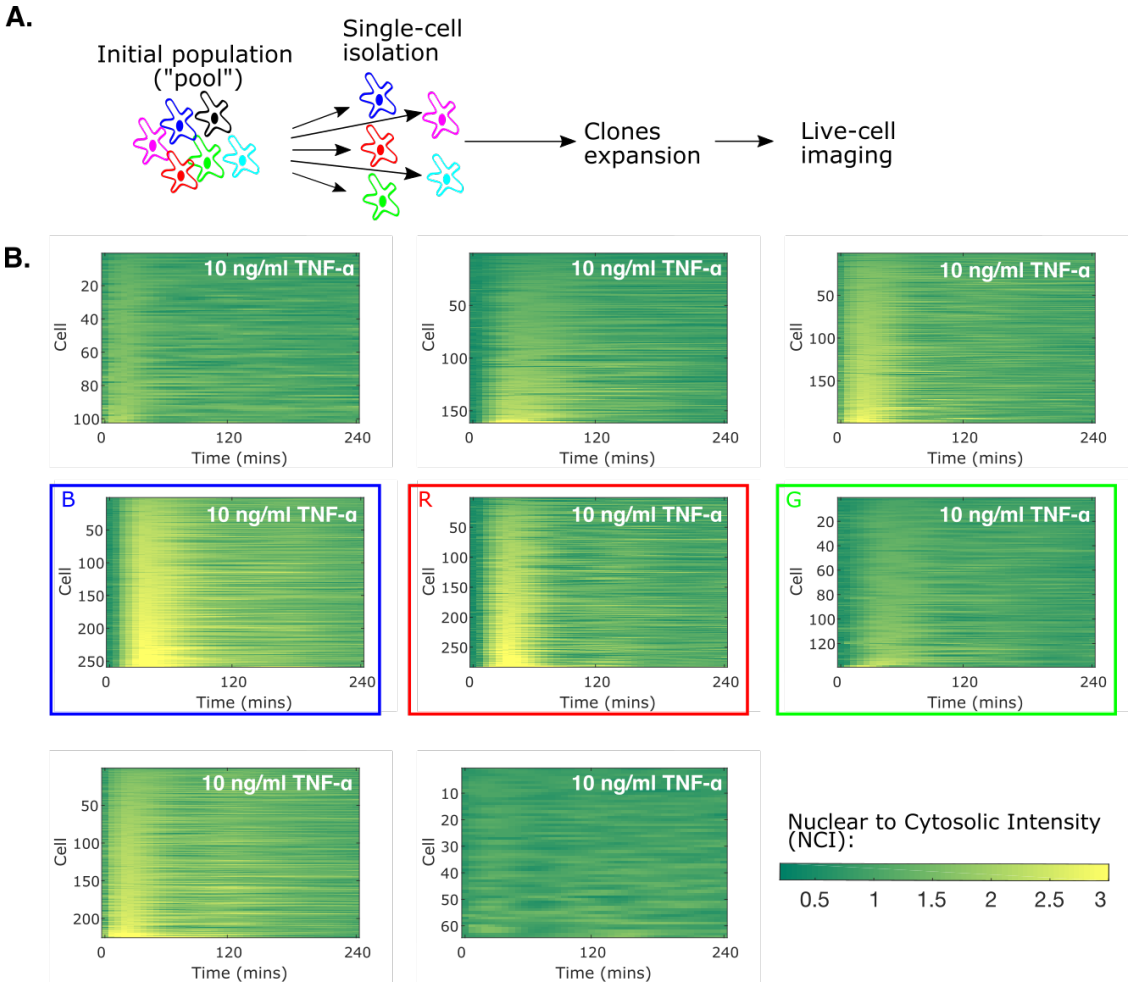

Figure 5.2. Single cell clones derived from an initial population of MEFs have distinct dynamics upon TNF-α stimulation. A. *Scheme shows the single cell cloning strategy from the initial MEF population (referred as Pool). Single cells were isolated from the pool by serial dilution and each single cell was plated in a well of a 96-well plate. Clones were then expanded and used for live-cell imaging.* ***B.*** *Dynamic heatmaps of 8 clones generated upon 10 ng/ml TNF-α stimulation (Clones B, R and G are highlighted).*

To have an unbiased confirmation of this observation, we utilized an unsupervised stochastic clustering approach using the k-means algorithm based on the Euclidean distance between the NF-κB dynamic profiles. The cells of the 8 clones were clustered according to their shapes into 8 different clusters (Figure 5.3A). Then we calculated the probability for two trajectories of each pair of clones to cluster together; the average result of many realizations of this stochastic procedure indicates that NF-κB dynamic profiles of cells of the same clone are more likely to cluster together than with profiles of cells of other clonal populations (Figure 5.3B). To quantify to what extent cells of the same clonal population cluster together we used an entropy-based clustering quantifier that gives high values if we randomly attribute the dynamics to

different clones, and zero if the trajectories of each clone are clustered together. This resulted in significantly high values in each of the realizations of the stochastic clustering than when the profiles are randomly mixed (Figure 5.3C), confirming that clones have distinct dynamics.

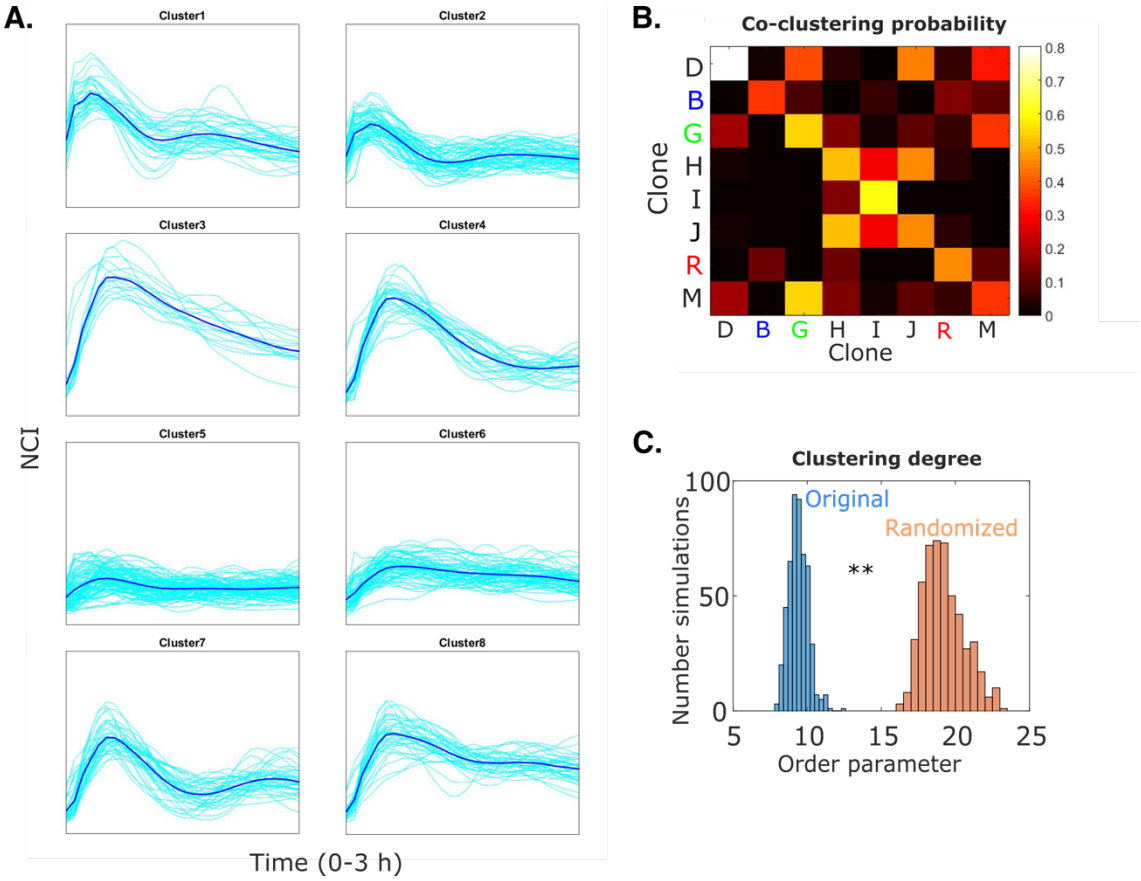

Figure 5.3. Clustering algorithms confirm clones possess distinct dynamics upon TNF-α stimulation. A. *8 clusters of NF-κB dynamic profiles obtained from an unsupervised stochastic clustering approach: a k-means algorithm based on the Euclidean distance between the NF-κB dynamic profiles.* ***B.*** *The color-coded plot shows co-clustering probability of NF-κB dynamic profiles between different clones.* ***C.*** *An entropy-like disorder parameter calculated for each realization of the original stochastic clustering versus a randomized dataset. The distributions do not overlap in 500 realizations of the stochastic clustering for the original and the randomized datasets, $p<2\cdot10^{-3}$.*

In summary, we find that isolated clones from a population of MEFs derived from a single embryo display distinct dynamical behaviors.

5.1.2 NF-κB dynamics and oscillatory behavior of the cells is different between clones yet heterogenous within clonal populations

We then decided to focus on three clones with archetypical dynamics reminiscent of those observed in the literature to investigate the origin of such differences. In particular, we focus on a clone with more persistent nuclear localization of NF-κB (Clone B, blue, Figure 5.2B), one with a first well-defined sharp peak (Clone R, red, Figure 5.2B) and a clone characterized by a low activation of NF-κB (Clone G, green, Figure 5.2B).

Clonal populations B, R and G had clear distinct NF-κB dynamics even by direct inspection of their time-lapses (Figure 5.4A). The average NF-κB activation profiles show how the three clonal populations respond distinctly to TNF-α, with a stronger response for clone B than for clone R, and for clone R than for clone G (Figure 5.4B). A compact way to represent this is through the order relation B>R>G.

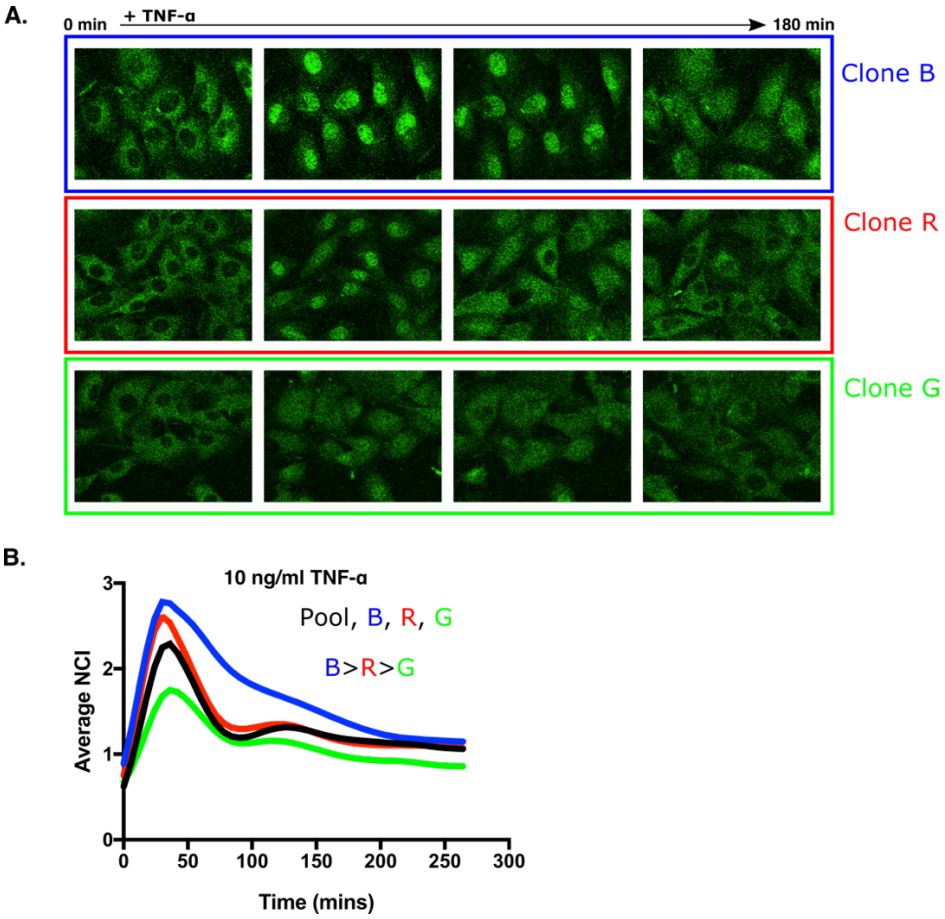

Figure 5.4. The selected clones B, R and G shows distinct dynamics upon TNF-α stimulation. A. *Representative images from our time-lapse movies for clones B, R and G upon 10 ng/ml TNF-α stimulation.* ***B.*** *NF-κB dynamic response of the clones to TNF-α as assessed by the average NCI.*

The dynamic response of our clones was strikingly robust across the experiments (Figure 5.5A). The differences in the average response were conserved for higher TNF-α doses (100 ng/ml) (Figure 5.5B) and also for many passages, even if the average response to TNF-α was weaker after 8 weeks (Figure 5.5C).

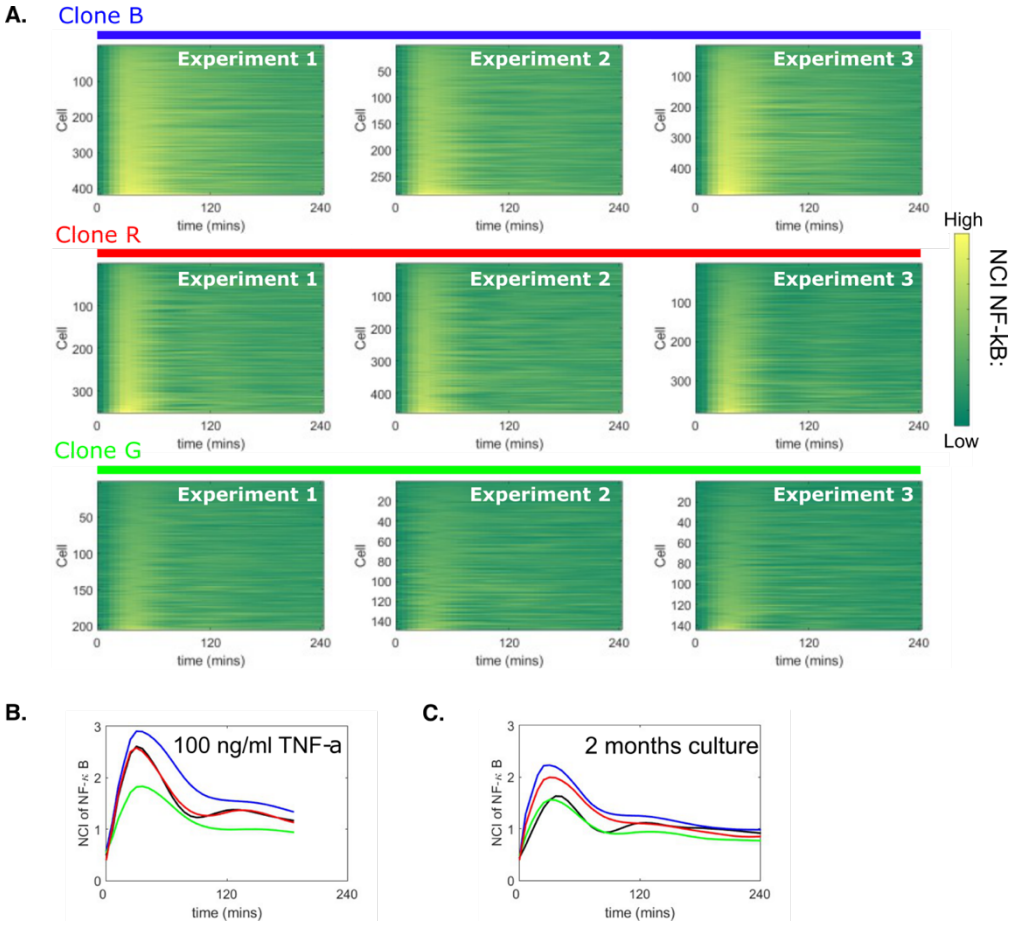

Figure 5.5. The differences on NF-κB dynamic profiles between the clones are robust. ***A.*** *Dynamic heatmap of the response of the clones B, R and G to 10 ng/ml TNF-α in three independent experiments.* ***B.*** *Average NF-κB dynamic profile for the three clones upon 100 ng/ml TNF-α.* ***C.*** *Average NF-κB dynamic profile for the three clones B, R, G kept in culture for 8 weeks.*

On the other hand, we also observed a certain degree of cell-to-cell heterogeneity, so we used our live-cell imaging quantitative setup to extract the key features of the dynamical response to TNF-α at single-cell level. We focused on classic quantifiers of NF-κB response, such as the height of the first peak, its timing, and the area under the curve (Tay *et al*, 2010; Zambrano *et al*, 2014). We find that the values of such quantifiers are heterogeneous, but yet there are statistically significant differences between the populations (Figure 5.6A). We indeed found that the values of the first

peak of activation are typically higher for clone B than for clone R, which in turn are much higher than for clone G (Figure 5.6A), so the B>R>G relation is also preserved. The timing of the first response peak is equally prompt within our experimental resolution in clones B and R, but slightly slower in clone G (Figure 5.6A). The stronger differences though are observed in the area under the curve (Figure 5.6A) which is much higher for clone B than for clone R, and is again the lowest for clone G. This captures well our observation that clone B has a more persistent NF-κB nuclear localization dynamics.

All the differences above were assessed using the nuclear to cytosolic intensity (NCI) of NF-κB. To further confirm our findings, we also used the absolute intensity of the nuclear signal and showed that B>R>G relation was conserved (Figure 5.6B). The initial nuclear intensity of the clones was low and similar across clones, but nonzero as expected (Figure 5.6B) (Zambrano *et al*, 2014). To exclude bias derived from the automated quantification, we also confirmed such relation by manually segmenting the cell's nuclei using Fiji (Figure 5.6C).

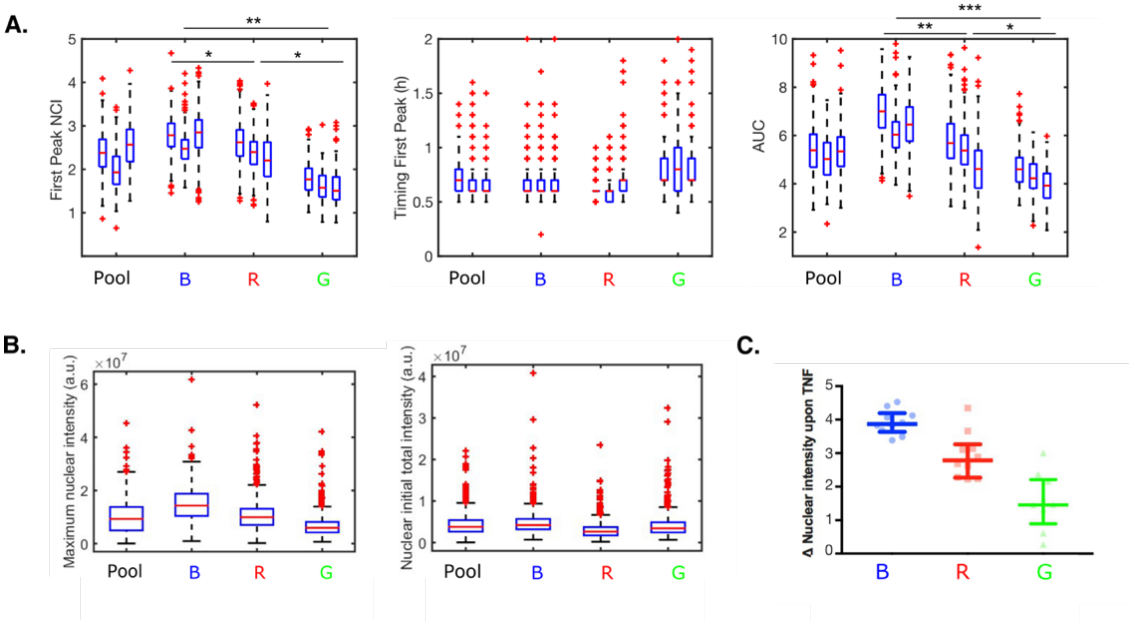

Figure 5.6. Manual and automated single cell analysis show intra-clonal response to TNF-α is heterogeneous but differences between clonal populations are significant
A. *Dynamical features of the response to TNF-α in three biological replicates: value of the first peak, timing of the first peak and area under the curve (AUC).* ***B.*** *Maximum nuclear intensity and nuclear initial intensity of the clones quantified by absolute NF-κB intensities instead of the internally normalized NCI.* ***C.*** *Maximum response to TNF-α calculated by manually segmented nuclei intensity difference before and after the stimulation. *p<10^{-2}, ** p<10^{-3}, *** p<10^{-4}, multiple comparisons through Kruskal-Wallis.*

Our data indeed indicate that each population has a distinct early NF-κB dynamic response to TNF-α, and that such differences are robust and accompanied by a consistent degree of intra-population heterogeneity.

Distinct NF-κB dynamics of single cell clones could be related to intrinsic or extrinsic factors such as cell cycle, which has been already shown to modulate the response to TNF-α (Ankers *et al*, 2016). Hence, we compared the cell cycle distributions of our clonal populations (Figure 5.7A). When we compared our strongest and weakest TNF-α responding clones (Clone B vs Clone G) we found that their cell cycle distributions are very similar, suggesting the cell cycle has a limited impact to explain inter-clonal dynamic differences. Instead, the distribution of cell cycle phases across Clone B and Clone R was more diverse. Therefore, we applied a computational correction for the differences in the population fractions in each cell cycle phase. We generated an artificial dataset of NCI time series of Clone R: the top 25% of the population was assumed to be the S-phase high responders (Ankers *et al*, 2016) and their percentage was increased to 43% by neglecting the corresponding fraction of the less responding cells. The resulting dataset had overall a higher value than before the correction, as expected, but yet it was a lower value of the AUC in comparison to Clone B (Figure 5.7B), suggesting that even after cell cycle correction the global differences in the dynamic responses between the clones are maintained.

A.

	G1 Mean	G1 CV	%G1	G2 Mean	G2 CV	%G2	%S	G2/G1
B	87175,78	8,10	43,39	167031,93	5,64	15,82	40,79	1,92

	G1 Mean	G1 CV	%G1	G2 Mean	G2 CV	%G2	%S	G2/G1
R	97138,36	8,11	50,84	181729,34	7,72	23,79	25,37	1,87

	G1 Mean	G1 CV	%G1	G2 Mean	G2 CV	%G2	%S	G2/G1
G	81811,96	8,43	41,06	153517,46	7,70	18,62	40,32	1,88

B.

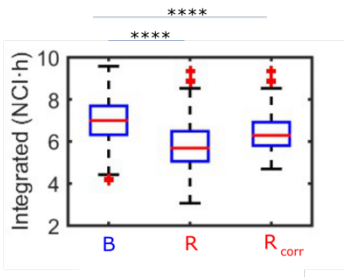

Figure 5.7. Cell cycle distributions has limited effect on the NF-κB dynamics of the clones A. *The table shows the cell cycle distributions of the clones by FACS analysis.* ***B.*** *The AUC (the integral of the NF-κB profiles) was calculated for Clone B, Clone R, and in-silico cell cycle corrected Clone R. *p<10^{-2}, ** p<10^{-3}, *** p<10^{-4}, multiple comparisons through Kruskal-Wallis.*

Our single cell data from clonal populations do also provide us an interesting perspective on whether NF-κB signaling dynamics can be considered oscillating or not, a topic that has been subjected to discussion (Barken *et al*, 2005; Kellogg & Tay,

2015; Nelson *et al*, 2004; Zambrano *et al*, 2016). Such oscillations should be characterized by the presence of multiple oscillatory peaks in our NF-κB dynamic profiles. Hence, we calculated the fraction of cells with 1, 2 or 3 oscillatory peaks for each clonal population upon 4 hours of treatment with 10 ng/ml of TNF-α. We found that such fractions are variable across the pool and the clonal populations, and it is possible to find for each clone a substantial fraction of cells that do not oscillate, having at most one peak (Figure 5.8A). However, there are also different fractions of cells in each population that have two or more peaks, from which we can conclude that some clones are more oscillatory than the others (Figure 5.8A), and that there are cells oscillatory to different degrees within each population. The period of the oscillations, computed as inter-peak timing, is slightly higher for clone B (Figure 5.8B). When analyzing instead the features of those oscillations at single cell level, we find a remarkable degree of heterogeneity in the peak value ratios, which is again consistently maintained in experimental replicates (Figure 5.8C). Our data then shows that being oscillatory is somehow a fuzzy phenotype in each population, and even single cell populations can be considered oscillatory to different degrees. This might explain the qualitatively different dynamics observed for different cell types, that can go from cells that oscillate in a sustained fashion for 20 hours and more (Kellogg & Tay, 2015) to those that oscillate in a more damped way with fewer oscillatory peaks (Zambrano *et al*, 2016) or not oscillating at all (Lee *et al*, 2014).

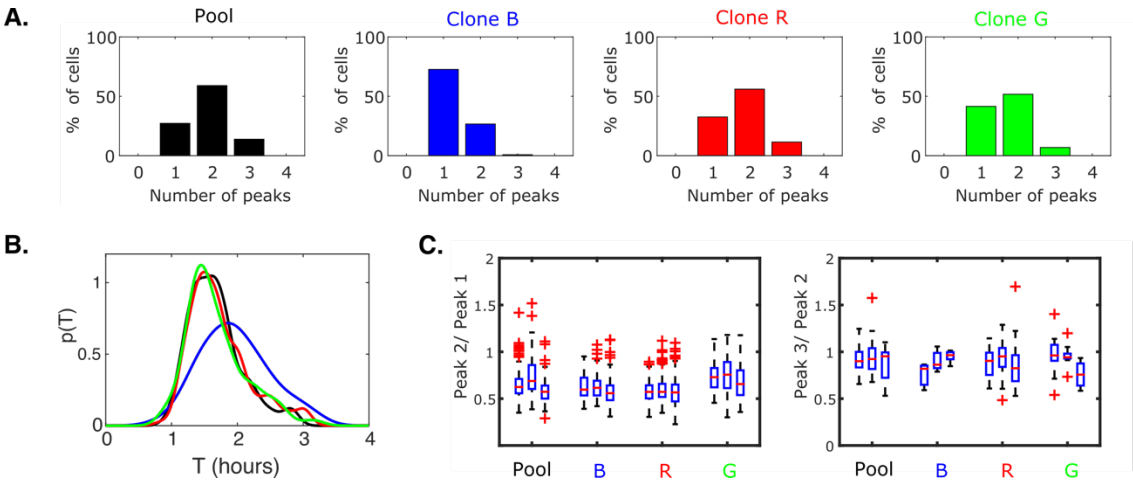

Figure 5.8. Clones show different degrees of oscillatory NF-κB dynamics A. *Frequency of the number of the oscillatory peaks observed for each population in 4 hours.* ***B.*** *Periods of the oscillations computed as the inter-peak timing for each population.* ***C.*** *Ratios of the oscillatory peak values for each clonal population in three independent experiments.*

Overall, we show how clonal populations of fibroblasts derived from the same mouse embryo have distinct yet heterogeneous dynamical features both in their early response to TNF-α and in the subsequent dynamics that is oscillatory to a different degree within each population.

5.1.3 Clonal populations have distinct transcriptional programs and control of target gene expression upon TNF-α

We next decided to further understand how different our clonal cell populations are and try to unveil the source of the differences in their NF-κB dynamic response by performing RNA-sequencing.

Our cells display quantitative differences on their average NF-κB dynamic response already after 1 hour TNF-α stimulation (Figure 5.4B). Therefore, we decided to perform the RNA-sequencing of cells untreated (UT) and treated 1 hour with TNF-α (Figure 5.9A). To gain statistical power and be able to confidently identify relatively small differences we generated 5 replicates per condition. We first checked the quality of our samples by dividing the number of reads mapped to a specific gene by the total number of mapped reads: a normalized gene expression unit known as counts per million reads (CPM). We found more than 10000 genes with CPM>1 showing the good quality of our samples (Figure 5.9B).

Next, we took advantage of the high quality of our samples to estimate genetic differences between clonal populations following an established procedure based on reads mapping (Yizhak *et al*, 2019). We aligned the reads from each population to a reference genome and identify single nucleotide polymorphisms (SNPs). The confidence level of SNP calling was based on the minimum coverage requested and then the single-nucleotide differences were calculated between the clones. We find that our clones differ in a range of 200-400 nucleotides; by dividing this by the length of the genome that we confidently mapped we obtain a mutation rate of $5 \cdot 10^{-7}$ per base pair (Figure 5.9C). This is compatible with somatic differences from cells of the same organism (Milholland *et al*, 2017) as expected.

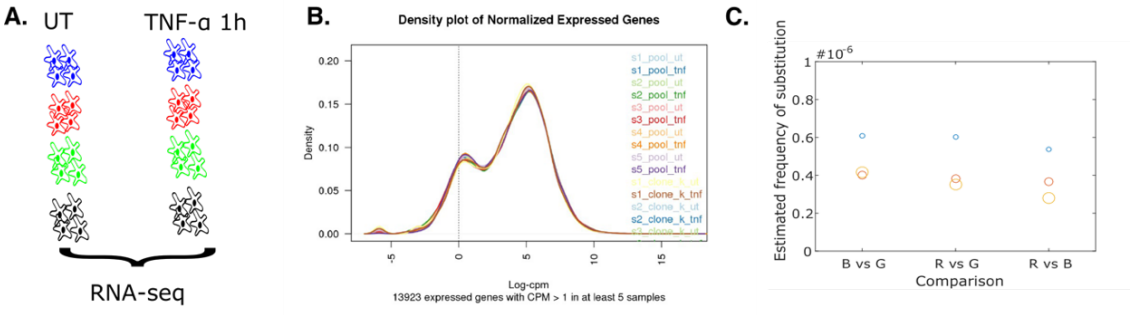

Figure 5.9. RNA-sequencing experimental setup, quality control and the mutation rates. A. *Scheme of the RNA-sequencing performed: cells treated 1 hour with TNF-α or untreated (UT).* ***B.*** *Density plot of normalized expressed genes for each sample* ***C.*** *Estimated frequency of substitution between clones calculated by the ratio of the number of SNPs and the length of the mapped genome. Increasing marker sizes indicate more stringent criteria for SNPs calling (See Methods for details).*

To be able to capture the transcriptomic variations in our samples we performed an unsupervised principal component analysis (PCA). This time we considered a gene length normalized expression unit: RPKM (reads per kilobase of transcript per million mapped reads) calculated by dividing the number of reads mapped to the genome by the total number of mapped reads and the length of the gene. For the analysis we only included genes that are RPKM>1 in at least five samples. We found that samples from different clones do cluster in different groups (Figure 5.10A) and such neat clustering is also preserved when we use additional dimensions (Figure 5.10B). Most of the variability was explained by only few dimensions showing the quality of the analysis (Figure 5.10C). When we performed PCA of our samples together with public transcriptomic data from other tissues our samples clustered together very closely and far from the outgroup sample. This shows the apparent transcriptional divergence between our clones is very small (Figure 5.10D).

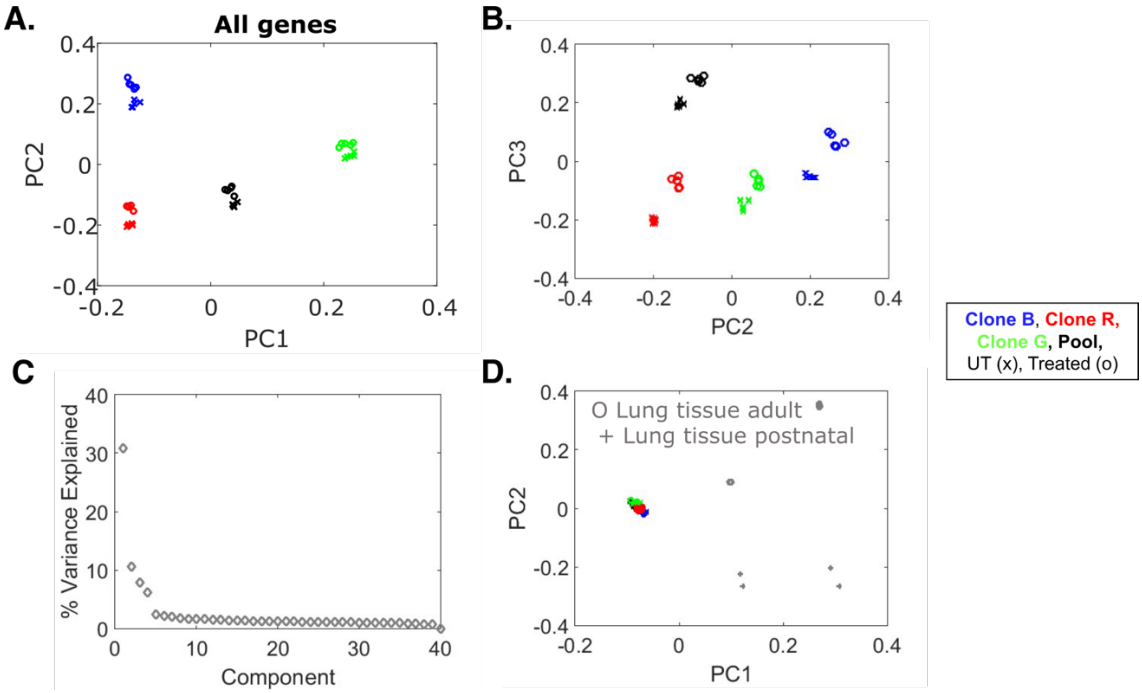

Figure 5.10. PCA show small but significant transcriptional variations between clones. A. *PCA of the UT and TNF-α treated samples of our clones B, R, G, and the pool, considering all genes.* ***B.*** *Additional dimensions of the PCA for our samples' transcriptomes.* ***C.*** *Fraction of variance explained per dimension.* ***D.*** *PCA of samples from our clones performed jointly with transcriptomic data from two other mouse tissues.*

Next, we decided to focus on how NF-κB controls the target gene expression in the three clonal populations and performed the PCA on 462 genes that have been previously established as differentially expressed upon TNF-α stimulation (Zambrano *et al*, 2016). Interestingly, now transcriptomes are clustered both by TNF-α treatment and by the population of origin (Figure 5.11A). Again, we found that such clusters were conserved on additional PCA dimensions (Figure 5.11B) and only few of them were needed to explain the transcriptional variability (Figure 5.11C). We then had a closer look at the differentially expressed genes upon TNF-α in each clone through volcano plots (Figure 5.11D). Interestingly, the number of upregulated genes correlates well with the strength of the NF-κB response and satisfies the relation B>R>G, the same order relation that we find for the average populational NF-κB response (Figure 5.4B). Overall, our results show that our clones have differently expressed NF-κB targets both before and after TNF-α stimulation.

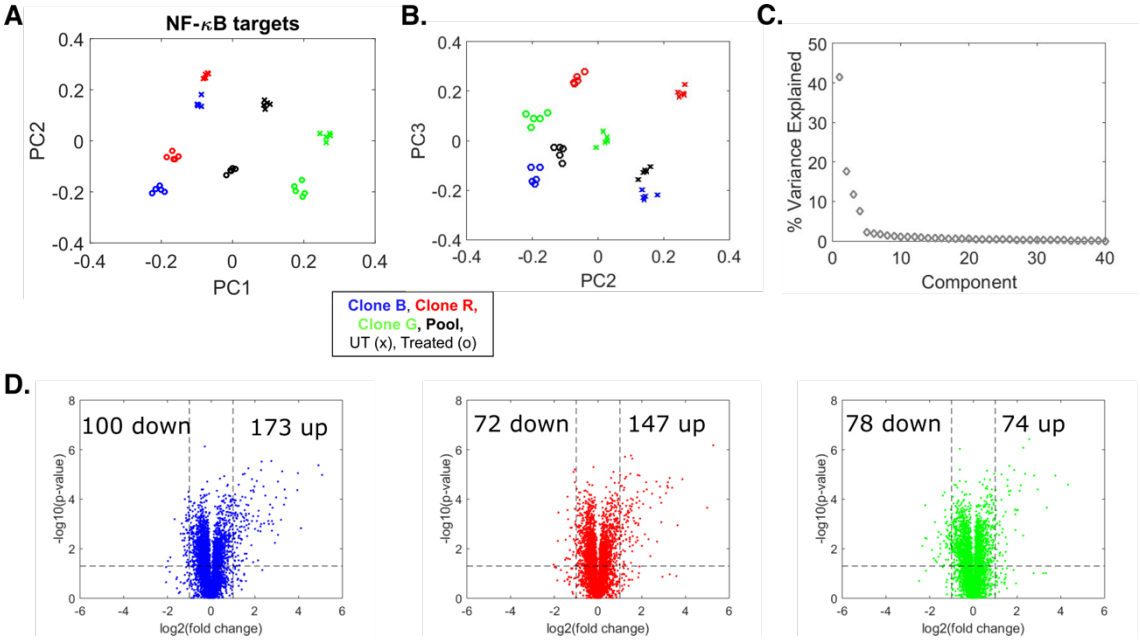

Figure 5.11. NF-κB target genes are differentially expressed in the clones before and after TNF-α stimulation. A. *PCA considering only expression levels of NF-κB target genes.* ***B.*** *Additional dimensions of the PCA when considering only NF-κB target genes.* ***C.*** *Fraction of variance explained per dimension.* ***D.*** *Volcano plots of gene expression upon TNF-α for clone B, R and G (each dot is a single gene).*

To gain insights on the identity of our cellular populations, we also looked at the differentially expressed genes between clones that were untreated. We find that the categories enriched are related with morphogenesis of different organs/tissues: epithelium, renal system, and skeletal system, to cite a few (Figure 5.12A). This suggests that our population of MEFs, which derives from an embryo, contains cells that presumably are already committed to different tissues or anatomical compartments. We also performed similar analysis on the upregulated genes upon TNF-α treatment; the recurrent categories included TNF-α response and innate immune responses as expected. However, we found different degrees of overlap with the different categories, suggesting that the clones activate slightly different transcriptional programs when treated with TNF-α (Figure 5.12B).

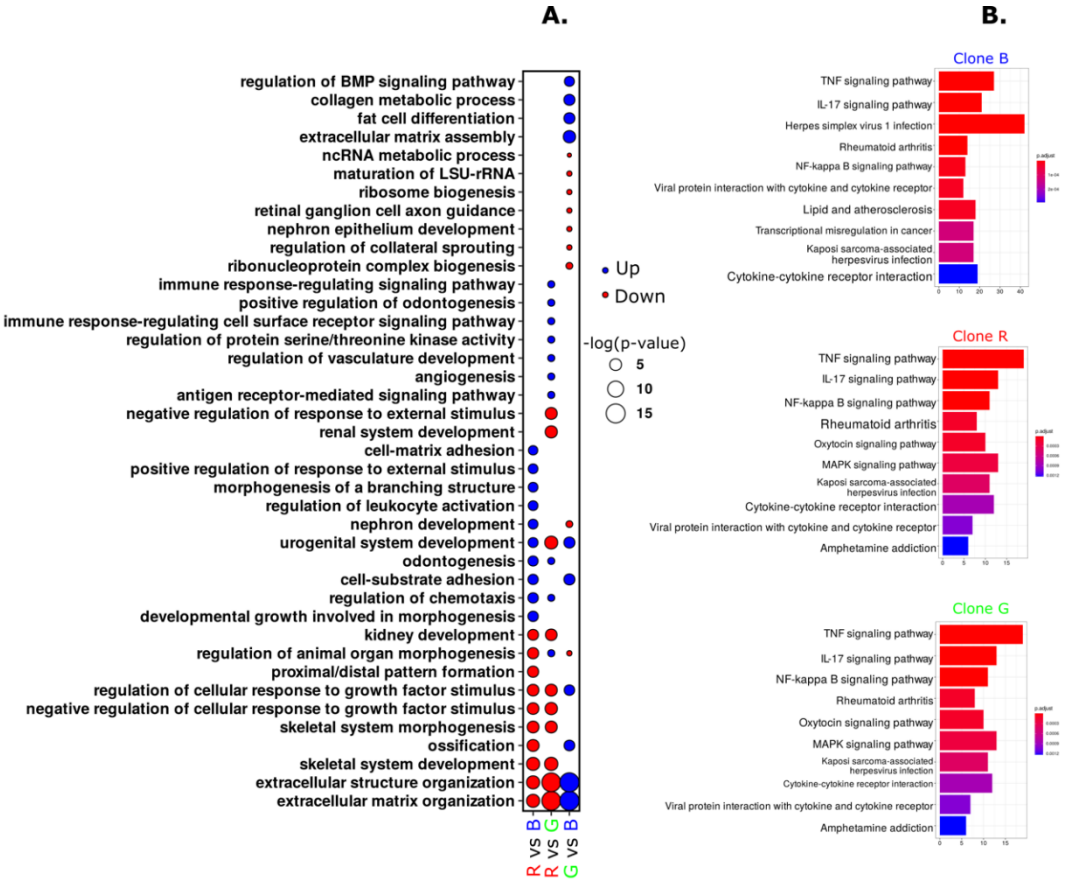

Figure 5.12. Pathway analysis show clones are committed to different tissues, and they have different transcriptional priorities upon TNF-α stimulation. A. *Gene ontology analysis of the differentially expressed genes between the untreated clonal populations.* ***B.*** *KEGG enriched pathways when looking at genes up/down regulated upon TNF-α in the indicated clones.*

Our results show that the clones differ mostly for their developmental identity, and that they differentially express targets of NF-κB. The strength of the NF-κB response is a key –but not the only one– determinant of NF-κB target gene expression levels upon TNF-α exposure.

5.1.4 Differences in the transcriptional levels of protein involved in NF-κB activation are predictive of the early response to inflammatory stimuli

Since the clearest phenotypic difference between our clonal populations is the dynamic response to TNF-α we decided to consider if there were transcriptional differences in elements involved in NF-κB regulation (as opposed to genes that are NF-κB targets). We used the *wikipathways* database to obtain a list of hundreds of genes involved in TNF-α signaling and performed a transcriptomic analysis on these genes. Unsupervised clustering shows our data cluster nicely across clones and treatments (Figure 5.13A). Interestingly, this hierarchical clustering identifies three groups of genes: a first group of genes that are highly expressed in clone G, a second one that are highly expressed in clone B, and a third one that are highly expressed in clone R (Figure 5.13A). We indeed find that also in the entire transcriptome the most common situation for any gene is to be more expressed in clone G (Figure 5.13B). Instead, when we only considered differentially expressed NF-κB targets we found that Clone B has the higher expression values as expected from its strongest NF-κB response (Figure 5.13C).

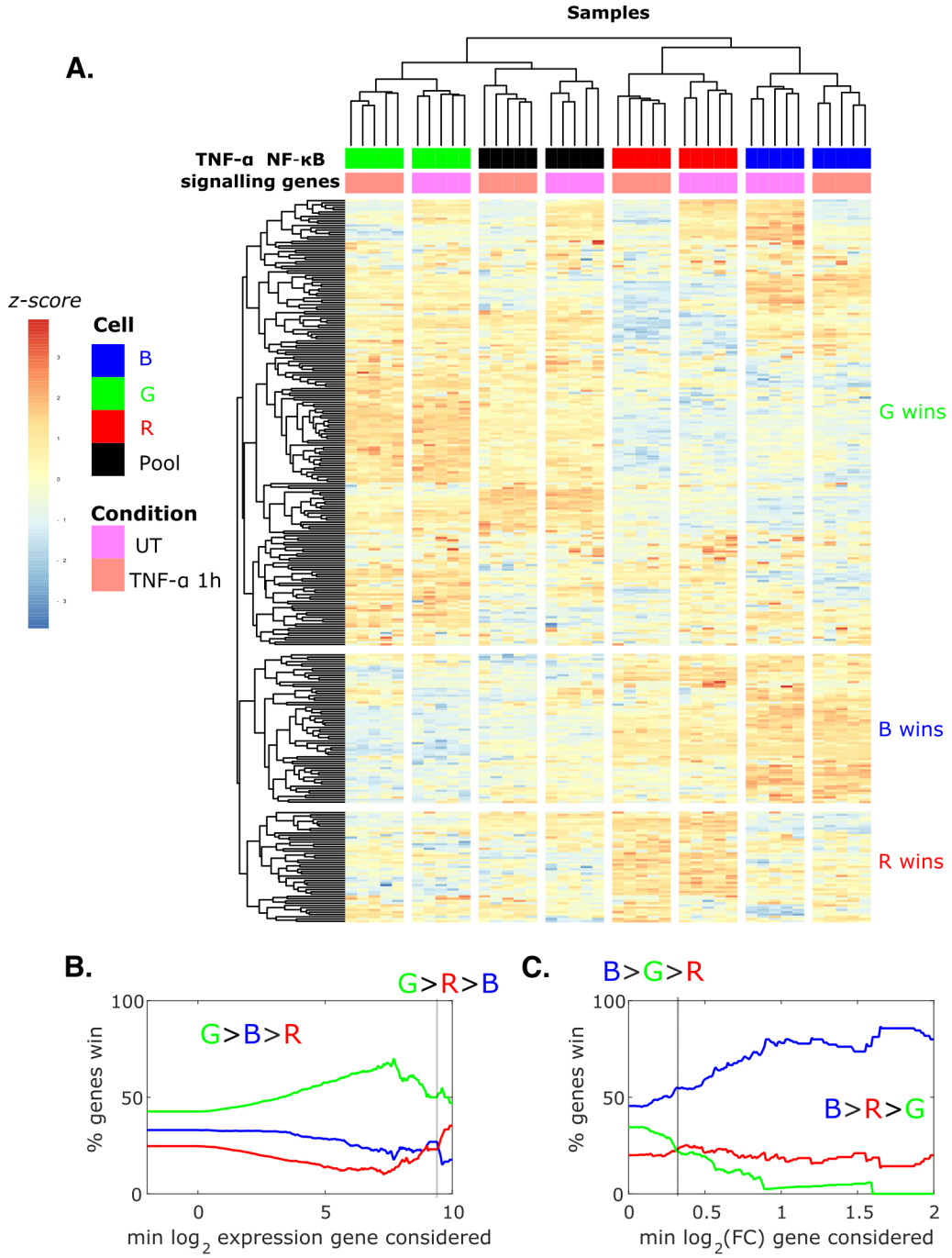

Figure 5.13. Clones have transcriptional differences in the elements of NF-κB signaling pathway A. *Hierarchical clustering of the genes from the "TNF-α NF-κB signaling pathway (Mus musculus)" list from wikipathways.* ***B.*** *Fraction of genes from untreated samples that are more expressed in B, R and G for different thresholds for the minimum expression considered. The predominant ordinal pattern of expression in each part of the graph is shown and the grey vertical line indicates the point where there is a change.* ***C.*** *Same as in B but now considering expression levels upon TNF-α treatment and for different thresholds for the minimum fold-change considered.*

Although this analysis indicates that the expression level of genes in the NF-κB regulatory circuit differs across our populations, it provides limited insights on why cells respond with different strengths and with notably different dynamics to TNF-α. This is also partly due to the fact that the elements in the regulatory circuit provided by *wikipathways* are understood in quite a broad sense, since the list include epigenetic regulators such as histone deacetylases or even the gene encoding for ribosomal and proteasomal proteins, resulting in an extremely complex scheme. Therefore, we decided to take a closer look into subsets of genes directly involved in NF-κB activation and dynamic control. We combined online databases and the literature (DeFelice *et al*, 2019; Hayden & Ghosh, 2008; Lee *et al*, 2016) to create a list of genes that might play a role in the strength of the nuclear localization of NF-κB upon TNF-α. Such list includes receptors, signal transducers and kinases and we labelled it as "TNF-α to NF-κB". We hypothesized that the level of expression of genes in the "TNF-α to NF-κB" list would affect the strength of NF-κB response in our clonal populations. Although the proportionality between transcript and protein amounts is not perfect nor constant (Schwanhäusser *et al*, 2011), for each gene we expect the proportionality to be very similar in each of our clonal populations. Indeed, when we checked the levels of expression of p65 (RelA) it correlated well with the protein amount (computed as fluorescent signal intensity) across the clones (Figure 5.14A).

We then focused on the basal levels of expression of the "TNF-α to NF-κB" genes in untreated samples. Although there is not a clear and constant order relation between the expression of such genes, we focused on a relatively simple quantifier to have a global view of their levels across the populations: the average relative expression levels. We define the average relative expression as the expression level divided by the average expression level across the clones B, R and G. By definition, for a given gene, the sum of their relative expression levels in clones B, R and G is always 3. For a given gene list we can calculate the relative expression value of each gene and then calculate the average value of the relative expression for each population, and we denoted them as <B>, <R> and <G>.

We found that the variation in average relative expression levels of "TNF-α to NF-κB" genes is moderate among clonal populations, and only in exceptional cases goes beyond 0.5 or 1.5 times the average expression of each gene (Figure 5.14B). We find that such average expression values follow the order relation B>R>G, which indicates that on average these genes are more expressed in B than in R, and in R than in G (Figure 5.14B). As the absolute differences seem small, we evaluated the statistical probability of getting the order relation with such differences or larger.

Before detailing the procedure, we can point out that for any given three numbers there are six possible order relations. Hence average relative expression levels of the three clones, that we denote <R>, <G> and <B>, can adopt six different order relations. Their sum is equal to three, so we can always present each combination of three values with just two of them, we chose here the R>-<B> plane. Each order determines a region in the 3-coordinate space <R><G><B>, each two regions are separated by a plane which intersects with the <R>-<B> plane with a straight line (Figure 5.14C). Hence, the <R>-<B> plane is divided in six sections that determine 6 possible order relations between <R><G><B>.

Bearing all this in mind, to assess the statistical probability of observing an order relation with the average relative expression values obtained, we created 20000 random gene lists with the same size and similar expression levels and computed the probability of different average relative expression levels projected on the <R>-<B> plane. We found that for the B>R>G order with such a different on average relative expression the p-value is smaller than 0.005 (Figure 5.14C) and concluded that clone B has a significantly higher basal expression of genes in the "TNF-α to NF-κB" list and this correlates with its higher NF-κB response to TNF-α (Figure 5.4B).

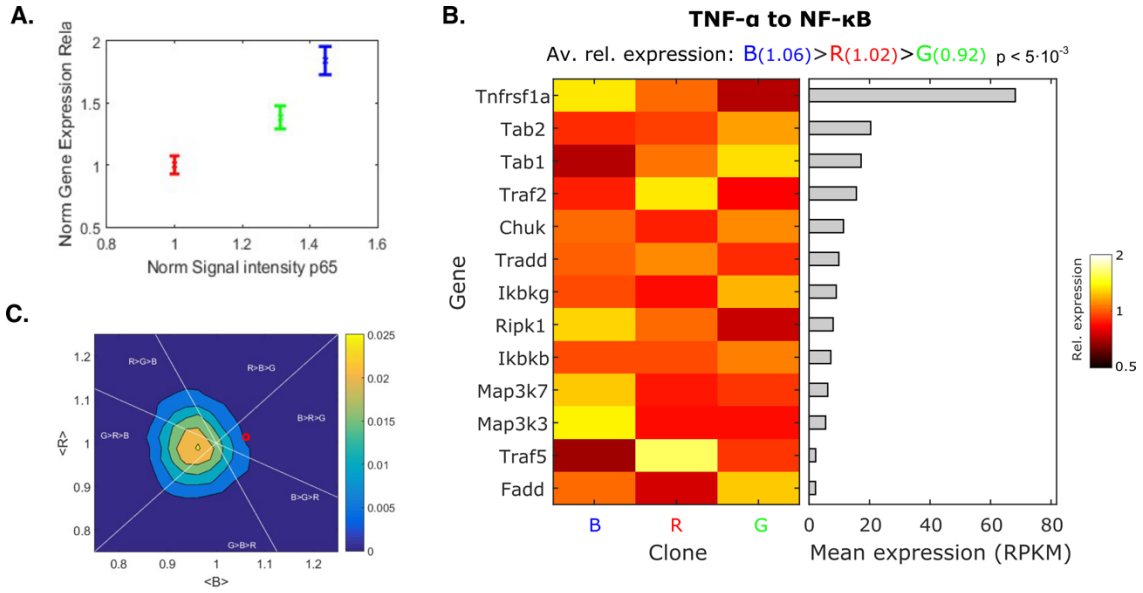

Figure 5.14. Gene expression of the TNF-α to NF-κB list predicts the TNF-α response. ***A.*** *Expression of RelA gene plotted against the fluorescent intensity of the protein in each clone.* ***B.*** *Relative expression levels (normalized in each gene by the average expression across clones) of genes encoding for proteins involved in "TNF-α to NF-κB" list (left) and average expression levels for each gene (right). The average relative expression of each clonal population and their order relation is shown on top.* ***C.*** *Probability distribution of average relative expression of genes for the clone B and the clone R (<R> and <B>, respectively) in datasets with features similar to that of the "TNF-α to NF-κB" list. The red circle represents the value of the average relative expression in the "TNF-α to NF-κB" list. Straight lines delimitate the regions for which different order relations of average relative expression values are satisfied.*

Since our approach correctly predicted the correlation between strength of the response and expression levels of the genes involved in TNF-α signal transduction, we asked if it could also predict the relative clonal differences in the response to a different inflammatory stimulus. We focused on IL-1β, a cytokine that is known to activate NF-κB through a pathway only partially overlapping with that of TNF-α, and characterized by its own regulatory mechanisms and dynamical features (DeFelice *et al*, 2019; Martin *et al*, 2020). We elaborated a list of "IL-1β to NF-κB" genes that now includes new genes such as *Ilr1r1*, the gene encoding the receptor, and *MyD88* (Figure 5.15A). In this list, we found again different levels of expression that typically do not exceed 2-fold (Figure 5.15A). Interestingly, in this case the order relation of the average expression was different: B>G>R. By reproducing the same analysis used before, we find that the order relation B>G>R is infrequent in random gene lists with similar features, with p<0.015 (Figure 5.15B).

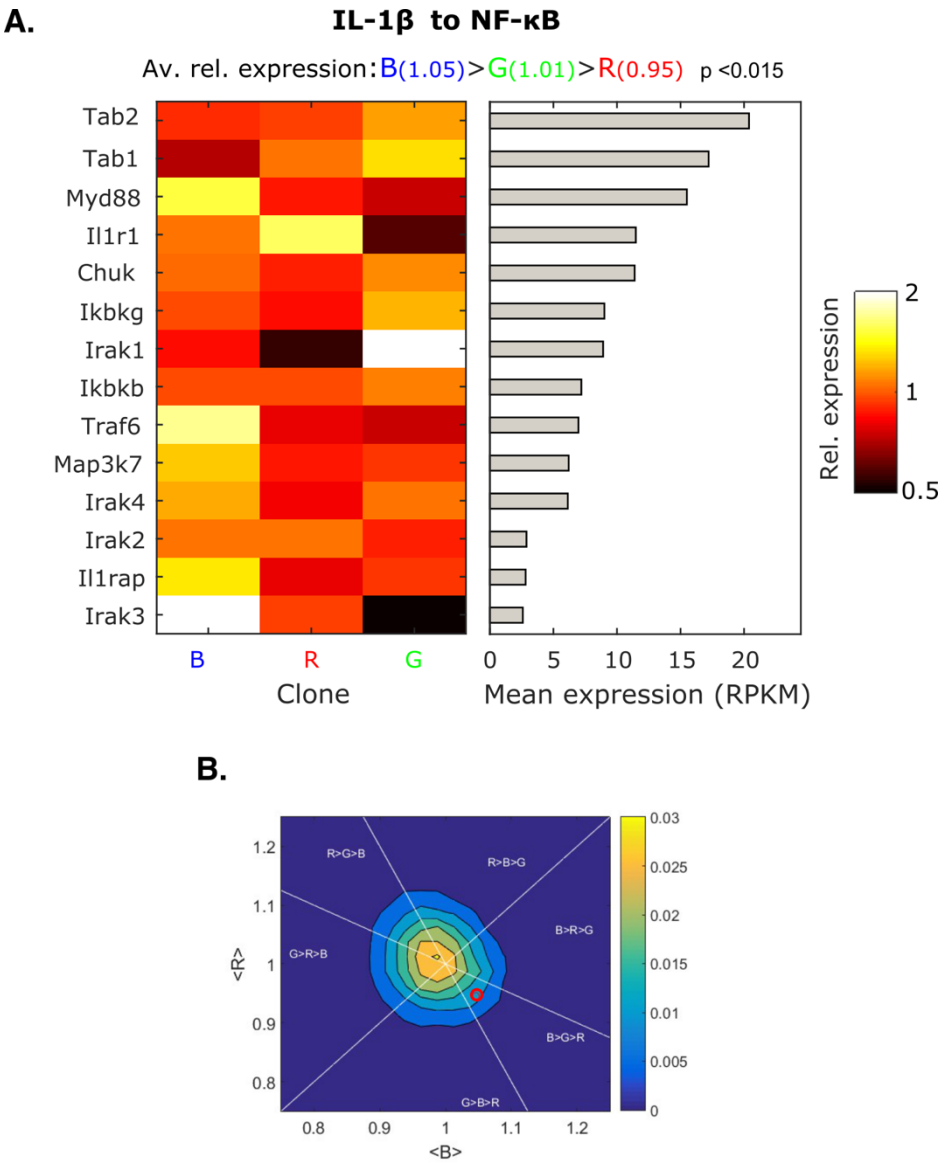

Figure 5.15. The gene expression of IL-1β to NF-κB list predicts differences in the order relation of clones in comparison to that of TNF-α ***A.*** *Relative expression levels (normalized in each gene by the average expression across clones) of genes encoding for proteins involved in "IL-1β to NF-κB" (left) and average expression levels for each gene (right). The average relative expression of each clonal population and their order relation is shown on top.* ***B.*** *Probability distribution of average relative expression of genes for the clone B and the clone R in datasets with features similar to that of the "IL-1β to NF-κB" list. The red circle represents the value found for "IL-1β to NF-κB" gene set. Straight lines delimitate the regions for which different order relations of average relative expression values are satisfied.*

We then performed live cell imaging of the clones upon 100 ng/ml IL-1β. All clones respond (Figure 5.16A), and in particular now clone G has a stronger response than to TNF-α; notably, the average NF-κB response reflects the order relation B>G>R (Figure 5.16B), as predicted. Our single-cell quantifications also show clear differences that indicate that clone G displays overall a stronger response than clone

R. However, clone B is the one with a higher response and a much higher AUC (Figure 5.16C).

Finally, upon IL-1β we find that the cells' oscillatory phenotype is also different with respect to TNF-α: more cells of clone G have at least two peaks (Figure 5.16D) and an oscillatory period at T=1.5h, similar to clone R (Figure 5.16E). Clone B remains the one with a less oscillatory phenotype (Figure 5.16D), suggesting that this behavior might be related with downstream regulators of NF-κB activity, an idea that we explore next.

Taken together, our data shows that the expression levels of proteins in two different signaling cascades upstream of NF-κB predict which cells respond more or less intensely to which inflammatory stimulus.

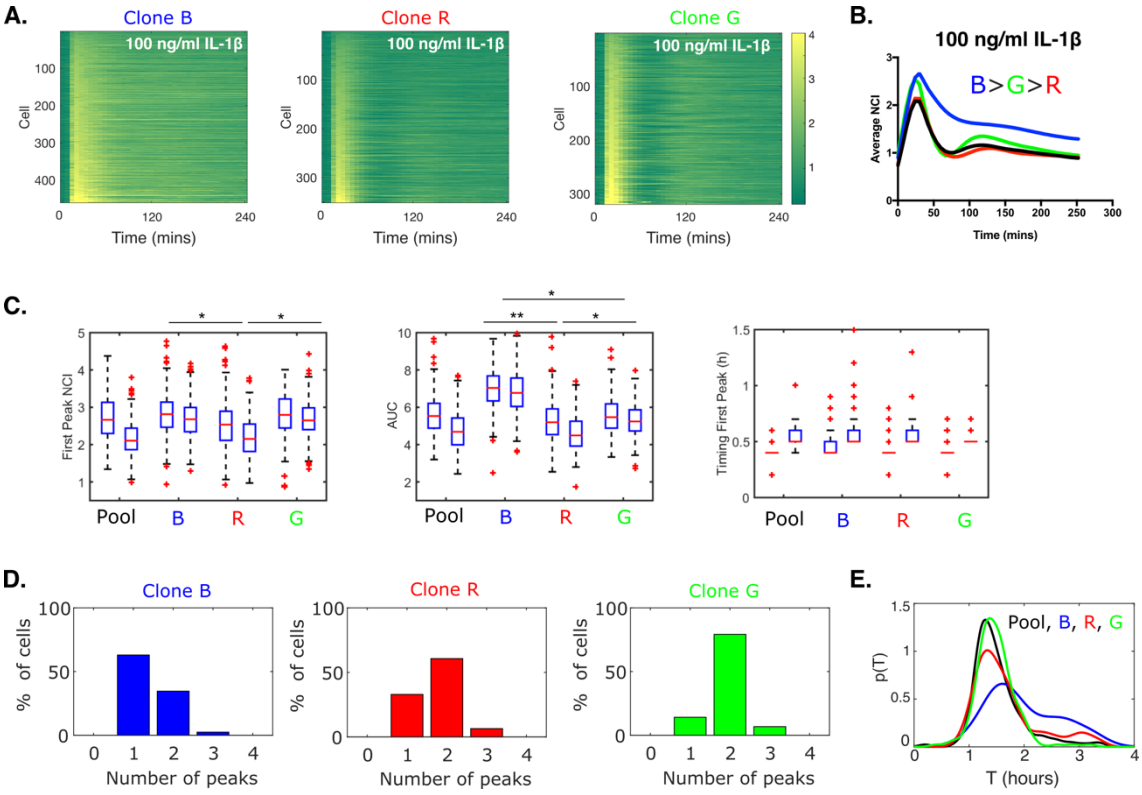

Figure 5.16. Experiments upon IL-1β stimulation confirms the predictions. A. *Dynamic heatmap of the responses of clone B, R and G to 100 ng/ml IL-1β.* ***B.*** *Average NF-κB response for the three clones to IL-1β stimulation.* ***C.*** *The boxplots of the dynamical features of the response to IL-1β in two biological replicates: value of the first peak, area under the curve (AUC) and the timing of the first peak.* ***D.*** *Fraction of the cells having 1, 2 or 3 oscillatory peaks on each of the populations considered upon 4 hours of IL-1β stimulation.* ***E.*** *Periods of the oscillations computed as the inter-peak time for each population. *p<10^{-2}, ** p<10^{-3}, *** p<10^{-4}, multiple comparisons through Kruskal-Wallis.*

5.1.5 Differences in the expression levels of the NF-κB feedbacks underpin distinct dynamics in the clonal populations

Beyond differences within the first 30 minutes, our clonal populations also show differences at later time points. For instance, clone B has more persistent nuclear localization of NF-κB whereas clone R has a sharp and more oscillatory dynamics. Therefore, we decided to investigate whether transcriptomic data could also shed light on the origin of such differences.

It is well established that NF-κB nuclear localization dynamics is tightly regulated by a system of negative feedbacks such as the inhibitors IκBα, IκBβ and IκBε that keep NF-κB in the cytosol (Hoffmann *et al*, 2002; Paszek *et al*, 2010) and the protein A20 that interferes with stimulus-mediated IκB degradation (Ashall *et al*, 2009; Son *et al*, 2021b); all of them are under the transcriptional control of NF-κB (Figure 5.17A).

To check if the methodology used to predict the relative differences in the early response to TNF-α across clones could also be informative about the subsequent dynamical responses, we elaborated a list of "NF-κB negative feedbacks". We find that these genes show relatively low expression in our untreated samples (Figure 5.17B, left) but they are highly expressed after 1 hour of TNF-α activation (Figure 5.17B, right). Indeed, these are among the genes that respond relatively quickly to the stimulation (Zambrano *et al*, 2016). Overall, we found that there are moderate differences in the expression of "NF-κB negative feedbacks" genes across the clones (Figure 5.17B). When considering the average relative expression levels, we find significant order relation of R>G>B for our untreated samples (Figure 5.17C, left) and highly significant order relation of R>B>G for our TNF-α treated samples (Figure 5.17C, right). These correlate well with the sharpness of the response of Clone R that we observed experimentally. Importantly, we are considering expression level as a proxy of protein levels and hence of the strength of the negative feedbacks, this is the reason why we focus on absolute levels and not in fold-change induction. We also showed that the expression levels of IκBα and IκBε are indeed higher in Clone R relative to Clone B in a separate plot (Figure 5.17D) and RT-qPCR results confirm that mRNA levels of negative feedbacks differ between the clones as shown for the RNA-seq data (Figure 5.17E).

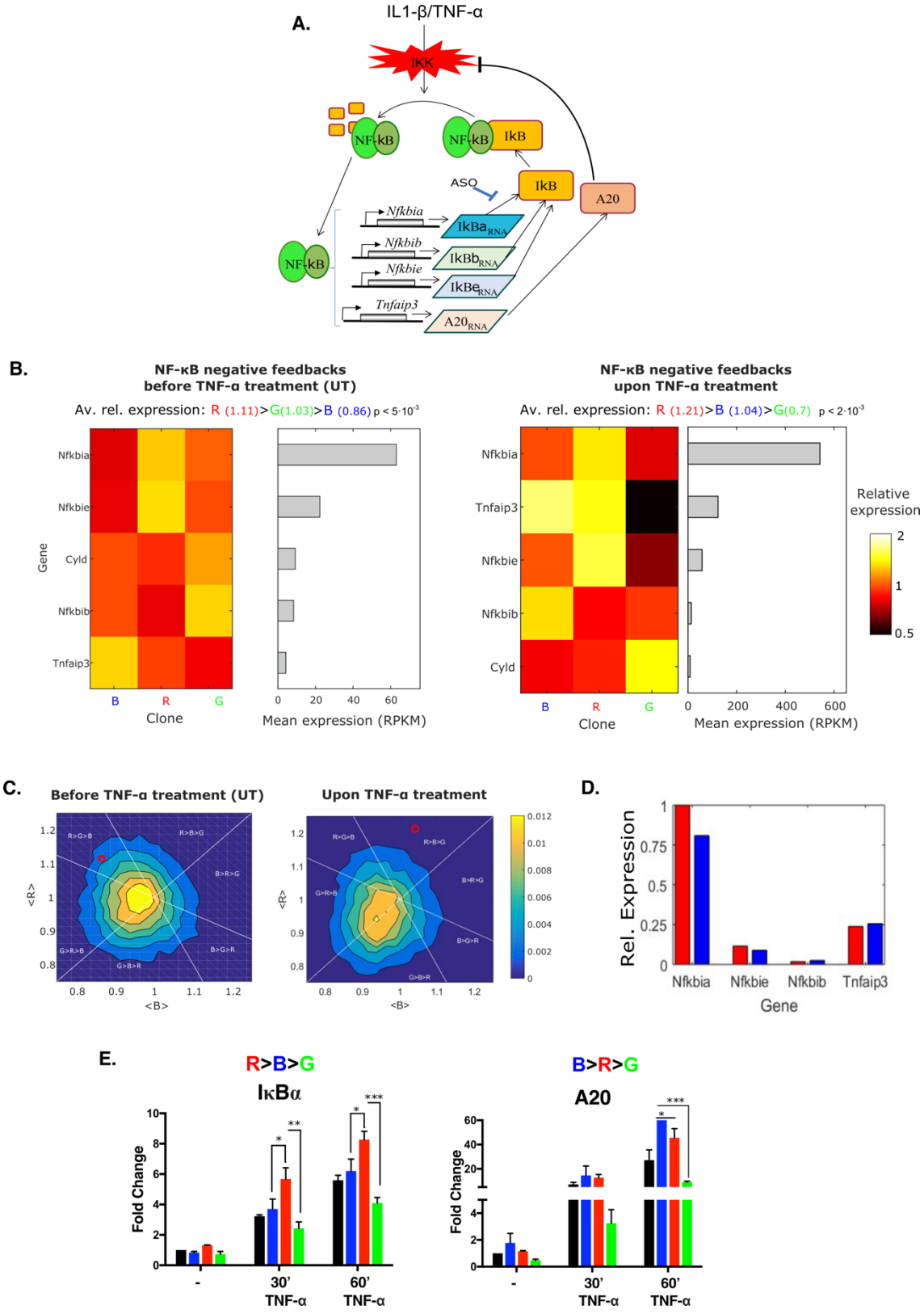

Figure 5.17. Clones differ in expression levels of NF-κB negative feedbacks. A. *Scheme of the main negative feedback regulators acting on NF-κB.* ***B.*** *Relative and average expression levels (normalized by the average expression across clonal populations) of genes of the "NF-κB negative feedbacks" list in untreated (left) or TNF-α treated samples (right). The order relation of the average relative expression levels is shown on top.* ***C.*** *Probability distribution of*

the average relative expression values of genes for clone B and clone R in datasets with features similar to that of "NF-κB negative feedbacks" list in untreated (left) or TNF-α treated samples (right). The red circle represents the values found for the "NF-κB negative feedbacks" list. Straight lines delimitate the regions for which different order relations of average relative expression values are observed. ***D.*** *Expressions of elements of the NF-κB negative feedbacks in clones B and R by RNA-seq data, relative to the expression level of IκBα for clone R.* ***E.*** *Fold change expression levels of IκBα and A20 for each cell population at different timepoints by RT-qPCR. Error bars show the standard deviation of replicates. *$p<10^{-2}$, ** $p<10^{-3}$, *** $p<10^{-4}$ comparisons through 2-way ANOVA.*

The negative feedback loops of NF-κB system have actually been extensively modelled (Hoffmann *et al*, 2002; Nelson *et al*, 2004; Paszek *et al*, 2010). Hence, mathematical modelling could provide us further insights on whether transcriptional differences in the "NF-κB negative feedbacks" are enough to explain the differences observed in the sharpness of the response across clones. Thus, we built a new mathematical model that is based on a simpler version available in our laboratory (Zambrano *et al,* 2016).

In our new model, we included the inhibitors IκBβ and IκBε in addition to IκBα and A20 feedbacks that were already included in the previous model. The new model contains the original set of parameters, and the new parameters are constrained in such a way to mimic the relative expression levels of the feedbacks in clone R. Then we took the clone R parameter set and modified it to obtain a new parameter set for clone B, so that the relation between the expression of the inhibitors between the clones are preserved. As expression levels of NF-κB between the clones was slightly different (Figure 5.14A) we also varied the NF-κB levels according to the experimentally observed ones. Interestingly, these moderate differences already lead to a change in the dynamics from sharp in the simulation of R to persistent in that of B, qualitatively similar to the one observed experimentally (Figure 5.18A).

Since our modelling result could be due to our particular selection of parameters, we performed simulations for randomly generated pairs of parameter sets that satisfied certain constraints (Figure 5.18B). Our constraints were the constant relative expression of the inhibitors within the Clone R simulations (Figure 5.18C) and between the clones (Figure 5.18D) observed experimentally. As a result of this procedure, we found moderate differences in the timing and the strength of the response (Figure 5.18E) in simulations performed with each element of the pair, whereas there is a more drastic decrease of the sharpness for clone B, as revealed by the AUC (Figure 5.18E). This mirrors the sharper NF-κB nuclear localization dynamics that we found experimentally for clone R with respect to B (Figure 5.4B,

5.16B) and indicates that the moderate transcriptional differences observed have a clear impact in the dynamics and might be the key driver of the differences observed.

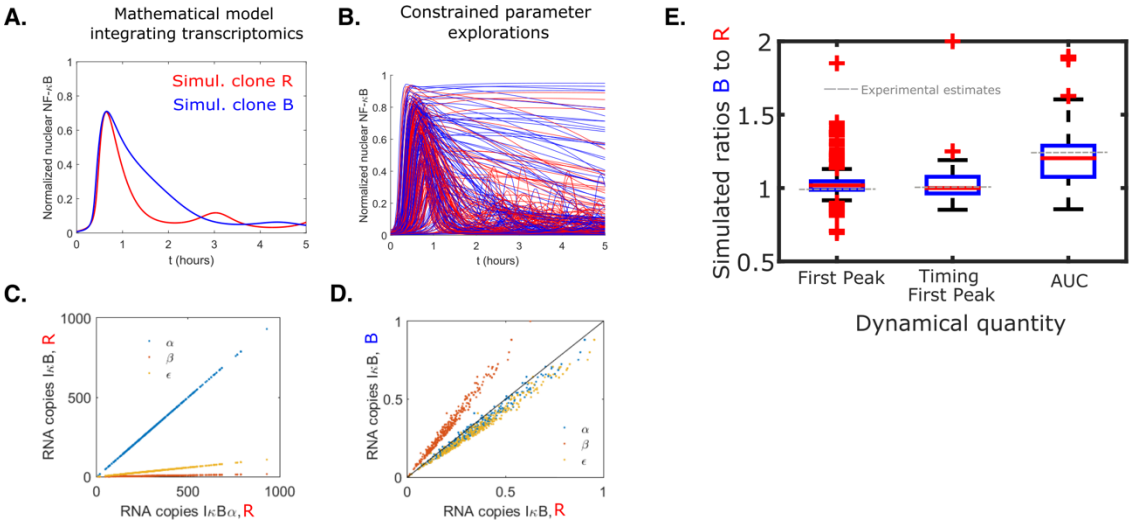

Figure 5.18. Mathematical modelling recapitulates experimental observations A. *Numerical simulation of clone R (red line) and transcriptionally constrained simulation of clone B (blue line).* ***B.*** *Example of numerical simulations of randomly generated parameters of clone B and clone R where the experimental ratios of expression of the inhibitors are kept constant.* ***C.*** *The ratios between the levels of expression of the inhibitors within the simulations of clone R. Each dot corresponds to a simulation.* ***D.*** *The ratios between values observed in clone B and clone R. Each dot corresponds to a simulation.* ***E.*** *Ratios between values observed for constrained simulations of clone B and R for the timing and value of the first peak and area under the curve.*

To confirm our bioinformatic and modelling analysis, we set out to experimentally test the effect of modulating the NF-κB negative feedback levels in the dynamic response to TNF-α. We focused on the key inhibitor IκBα, whose absence gives rise to a non-oscillatory phenotype (Hoffmann *et al*, 2002; Cheng *et al*, 2021).

To modulate the mRNA levels of IκBα we took advantage of antisense oligonucleotide (ASO) technology. The single-stranded synthetic nucleic acid analogs (2'-deoxy-2'-fluoro-β-d-arabino nucleic acid, FANA) were designed to be self-delivered to the cells and target the mRNA of interest with high affinity. They induce the mRNA cleavage by RNAseH to reduce the synthesis of the encoded protein (Figure 5.17A). We first tested the ASOs on our pool. We pre-treated the cells with a final concentration of 5 μM ASO for 24 hours prior to imaging. The internalization of the ASOs (both scrambled and IκBα targeting) was visible as they get stained by Hoechst (Figure 5.19A). We found that ASO treatment did not change the strength of the TNF-α response whereas the area under the curve was much higher for ASO treated cells

indicating the transcriptional disruption of the IκBα negative feedback. We also checked the effect of ASOs on the mRNA levels and found that they led to moderate but significant decrease on the expression of IκBα (Figure 5.19C).

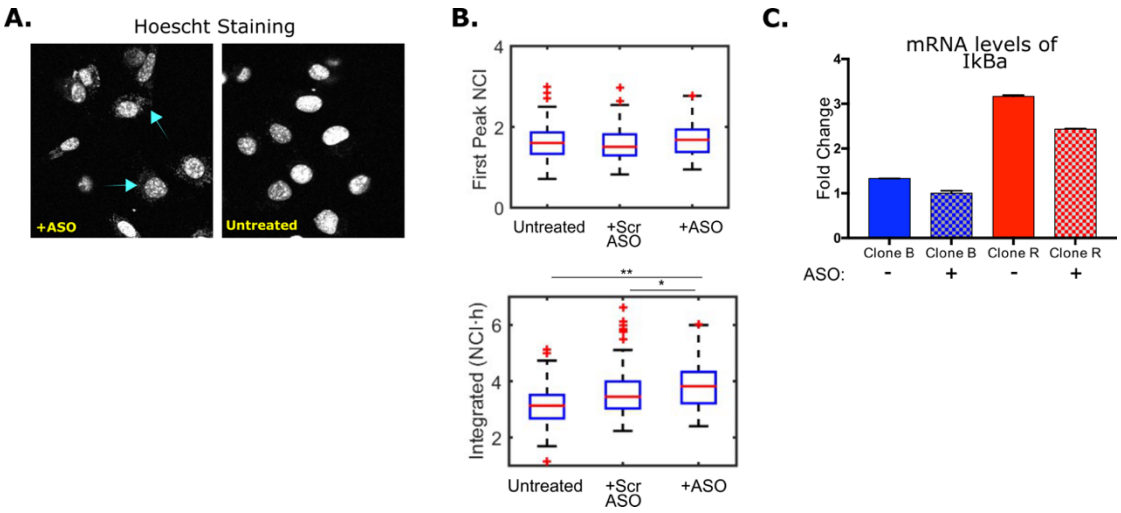

Figure 5.19. IκBα targeting ASOs get internalized and disrupt the gene expression ***A.*** *Representative images of the Hoechst channel showing (blue arrows) internalization of the ASOs after 24 hours.* ***B.*** *Effect of the scrambled and IκBα targeting ASOs on the value of first peak and AUC of the pool population upon TNF-α stimulation.* ***C.*** *Relative mRNA levels of IκBα after 24 hours of ASO treatment. Error bars show the standard deviation of replicates.*
** $p<10^{-2}$, ** $p<10^{-3}$, *** $p<10^{-4}$, multiple comparisons through Kruskal-Wallis.*

We then treated Clone B and R with IκBα targeting ASOs. We indeed observed that, upon TNF-α, the response of both clone B (Figure 5.20A, top) and clone R (Figure 5.20A, bottom) was characterized by a more persistent NF-κB nuclear localization, indicating that partial transcriptional disruption of the IκBα negative feedback is enough to produce a qualitative change in the dynamics. Our more detailed quantification of the dynamics shows that the ASO treatment does not affect the maximum value of the NF-κB response (Figure 5.20B), as expected. However, the area under the curve increases for both clones, and in particular for clone R, so that the AUC value of clone R is much more similar to that of clone B response (Figure 5.20B).

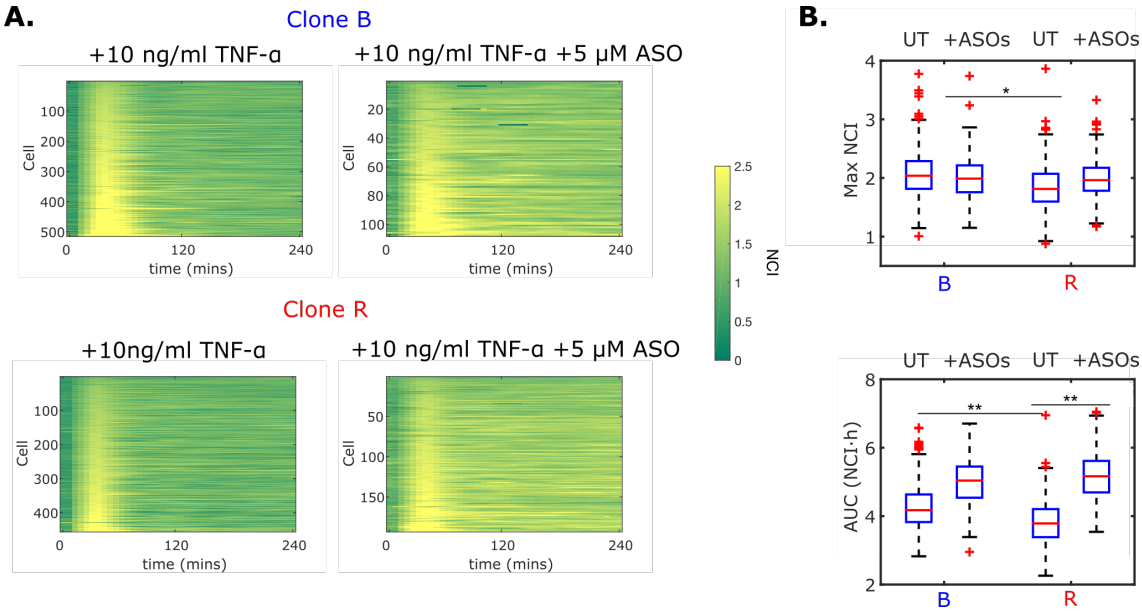

Figure 5.20. ASO treated clones show persistent nuclear localization of NF-κB upon TNF-α stimulation. A. *Representative dynamic heatmaps of clone B (top) and clone R (bottom) upon TNF-α for both untreated and ASO-treated cells.* ***B.*** *Quantification of the maximum response and AUC for untreated and ASO-treated cells upon TNF-α. *$p<10^{-2}$, ** $p<10^{-3}$, *** $p<10^{-4}$, multiple comparisons through Kruskal-Wallis.*

Overall, we have shown how the expression levels of the negative feedbacks correlate with the differences of NF-κB dynamics observed across our clones, and especially with the observed sharp versus persistent NF-κB response. Our experiment-driven simulations also indicate that the transcription levels of the NF-κB negative feedbacks are key determinants of the distinct dynamics observed in our clonal populations. Finally, our experiments with ASOs show how even a mild targeted modulation of the expression of IκBα can distinctly alter the dynamics of clone R to resemble that of clone B, and therefore to reprogram it from a sharper (and oscillatory) to a persistent dynamical phenotype of NF-κB activation.

5.2 The role of spatial information on NF-κB dynamics

5.2.1 NF-κB spatial activation heterogeneity can be observed in tissues

Immune cells are the key players to orchestrate immune response upon pathogen exposure. They communicate danger signals to neighboring cells through cytokines (Nourshargh & Alon, 2014). The length scale of such communication is an important parameter to know especially relating to the size of the organ. When the communication length is equal or higher to the size of an organ, homogenous cytokine fields are achieved (Perona-Wright *et al*, 2010b). On the other hand, when the length scale of communication is shorter than the organ size it results in localized cytokine niches (Pangault *et al*, 2010). Cells located in such niches are exposed to cytokines more than other cells of tissue. Thus, we speculated that cytokine concentration heterogeneity in a tissue could translate into variability of NF-κB activation.

We first wondered whether the emergence of cytokine niches can result in heterogenous distribution of NF-κB activation within a tissue. To see whether we can capture such spatially inhomogeneous NF-κB activation patterns in liver tissue (as a simple to retrieve and well-structured tissue) in a simple experimental method we performed TNF-α injection in wild-type mice and decided to select time points that are relatively soon after the injection. In this way we aimed to observe inhomogeneous patterns of NF-κB temporal activation starting from cells that are near portal vein. We sacrificed mice 10, 20, 30 and 60 minutes after the injection and checked the activation status of liver tissue. To do so, we setup an immunohistochemistry protocol for NF-κB staining in liver. We found an overall activation of the liver tissue as early as 30 minutes, but we were not able to capture any heterogeneity in earlier time points (Figure 5.21A). This could be due to fast distribution of TNF-α upon injection in the liver tissue. However, this experiment shows that activation of NF-κB can clearly be observed by liver immunohistochemistry.

Then we decided to focus on a different situation where inhomogeneous NF-κB activation was reported. Hepatocellular carcinoma (HCC) carrying mice show heterogeneous NF-κB activation in a cluster of cells in liver tissue (Pikarsky *et al*, 2004). Therefore, taking advantage of our immunohistochemistry setup, we performed NF-κB staining on liver sections of HCC mice. We confirmed such activated cell clusters (Figure 5.21B, yellow circle) and also found individually activated cells

(Figure 5.21B, yellow arrows) within the liver of HCC carrying mice. This allowed us to show very clear inhomogeneous activation of NF-κB in this tissue.

We then reasoned other types of liver damage could also result in heterogeneity of NF-κB activation. In general, it is known that tissue-resident immune cells promote infiltration of leukocytes by secretion of inflammatory cytokines when there is a tissue damage (Szekanecz & Koch, 2017). Acetaminophen (APAP) intoxication has been previously shown as an acute liver damage model that recruits leukocytes to the damage site starting from day 1 to day 7 post injury (Ferrara *et al*, 2020). We used this model to check activation status of NF-κB. As leukocyte infiltration has been shown to start already at day 1 post APAP intoxication we selected this timepoint to perform immunohistochemistry. We found individual activated cells (Figure 5.21C, yellow arrows) as well as activated cell clusters (Figure 5.21C, yellow circle). Hence, we showed also in these settings that activated cells can coexist with non-activated cells in liver tissue.

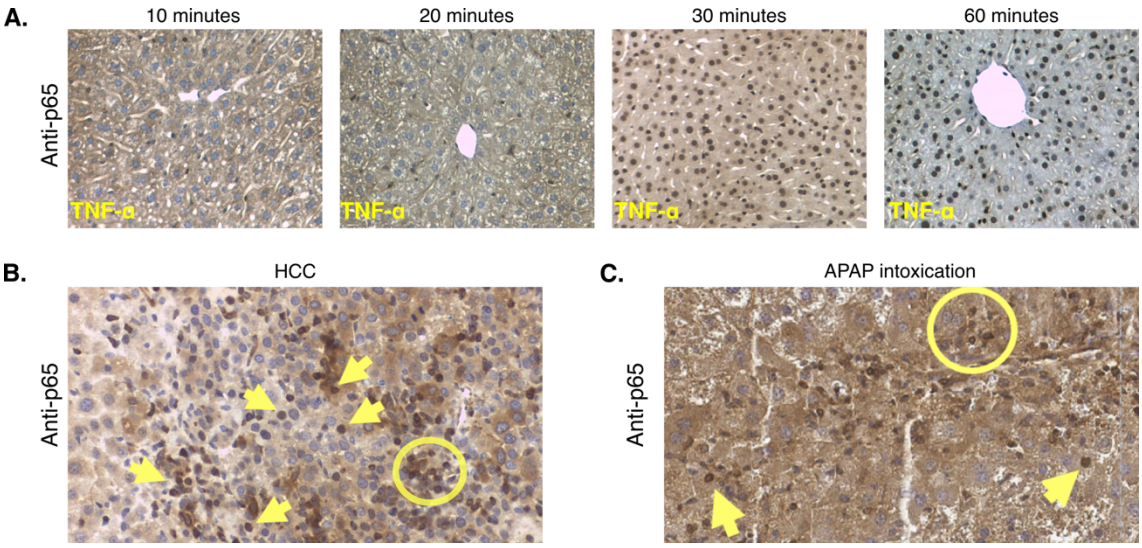

Figure 5.21. NF-κB spatial activation heterogeneity can be observed in vivo. A. *Immunohistochemistry against p65 in wild-type mice liver sections that were TNF-α injected and sacrificed at given timepoints**. B.*** *Immunohistochemistry against p65 in liver sections of hepatocellular carcinoma (HCC) carrying mice **C.** Immunohistochemistry against p65 in liver tissue damaged by APAP injection. Activated individual cells are indicated by yellow arrows and clusters of activated cells are shown in circles.*

Overall, we found that heterogeneity in activation of NF-κB could be observed in compromised liver tissue such as the case of hepatocellular carcinoma and acute tissue injury. These proof-of-principle in vivo experiments show that the location of cells in tissue has an important role in NF-κB activation, as clusters of NF-κB activated

cells can coexist with tissue regions where there is no activation. In principle, an activated cell could secrete NF-κB activating cytokines to communicate a danger signal to neighboring cells also in healthy tissue. The clusters of activated cells that we observed suggest the existence of cytokine niches that can translate into variability of NF-κB activation in tissue. However, it is still unclear how far the length scale of this communication goes or whether it can be modulated. We are also far from understanding how the activation of these cells occur over time because static immunohistochemistry images provide only spatial information about NF-κB activation. In short, how being a neighbor of an activated and/or cytokine secreting cell could affect NF-κB in neighboring cells in space and time is experimentally challenging to characterize in vivo. However, as previously argued in this thesis, NF-κB can only be fully understood using a dynamic point of view. Hence, we decided to use in vitro approaches to characterize the key features of NF-κB dynamics in cytokine niches.

5.2.2 NF-κB spatial activation heterogeneity can be imaged in vitro

We next checked if NF-κB activation heterogeneity could be captured in an in vitro 2D culture system. Biophysical estimations show that a cytokine/chemokine secreting cell communicates the signal to its neighboring cells via generation of a concentration gradient within the cytokine niche (Francis & Palsson, 1997), (Figure 5.22A). It has been also shown that these concentration gradients are shaped by certain factors such as diffusion rate of cytokines and consumption by surrounding cells (Oyler-Yaniv *et al*, 2017). Such cytokine gradients could result in gradient activation of NF-κB, but this has never been observed or characterized in traditional 2D culture systems. It is also a common belief that the fast diffusion of cytokines like TNF-α does not allow to observe differences in 2D cultures, where molecules can freely diffuse in the culture medium above the cells. TNF-α has a diffusion coefficient of the order of magnitude D=30 $\mu m^2/s$ (Francis & Palsson, 1997) and it would on average travel a distance of the order of 1 cell size in few seconds.

We performed a simple experiment to demonstrate the opposite: that when a cytokine is secreted in a certain location in a 2D culture, we can observe inhomogeneous activation of NF-κB. To do so, we simply gave a drop of TNF-α only to one corner of the cell culture well (Figure 5.22B) and we checked the activation strength of our MEFs depending on their distance to that corner. We found that cells in proximity to the TNF-α corner respond fast and strongly compared to cells in the

opposite corner, which respond many minutes later and with less strength (Figure 5.22C, D, E).

As an alternative model, closer to the situation of a cytokine-secreting cell that we are interested in, we used agarose beads to immobilize TNF-α in order to have a better control on its localization. These beads have been used in the literature as an attraction source as they create a concentration gradient by diffusion of growth factors over time (Bonanomi *et al*, 2012). We soaked these beads in TNF-α and added them to the medium of our MEFs to generate TNF-α gradients around them. The addition of beads to the medium led them to settle on top of our cells within minutes and this allowed us to locate them by their shadow in transmitted light (Figure 5.22F, outlined with yellow dashes). We immediately observed strong activation for cells under the beads (Figure 5.22F). By calculating activation of cells at T=0 (hence right after bead addition to medium) we found cells that are 1-2 cell away from the bead showed distance-dependent activation proving the gradient formation around the bead (Figure 5.22G). Following the beads for long live imaging experiments was not possible due to their lack of stability.

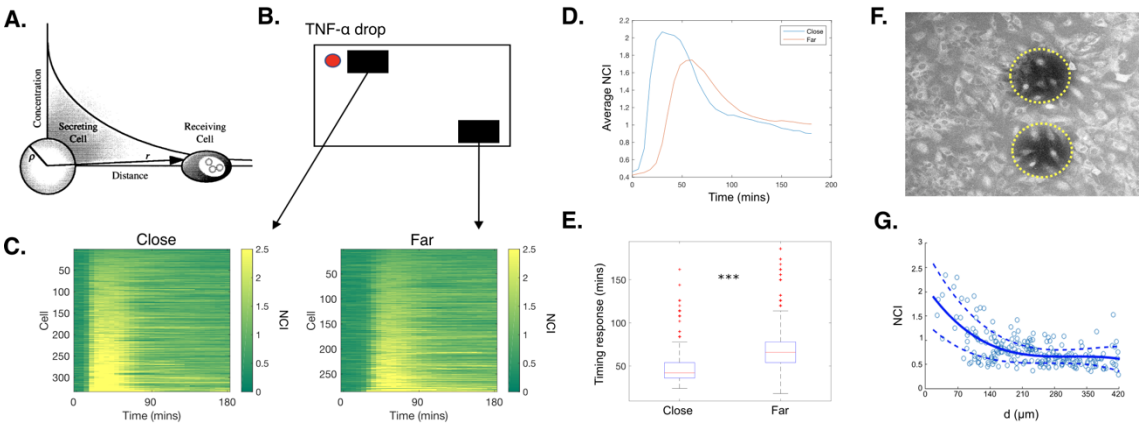

Figure 5.22. NF-κB spatial activation heterogeneity can be observed in vitro. A. *The scheme taken from (Francis & Palsson, 1997) shows how a cytokine secreting cell can form a concentration gradient.* ***B.*** *Experimental design for generation of transient concentration gradients in vitro.* ***C.*** *Heatmaps showing activation of close (left) and far cells (right).* ***D.*** *Average activation of close and far cells* ***E.*** *Timing of the response for close and far cells. ***$p<10^{-4}$, Kruskal-Wallis.* ***F.*** *An image (488 channel and brightfield) showing agarose beads on cells. Beads are outlined with yellow dashes.* ***G.*** *Activation of cells as a function of distance from beads. Each circle represents a cell, continuous line shows non-linear regression and dashed lines show the variance in data.*

These experiments show that in a monolayer of cells we can indeed observe differences in the strength of NF-κB activation as a function of the cell's position with

respect to the stimulus source. This aligns well with biophysical estimations of cytokine diffusion models (Francis & Palsson, 1997) and with the observation of clusters of NF-κB activated cells in vivo (Fig. 5.21). Hence, how a cytokine-sending cell might activate NF-κB in neighboring cells via cell-to-cell communication is the next topic we wanted to explore.

5.2.3 RAW 264.7 cells secrete NF-κB activating signals

To generate cytokine niches leading to cell-to-cell communication an efficient cytokine secreting cell is necessary. We used RAW 264.7 cells that are monocyte/macrophage-like and originated from BALB/c mice carrying tumors induced with Abelson leukemia virus. This cell line is widely accepted as an appropriate model of macrophages (Sung *et al*, 2014; Frank & Tay, 2015; Junkin *et al*, 2016; Bagnall *et al*, 2018). By co-culturing RAW 264.7 cells with the same MEFs that we previously used to characterize NF-κB signaling we aimed to study cell-to-cell communication within cytokine niches.

We first assessed a stimulation condition that can activate RAW 264.7 cells but unable to do so for MEFs. In this way we can observe MEF activation solely by cell-to-cell communication in our co-culture experiments. To achieve this, we used a very low dose of LPS. As RAW 264.7 cells do not possess tagged NF-κB we checked NF-κB activation upon LPS by immunofluorescence. We found that stimulation with as low as 1 ng/ml LPS led to nuclear localization of NF-κB in RAW 264.7 cells, showing their activation (Figure 5.23A). The same dose was not able to activate MEFs (Figure 5.23B). Hence, we choose this concentration for further experiments.

We next checked the mRNA levels of newly synthesized TNF-α to estimate RAW 264.7 cells' secretion upon activation upon LPS. We also use TNF-α as a control stimulation. We found that LPS stimulation induces TNF-α production as early as 30 minutes and high levels were kept until 2 hours post stimulation (Figure 5.23C), much higher than TNF-α stimulation (Figure 5.23C). Overall, we confirmed that RAW 264.7 cells are producing mRNAs of NF-κB activating cytokines upon LPS stimulation that could potentially generate cytokine niches in co-cultures.

Next, we tested whether production of TNF-α mRNAs translates into secretion of NF-κB activating cytokines in the medium of RAW 264.7 cells. Hence, we performed a medium transfer experiment where we used the medium of either LPS activated or naïve RAW 264.7 cells to stimulate MEF cells. We found that LPS activated medium of RAW 264.7 cells was able to activate MEFs (Figure 5.23D, blue line). Interestingly,

we also found a slight activation when we use medium of naïve RAW 264.7 cells medium (Figure 5.23D, green line). This suggests RAW 264.7 cells basally secrete low doses of NF-κB activating cytokines. As a control we stimulated MEF cells with same dose of LPS (1 ng/ml), which did not result in any activation (Figure 5.23D, black line).

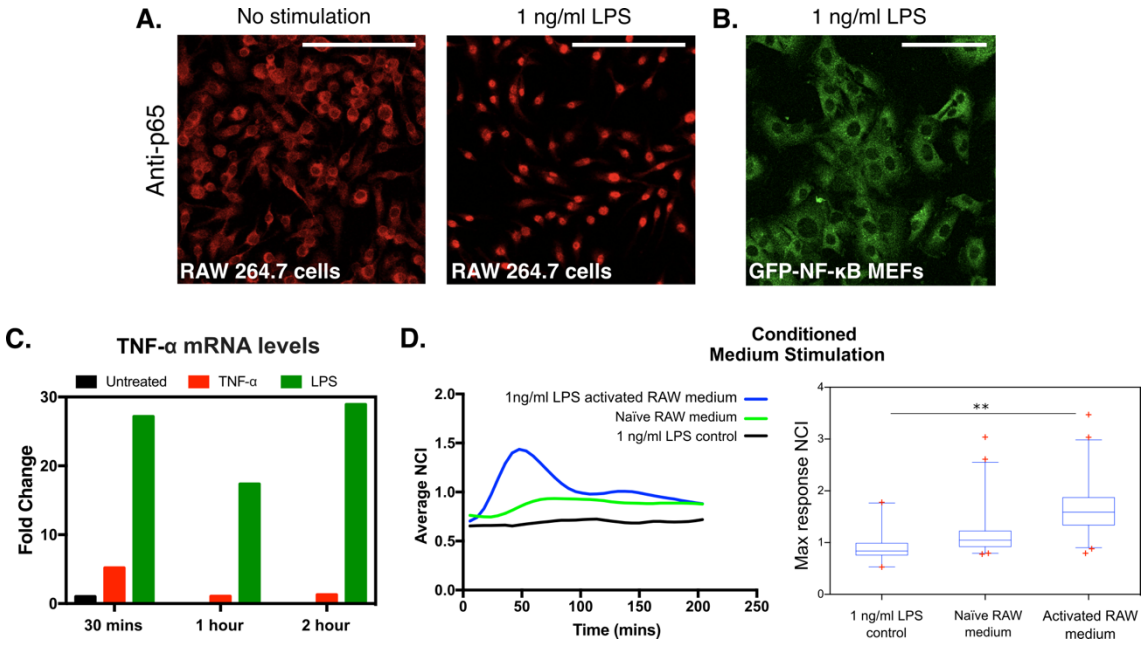

Figure 5.23. RAW 264.7 cells secrete NF-κB activating cytokines A. *Immunofluorescence against p65 showing nuclear localization of RAW 264.7 cells upon 1 ng/ml LPS.* ***B.*** *A snapshot of live-cell imaging upon 1 ng/ml LPS stimulation of GFP-NF-κB MEFs.* ***C.*** *Graph shows fold change of TNF-α mRNA production by real time PCR upon activation of RAW 264.7 cells with 10ng/ml TNF-α or 1 ng/ml LPS.* ***D.*** *Average NCI (left) and max response NCI values for MEFs that are stimulated with conditioned medium of 1 ng/ml LPS activated or naïve RAW 264.7 cells. Conditioned medium was collected 1 hour after LPS activation. 1 ng/ml LPS stimulation shown as a control. Scale bars show 100 μm. **$p<10^{-3}$, Kruskal-Wallis test.*

Overall, we confirmed production and secretion of NF-κB activating cytokines by RAW 264.7 cells upon activation with LPS. Interestingly, we found they have a basal secretion of such factors. We next explored inter-cellular signaling between RAW 264.7 and MEF cells in co-culture experiments and examined if basal secretion by RAW 264.7 cells can influence the cell-to-cell communication.

5.2.4 Cell-to-cell communication determines NF-κB activation of fibroblasts

To study cell-to-cell communication from RAW 264.7 cells to MEFs we co-cultured the two cell types in various ratios. Although morphologically RAW 264.7 cells already differ from MEFs in their smaller size we still used a red fluorescent dye to better distinguish them. We then diluted fluorescently labelled RAW 264.7 cells in MEFs (1:1, 1:10 and 1:100) and kept the final number of cells constant for each dilution (Figure 5.24A).

Upon LPS activation of RAW 264.7 cells we observed activation of MEFs in RAW 264.7 to MEF co-culture ratios of 1:1 and 1:10, but not of 1:100; since MEFs do not respond to this LPS dose this shows a clear cell-to-cell communication. Moreover, we found a strong correlation between the number of RAW 264.7 cells and the activation strength of MEFs (Figure 5.24B). As a control we used only MEF monoculture and gave the medium that was retrieved from LPS activated RAW-MEF coculture (1:1 ratio). Interestingly, the same medium resulted in stronger activation in the monoculture in comparison to the co-culture (Figure 5.24B, MEFs+cond). We also found that when we increase the number of RAW 264.7 cells in co-cultures initial NCI values are also slightly increased (Figure 5.24C).

Overall, these results suggest that the number of RAW 264.7 cells in the co-cultures plays an important role in determining how strongly MEFs respond to paracrine signaling. However, the response in co-cultures is quantitatively different from the response that we observed by a mere medium transfer experiment. On the other hand, we found that higher numbers of RAW 264.7 cells in the co-cultures result in increased initial activation of fibroblasts (above our NCI activation threshold of 1). We speculated this could be due to basal secretion of RAW 264.7 cells that was mentioned earlier. Next, we focus on spatial analysis of NF-κB activation to understand how far RAW 264.7 cells can send their signal to communicate with MEFs.

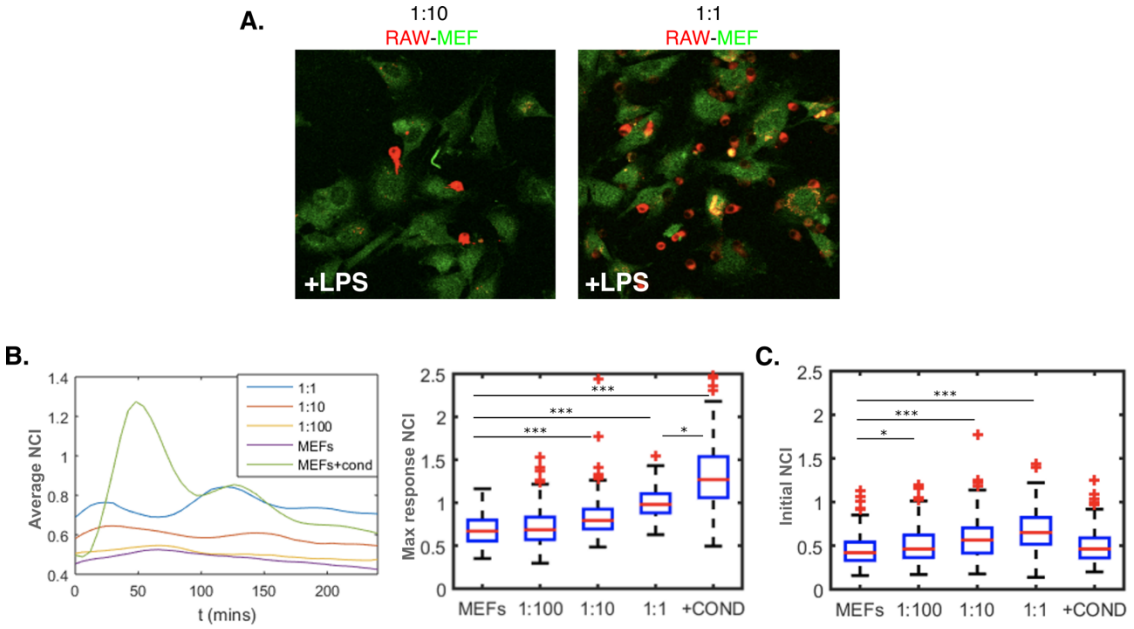

Figure 5.24. Upon LPS activation, RAW 264.7 cells activate NF-κB in co-culture with fibroblasts. A. *Images show RAW 264.7 (red) and MEF cells (green) co-cultured in 1:10 (left) and 1:1 (right) ratio upon LPS stimulation.* ***B.*** *Average (left) and single cell (right) NCI values of MEFs co-cultured with RAW 264.7 cells upon LPS.* ***C.*** *Initial NCI value of MEFs prior to LPS stimulation. Conditioned medium was used to stimulate only MEFs as a control and showed as +Cond in graphs. *p<10^{-2}, ** p<10^{-3}, *** p<10^{-4}, Kruskal-Wallis test.*

5.2.5 Co-culture of RAW 264.7-MEFs hints towards a spatial effect of NF-κB activation dynamics within cytokine niches

The biophysical model described earlier suggest that the concentrations are higher as we get close to the sending cell. When moving away from the source the concentration gradually decreases. To be able to see if this is also the case for our cytokine sending RAW 264.7 cells, we decided to spatially quantify NF-κB activation of MEFs. Hence, for each MEF we calculated their distance to closest RAW 264.7 cell and included this spatial information in our single cell quantifications. In this way we were able to associate activation strength of MEFs with their distance from the cytokine source (RAW 264.7 cells).

We used different metrics to calculate the role of distance to senders in the NF-κB response of the MEFs. As previously, we considered different ratios of RAW 264.7 to MEFs in co-cultures and kept the final number of cells equal in each dilution. We first checked response of receiver cells as a function of distance from the senders (Figure 5.25A). We found that there is a weak inverse correlation for all the conditions, which is slightly stronger in 1:1 RAW 264.7-MEF co-culture ratio (Figure 5.25A). However, all three co-culture ratios showed high heterogeneity on their distance dependent

NF-κB activation. To better extract and understand trends of our data, we next categorized the cells depending on their response. We found in general responding MEFs (defined as NCI>1) tend to be closer to RAW 264.7 cells in comparison to non-responding MEFs (Figure 5.25B). This trend was clear for all conditions, but more significant in co-cultures that contain a smaller initial number of RAW 264.7 cells. A larger initial number of RAW 264.7 cells resulted in similar trends but with a strong heterogeneity in the response (Figure 5.25B). Similarly, we also checked maximum activation NCI value of the cells that we categorize as Close or Far depending on a threshold of 50 μm, which is of the order of magnitude of 1-2 cells that we chose based on our calculations on biophysical estimations of cell-to-cell communication (See Methods for detailed explanations on threshold selection, some parameters used in this calculation is based on experiments that will be shown in the following sections of this thesis). We found that MEFs close to RAW 264.7 cells showed higher activation in comparison to the further ones (Figure 5.25C). This trend was also blurred when we increase the initial number of RAW 264.7 cells (Figure 5.25C). Moreover, we found a slight correlation between timing of the response and the distance from senders in 1:1 RAW 264.7-MEF co-cultures (Figure 5.25D, top). However, we were not able to capture any statistically significant timing difference on NF-κB activation between close and far cells in these experimental settings (Figure 5.25D, bottom).

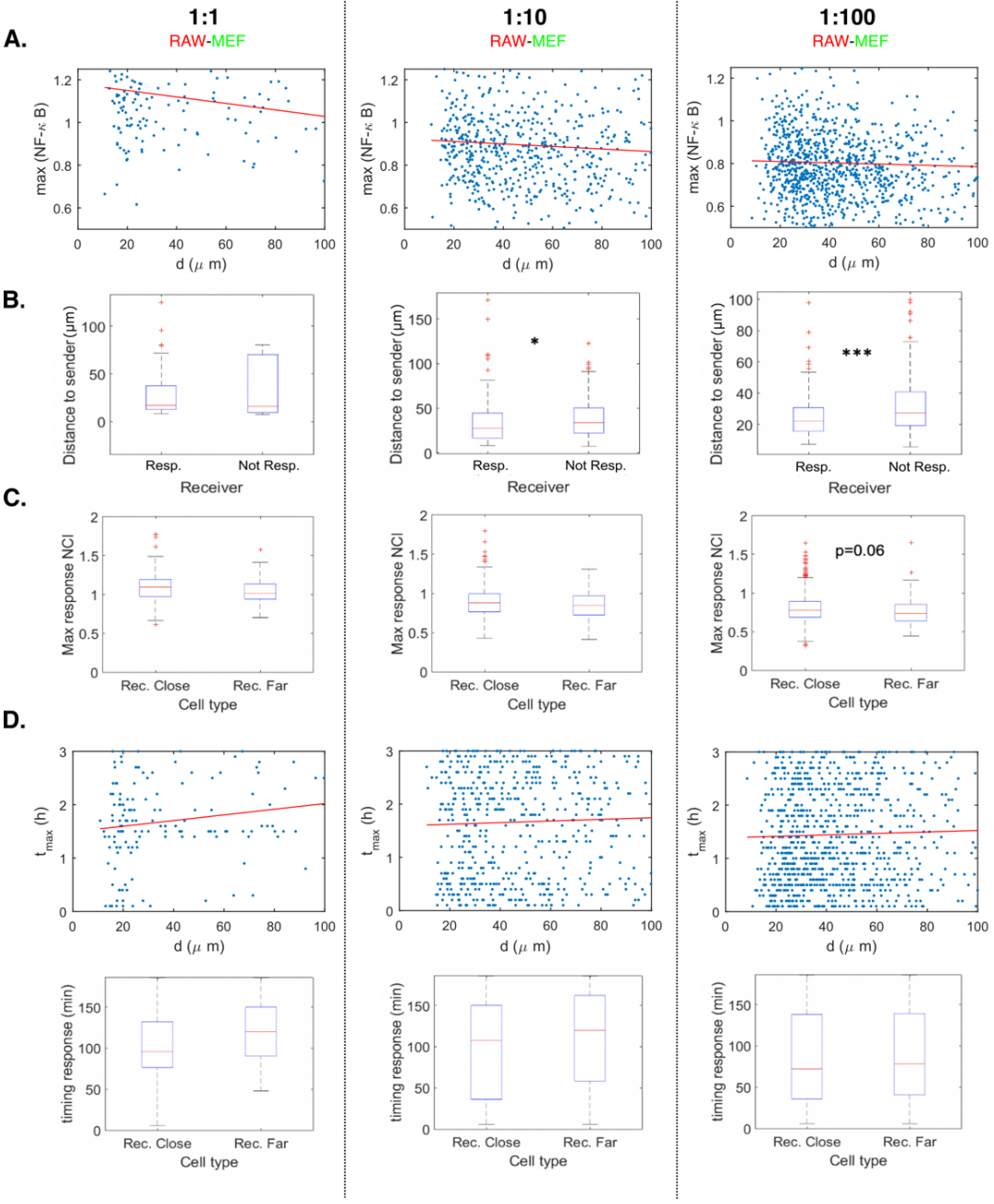

Figure 5.25. Spatial activation of MEFs highly depend on initial number of RAW 264.7 cells. A. *Scatter plots show maximum activation of receiver cells as a function of their distance from senders in 1:1, 1:10, 1:100 RAW 264.7 to MEF co-cultures. Red lines show the linear regression.* ***B.*** *Boxplots show responding and non-responding MEFs' distance to a sender and* ***C.*** *maximum response of close and far receivers in RAW 264.7-MEF co-cultures.* ***D.*** *(Top) Scatter plots show timing of maximum activation for receiver cells as a function of their distance from senders in 1:1, 1:10, 1:100 RAW 264.7 to MEF co-cultures. Red lines show the linear regression. (Bottom) Response time of close and far receivers in RAW 264.7-MEF co-cultures. *$p<10^{-2}$, ** $p<10^{-3}$, *** $p<10^{-4}$ through Kruskal-Wallis test. Graphs lacking the significance show no statistical difference.*

Overall, we find evidence of a positive correlation between being close to a cytokine source and NF-κB activation. Such trends are not very strong and the response of MEFs is very heterogeneous. The activation observed in these co-cultures are very weak in comparison to what we observed when the cells were treated with conditioned medium of activated RAW 264.7 cells. We found the initial number of RAW 264.7 cells play an important role in the way that NF-κB seems to encode for spatial information about the position of the cytokine source. It has been shown by others that previous exposure to TNF-α can reduce the cells ability to respond to subsequent stimuli (Son *et al*, 2021b). We reasoned the basal secretion of RAW 264.7 cells that we previously reported could play a role in this context. We indeed find higher initial NCI levels as we increase the concentration of RAW 264.7 cells in the co-culture. Since this preconditioning by RAW 264.7 cells negatively correlates with the activation strength of receivers, we called this as desensitization effect. This desensitization on MEFs, if confirmed in our settings, could somehow counteract the formation of a cytokine gradient that each immune cell might form around it. Uncoupling these two features to characterize how NF-κB dynamics carries spatial information using this co-culture system is technically challenging as basal secretion of RAW 264.7 cells is not controllable. Furthermore, in some extreme occasions we observe experimentally that RAW 264.7 cells at high density affect the morphology of our MEF cells (Figure 5.26). This suggests the existence of other interactions between RAW 264.7 and MEF cells that are not specific in the context of inflammatory cell-to-cell communication. Furthermore, it has also been reported single cell responses to LPS stimulation are heterogenous in RAW 264.7 cells resulting in highly variable cytokine production in single cells (Junkin *et al*, 2016). For these reasons, we decided to build a more controllable system to investigate desensitization and eventually study spatial and temporal activation of NF-κB.

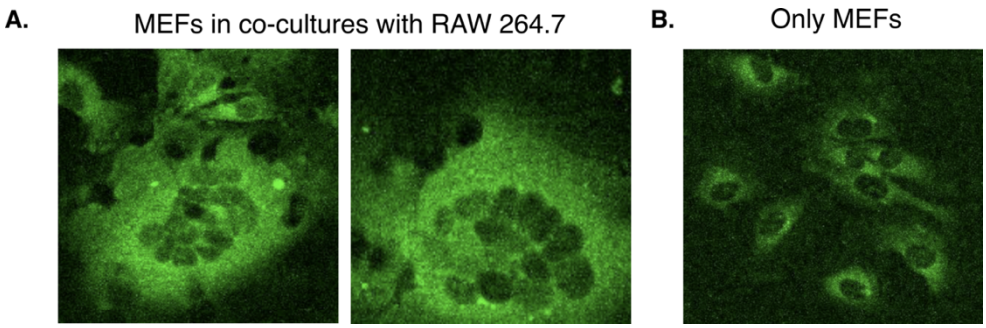

Figure 5.26. Morphology of a subset of MEFs is affected when co-cultured with RAW 264.7 cells. A. *Snapshots of MEFs co-cultured with high number of RAW 264.7 cells (not visible), showing altered morphology.* ***B.*** *A snapshot of a monoculture of MEF cells.*

5.2.6 Generation of a highly controllable sender receiver system

We reasoned that, to achieve a highly controllable in vitro system of cell-to-cell communication, we needed to use signal sending and signal receiving cells of only one type. Our ideal in vitro model consists of an inducible sender cell line that is engineered to send signals to neighboring cells upon controllable induction. As a receiver cell line, we could simply use our GFP-NF-κB MEFs.

To generate the sender cells, we engineered our GFP-NF-κB MEFs for inducible overexpression of fluorescently labelled TNF-α. To induce TNF-α secretion we took advantage of an established method called "Retention Using Selective Hooks (RUSH)" that allows synchronized secretion of proteins (Boncompain *et al*, 2012). The RUSH system uses two proteins to allow inducible secretion: a streptavidin fused compartment-specific hook and a streptavidin binding protein (SBP) fused to the protein of interest to be secreted by the cells. The interaction between streptavidin and SBP can easily be disturbed by addition of biotin to the cell culture medium. Once added, biotin binds the streptavidin fused hook, and this releases the secretory protein from its hook to follow the secretory pathway (Figure 5.27A).

We chose an endoplasmic reticulum (ER) protein KDEL as a hook to retain in this compartment streptavidin fused to an RFP tagged TNF-α. We co-transduced GFP-NF-κB MEFs with the hook and TNF-α containing lentiviral particles and then performed antibiotic selection for the presence of both constructs. Surviving cells were then cloned for live-cell imaging characterization. We identified a clone that showed no nuclear activation in basal conditions (Figure 5.27B, left). Only upon addition of biotin to cell culture medium we observed activation of cells which suggested TNF-α secretion that leads to autocrine/paracrine signaling (Figure 5.27B). We then chose this clone for further experiments.

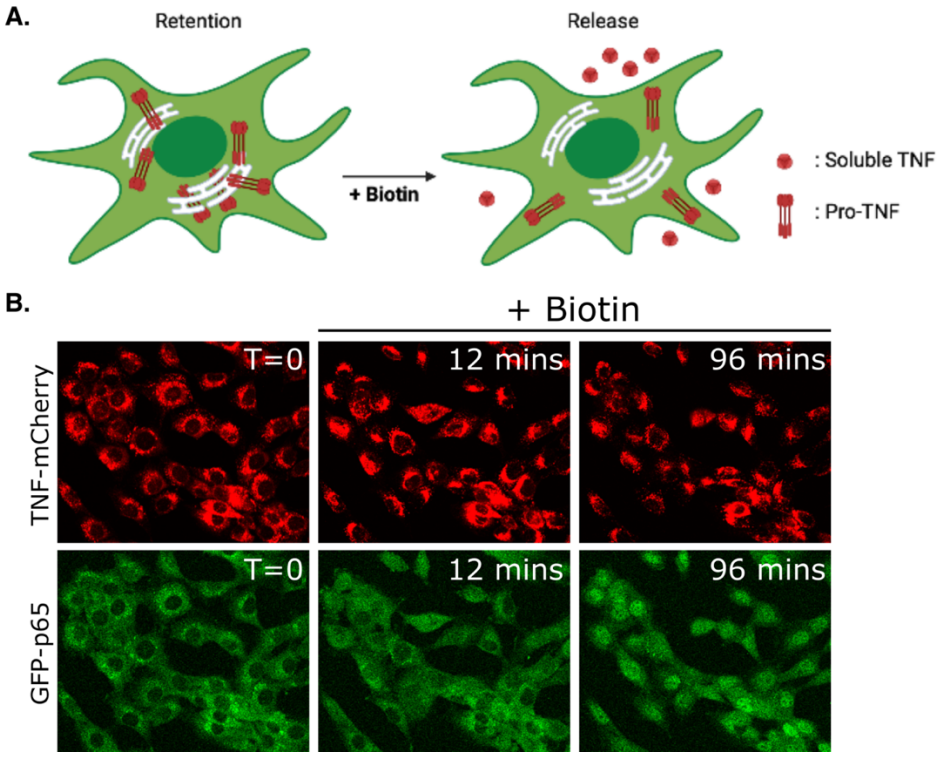

Figure 5.27. Generation of the sender cells. A. *Scheme showing the RUSH system that we used to generate senders (Created with BioRender.com).* ***B.*** *Snapshots of a live-imaging experiment showing the activation of sender cells upon addition of biotin to cell culture.*

The traditional inducible systems (such as Tetracycline-responsive Tet promoters) control the ectopic expression of proteins at transcriptional level. Although these inducible systems provide advantageous expression of proteins only when needed, it is already known that these systems can be leaky (Meyer-Ficca *et al*, 2004). In our RUSH inducible system, the induction is controlled at protein level and the balance between the two protein is a critical parameter that could lead to leakiness. Although our sender cells basally did not show any clear activation, we checked TNF-α levels in the medium by enzyme-linked immunosorbent assay (ELISA). We indeed detected soluble TNF-α in the medium of senders in basal conditions (Figure 5.28A). Biotin induction led to an increase in the concentration, confirming further secretion. To check whether secreted TNF-α was functional we performed a medium transfer experiment. Treating receiver cells with the medium of untreated sender cells resulted in NF-κB activation (Figure 5.28B). This shows that the medium of sender cells indeed contains functional TNF-α that they no longer respond to, potentially because of the desensitization effect that was mentioned earlier. We thought that this property might be useful to characterize desensitization in a more controlled setting.

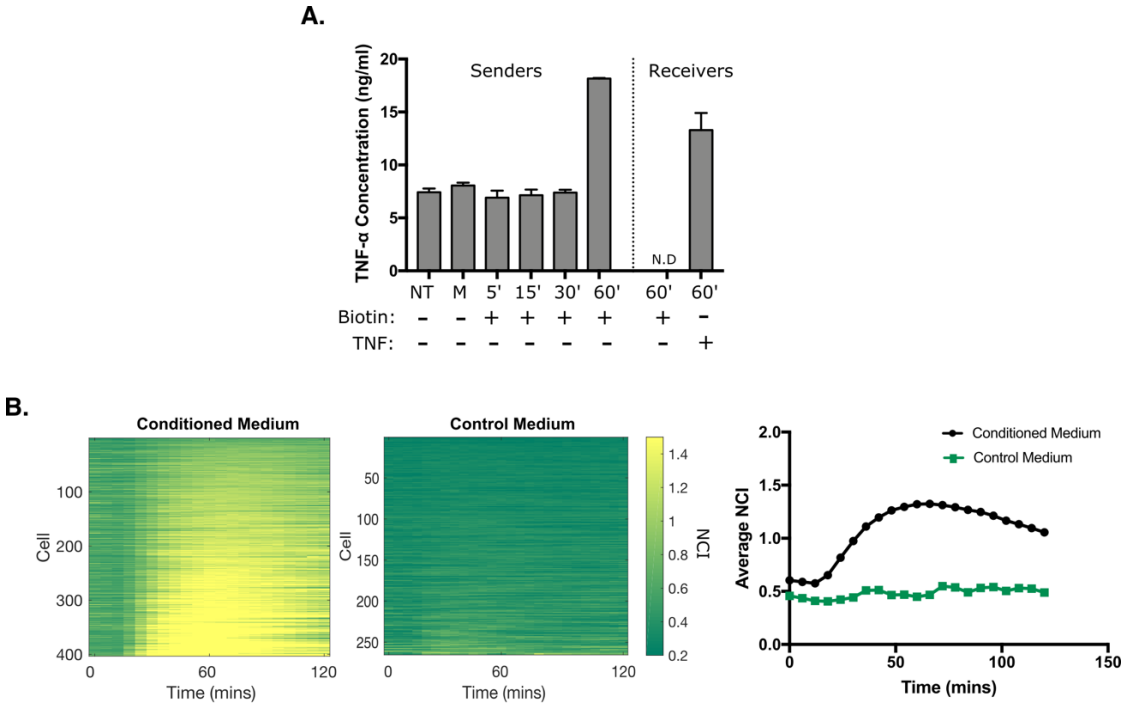

Figure 5.28. Sender cells secrete TNF-α, but they also leak some before induction. A. *ELISA showing the senders do secrete TNF-α upon biotin but they are also leaky.* ***B.*** *Heatmap for single cell NCI value (left) and average NCI (right) for receivers upon conditioned medium of senders confirming their leakiness of functional TNF-α.*

After generation of sender cells, we next performed co-culture experiments of our in vitro system. To see if leakiness affects the co-culture's initial activation value, we diluted sender cells in receivers at final percentages of 5, 15 and 66 and kept the final total number of cells constant for each dilution (Figure 5.29A). We found that increased number of senders in the co-cultures did not change the morphology of the receivers. To quantify initial NCI value of senders and receivers separately in the co-cultures we took advantage of our software that identifies the cells based on the signal intensity of red channel. We set a stringent threshold for detection of senders to ensure correct labeling of the cells even in crowded co-culture conditions. To check if our selection of the threshold correctly detects the senders, we plotted the average red signal intensity for detected senders and receivers to ensure no signal was detected from the receivers (Figure 5.29B). Once senders and receivers are successfully identified we then used our routine quantifications to calculate NF-κB activation based on the NCI value. We found initial NCI value of receivers in co-cultures were kept low (Figure 5.29C). This suggests receivers are not disturbed by co-culturing conditions due to basal secretion of senders as opposed to what was observed using RAW 264.7 cells.

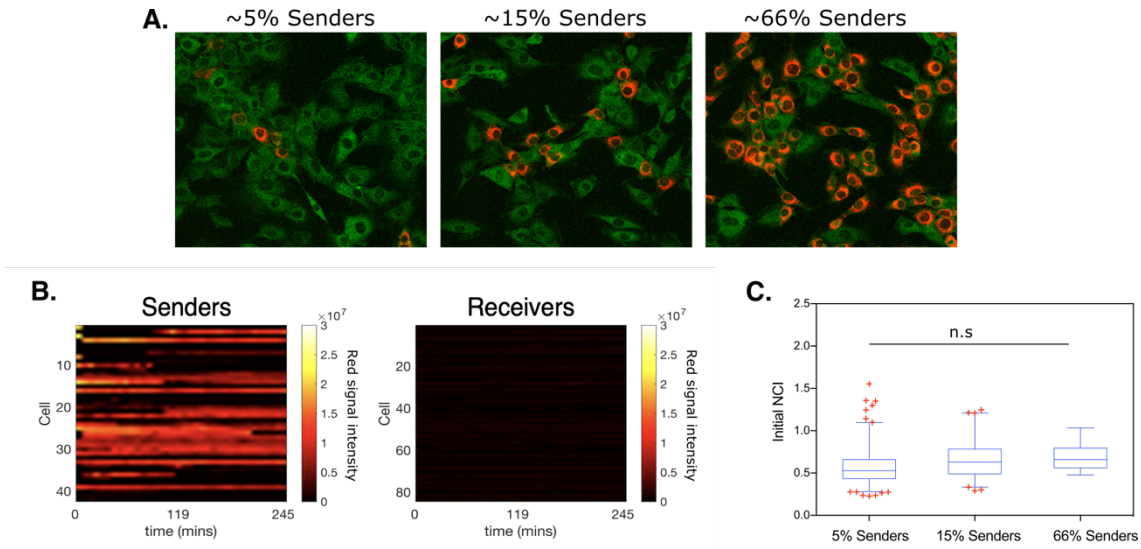

Figure 5.29. Receiver cells are not disturbed by co-culturing with sender MEFs A. *Images from 5, 15 and 66 percent senders containing co-cultures.* ***B.*** *Average red signal intensity for selected sender and receiver cells.* ***C.*** *Initial NCI value of receivers in co-cultures. p value is calculated through Kruskal-Wallis test (n.s: not significant).*

In sum, we generated sender cells that can successfully secrete TNF-α when induced. Their basal leakiness of TNF-α resembles what we observed for immune-like cells but without affecting receivers' morphology. This allows us to modulate the desensitization effect by targeting the number of initial sender cells without disturbing receivers' initial behavior. Next, we try to characterize how desensitization can change receivers' overall behavior in cell-to-cell communication.

5.2.7 Continuous exposure of soluble TNF-α desensitize the cells

Previously we termed preconditioning of receiver cells by RAW 264.7 cells as desensitization and speculated that this is due to previous exposure to NF-κB activating cytokines. To confirm this effect occurs solely by basal secretion we take advantage of our sender-receiver model and setup a side-by-side co-culture experiment where cells can share the medium but lack cell-to-cell contact.

We used a 3-well culture chamber that allowed us to separate cells from each other with 500 μm distance. We plated senders, receivers and some more receivers next to each other in this chamber (Figure 5.30A). To allow medium sharing we removed the chamber one day before imaging experiment leaving them approximately 24 hours in medium contact. During this time cells were not able to reach cell-to-cell contact. As control, to avoid medium sharing we did not remove the chamber until right before imaging.

We then induced TNF-α secretion by senders by addition of biotin to the medium. Upon biotin induction we first observed activation of sender cells in both conditions (Figure 5.30B, red lines). Receiver cells that are in contact with sender's medium did not respond to secreted TNF-α during 3 hour of imaging experiment (Figure 5.30B, 30C left). Naïve receivers that did not share the medium showed activation after 1.5 hour (Figure 5.30B, 30C right). This suggests desensitization effect is indeed caused by previous exposure of basally secreted TNF-α. Interestingly, in the condition in which no medium was shared, we found that receivers that are close to senders got activated stronger than the further ones upon induction of TNF-α secretion (Figure 5.30B). This confirms successful formation of a concentration gradient by sender cells.

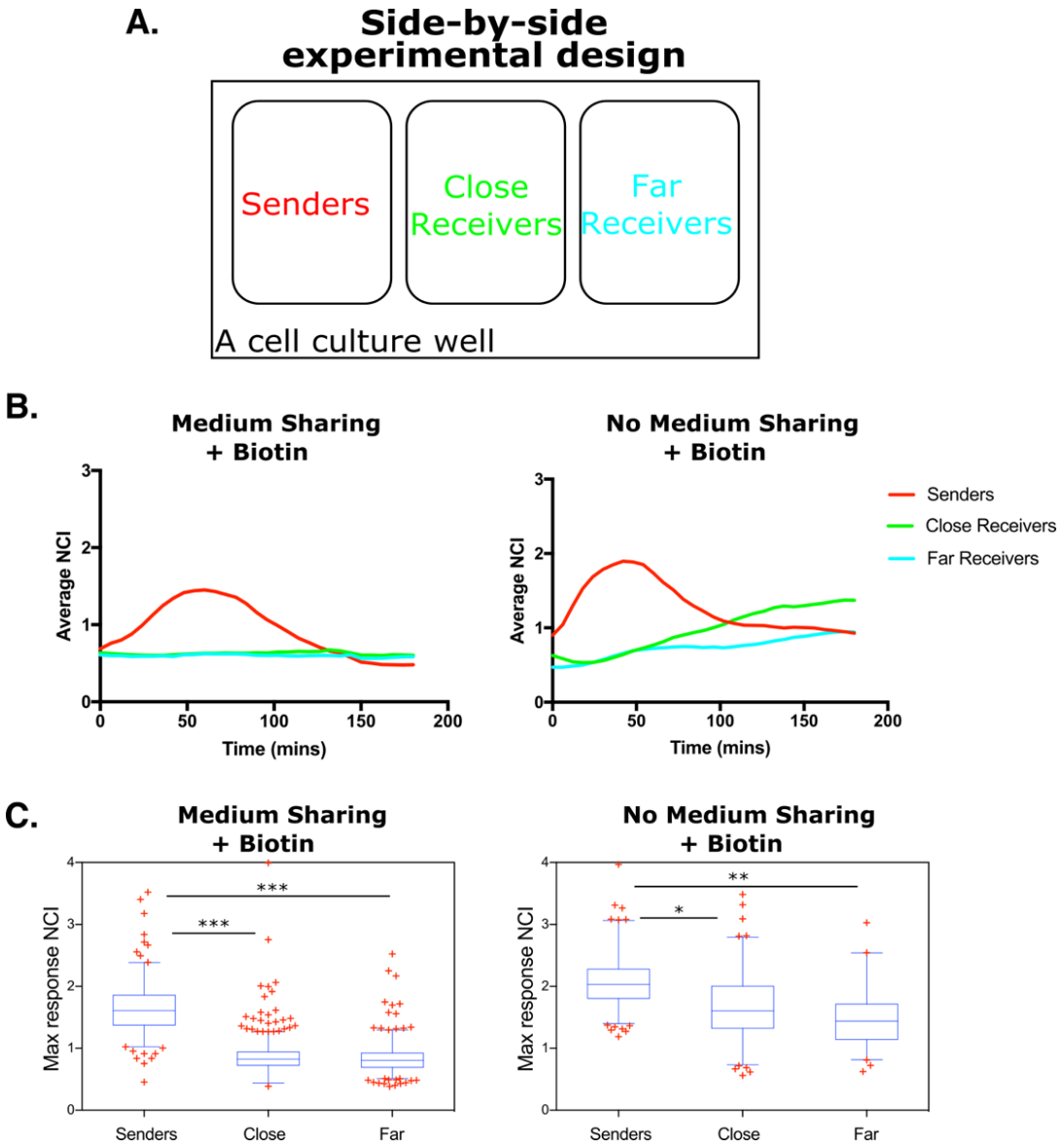

Figure 5.30. Senders spatially desensitize receiver cells by soluble TNF-α. A. *Experimental design for side-by-side co-cultures with a 3-well cell culture insert.* ***B.*** *Average activation of sender, close and far receivers upon biotin induction in medium sharing (left) and no sharing (right).* ***C.*** *Max response NCI values of senders, close and far receivers upon biotin induction in medium sharing (left) and no sharing (right) conditions. *$p<10^{-2}$, ** $p<10^{-3}$, *** $p<10^{-4}$ Kruskal-Wallis test.*

In sum, we concluded that the desensitization effect is caused by previous exposure to soluble TNF-α that alters the TNF-α response in receiver cells without the need of cell-to-cell contact. Interestingly, despite being the most TNF-α exposed cells, sender cells are highly responsive to their own induction. We speculate their activation could be a result of their action of secretion through another mechanism. We next explore the spatiotemporal effect of desensitization for our sender and receiver MEFs in random co-cultures.

5.2.8 Senders spatially desensitize receivers at single cell level

To understand how desensitization affects sender and receiver cells in random co-cultures we cultured them at different ratios and stimulated with TNF-α. We used final percentages of 5, 15 and 66 senders and kept the final total number of cells constant for each dilution. For spatial analysis we set a distance threshold of 50 μm to categorize receiver cells as close or far receivers based on their distance from senders.

We first checked overall activation of NF-κB upon TNF-α stimulation in sender and receiver cells. Interestingly, sender cells showed very little to no activation upon TNF-α regardless of their initial number (Figure 5.31A). Receiver cells instead showed very distinct overall responses at different sender to receiver dilutions. Specifically, we found that co-cultures containing the lowest number of initial sender cells respond strongly to TNF-α, whereas co-cultures containing the highest number of senders were the weakest TNF-α responders (Figure 5.31B). This confirmed the presence of desensitization effect also in this co-culture setting. We then checked if such desensitization effect plays a role in space at single cell level. Following our spatial quantifications, we found that the maximum response of far receivers was stronger than that of close receivers (Figure 5.31C). We found this to be significant for both 5% and 15% sender containing cocultures. We did not identify any far receivers for the 66% sender containing coculture as the number of senders was high and the chance of being far from a sender was low (Figure 5.31C).

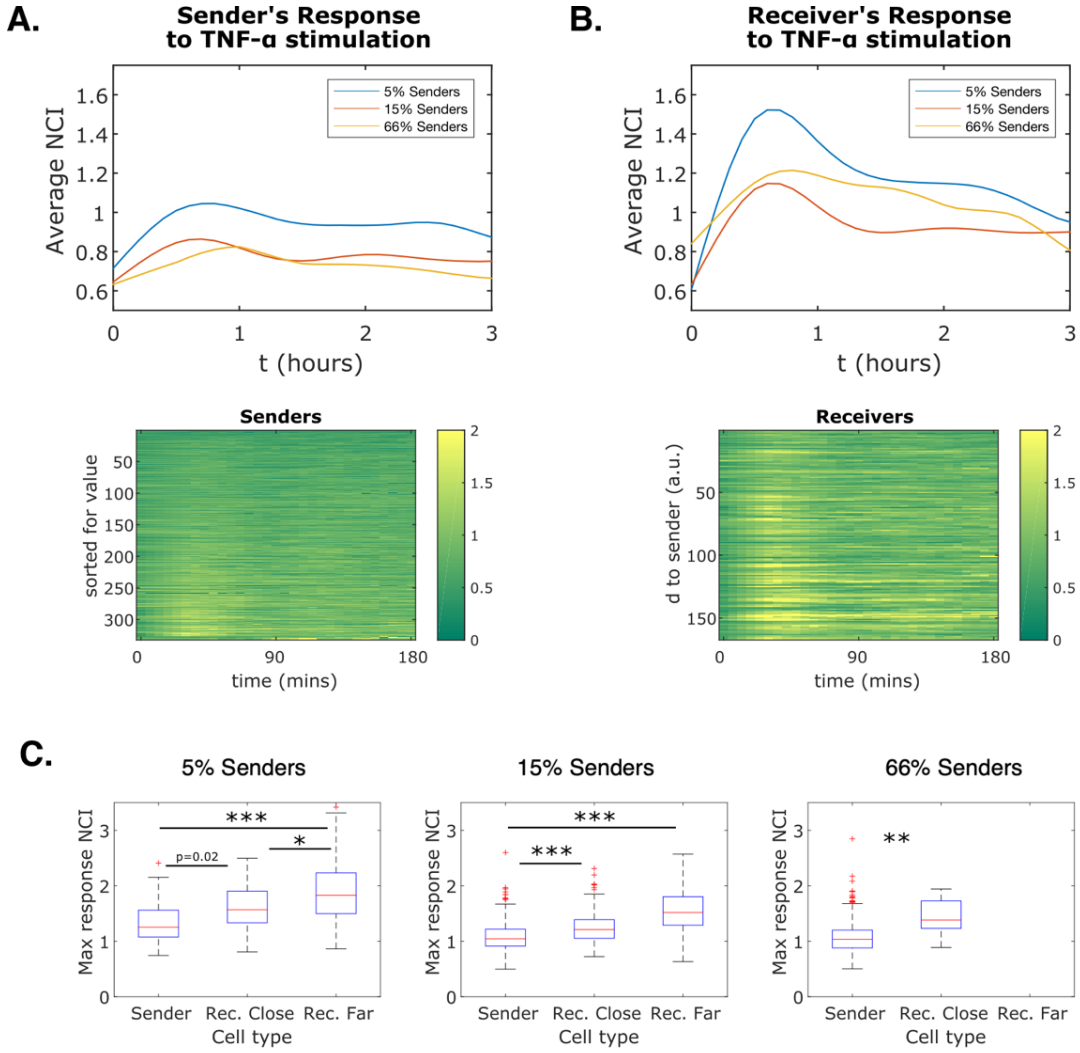

Figure 5.31. Senders spatially desensitize receivers at single cell level. A. *Average response of senders upon TNF-α stimulation in co-cultures (top) and an example of single cell NCI values in color plots (bottom, data shown is from 15% senders containing co-culture).* ***B.*** *Average response of receivers upon TNF-α stimulation in co-cultures (top) an example of single cell NCI values in color plots (bottom, data shown is from 15% senders containing co-culture).* ***C.*** *Boxplots show maximum response of senders, close and far receivers in co-cultures. *p<10^{-2}, ** p<10^{-3}, *** p<10^{-4}, Kruskal-Wallis test.*

In summary, we found that sender cells do not respond to soluble TNF-α despite they respond to their own TNF-α that is secreted after biotin induction. The behavior of receivers upon TNF-α stimulation showed that the desensitization effect is distance-dependent also at single cell level. Next, we wondered how this preconditioning affects spatial and temporal activation of receivers when we induce formation of TNF-α niches within sender-receiver monolayer.

5.2.9 Formation of TNF-α niches overcomes desensitization

We next wondered how receivers behave under desensitization effect when there is secretion from sender cells. Hence, we followed the same random co-culture settings that are described in the previous section and induced TNF-α secretion by addition of biotin to cell culture medium (Figure 5.32A). We first checked average cell response of senders and receivers in 5, 15 and 66% senders containing co-cultures. We found that initial number of senders does not affect the strength of overall activation of senders (Figure 5.32B) nor receivers (Figure 5.32C) upon biotin induction. For receiver cells this is contrary to what we observed for TNF-α stimulation. When we compare the average response of senders with receivers, we found that NF-κB activation in sender cells is stronger and earlier in comparison to receivers' response (Figure 5.32).

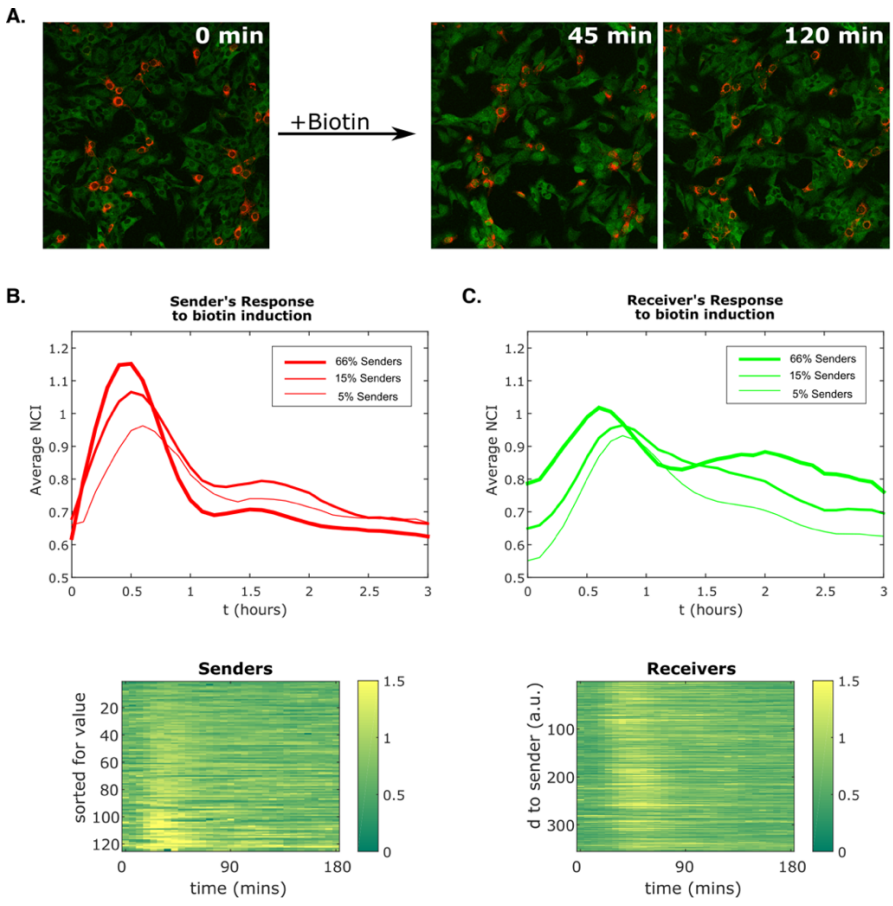

Figure 5.32. Biotin induced activation does not depend on initial number of senders. ***A.*** *Images showing sender-receiver co-cultures before and after biotin stimulation.* ***B.*** *Average response of senders upon biotin induction in co-cultures (top) and an example of single cell NCI values in color plots (bottom, data shown is from 15% senders containing co-culture).* ***C.*** *Average response of receivers upon biotin induction in co-cultures (top) and an example of single cell NCI values in color plots (bottom, data shown is from 15% senders containing co-culture).*

To understand how receivers behave around TNF-α niches that are generated by senders we next performed spatial quantifications on biotin induced co-cultures. We found in both 5 and 15% sender containing co-cultures responding receivers (defined as NCI>1) are closer to a sender than those that are non-responding (Figure 5.33A) as opposed to what we observed for TNF-α stimulation.

Lastly, we checked the timing of the response for sender and receiver cells. We showed that biotin induction leads to faster activation of senders than receivers (Figure 5.33B); close receivers respond faster than far receivers (Figure 5.33B), both for 5 and 15% sender containing co-cultures, with a certain heterogeneity observed in the latter.

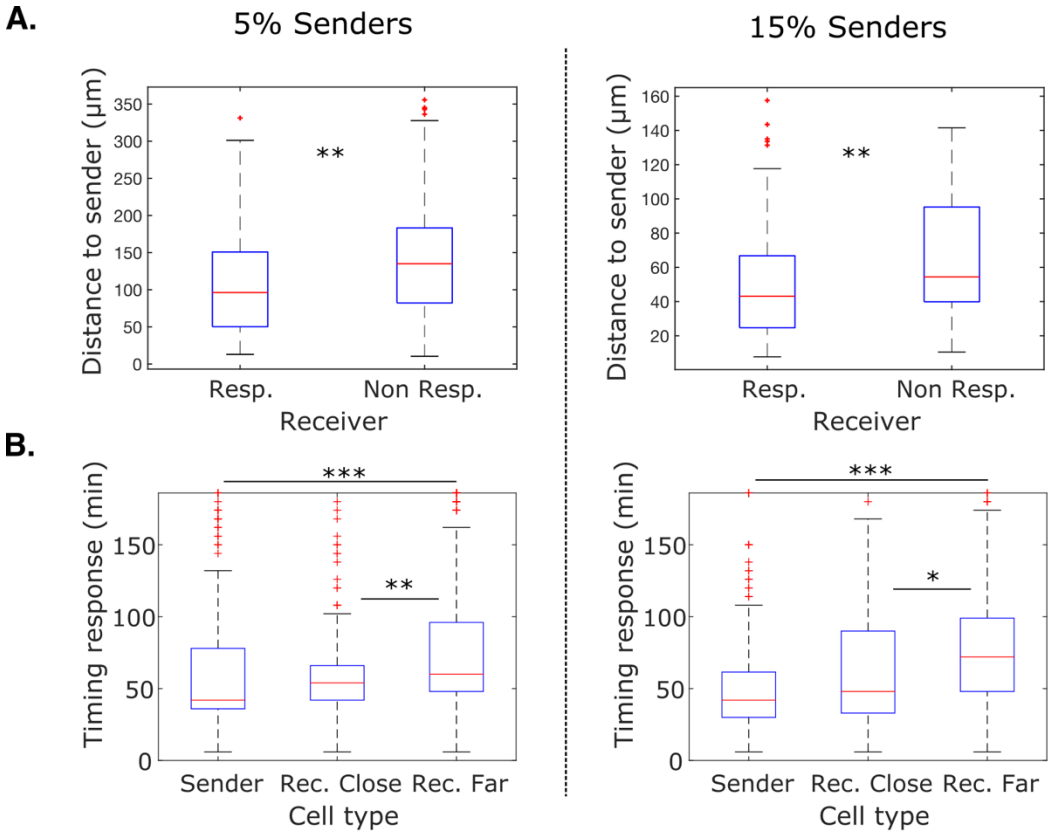

Figure 5.33. NF-κB dynamics encode spatial and temporal information at single cell level. A. *Boxplots show maximum response of sender, close and far receivers in co-cultures* ***B.*** *Boxplots show response timing of senders, close and far receivers in co-cultures. *$p<10^{-2}$, ** $p<10^{-3}$, *** $p<10^{-4}$, Kruskal-Wallis test.*

In summary, we built a sender-receiver system to study spatial and temporal activation of NF-κB. In basal conditions, we found desensitization causes a trade-off between being nearby to a TNF-α source and having strong NF-κB response to TNF-α. However, when immune cells are induced to create cytokine niches, cells nearby overcome desensitization effect due to an increased local concentration. In this condition, being nearby to a cytokine source results in stronger activation and the activation strength gradually decreases within the cytokine niches. Importantly, this occurs also in time-dependent manner resulting in nearby cells to respond faster than those further. Taken together, we report that single cells carry spatial and temporal information that defines their complex dynamic response during inflammation, as hypothesized. We speculate that such behavior is shaped by a desensitization effect that can contribute to produce an average moderate response within the population for a wide range of cytokine-sending cell concentrations.

6. DISCUSSION

Discussion presented in the following chapter of this thesis (6.1) is published in BioRxiv preprint server (Kizilirmak *et al,* 2021).

6.1 Small transcriptional differences lead to distinct NF-κB dynamics in quasi-identical cells

Single-cell imaging studies of NF-κB dynamics have shown that there is a high degree of heterogeneity within cell populations (Lee *et al*, 2014; Nelson *et al*, 2004; Paszek *et al*, 2010; Sung *et al*, 2009; Tay *et al*, 2010; Zhang *et al*, 2017a). Our work, performed on a homogenous cell population of mouse embryonic fibroblasts immortalized by serial passages and derived from a single embryo, indicates that NF-κB dynamic heterogeneity might be due in part to the coexistence of subpopulations of quasi-identical cells that do respond distinctly to the stimuli. Extrinsic factors such as the cell cycle phase have been shown to affect NF-κB dynamics (Ankers *et al*, 2016) but we cannot attribute inter-clonal differences to differences in the cell cycle. Instead, we show that the expression levels of genes coding for elements of the NF-κB regulatory circuit can explain the clonal differences, suggesting that they are a key determinant of the dynamical heterogeneity observed in the original population.

The link between NF-κB dynamics and transcription is typically analyzed in one direction (Lane *et al*, 2017; Lee *et al*, 2014; Tay *et al*, 2010; Zambrano *et al*, 2016): how does NF-κB nuclear localization dynamics drive gene expression? Here we consider the same question in the other direction: how can transcriptomic differences affect dynamics? We developed a computational framework based on the average expression levels of key genes coding for regulatory elements upstream of NF-κB, which explains differences in the strength of the response of clones to TNF-α. The same framework predicts clonal differences in the response to IL-1β. The expression level of these genes coding for upstream positive regulators could indeed determine the amount of IKK complex formed upon both stimuli, which has been recently shown to correlate with NF-κB activation (Cruz *et al*, 2021). We also showed how the expression levels of the components of the negative feedback of NF-κB predict whether the NF-κB response will be sharp or persistent. The prediction is supported by mathematical modelling and experimental data showing that a moderate reduction in IκBα level induced by antisense oligonucleotides can lead to relatively large differences in the NF-κB dynamics. Knock-out of IκBα coding gene Nfkbia has been shown to induce a change from oscillatory to sustained dynamics (Cheng *et al*, 2021),

our work shows how a finer tuning of the feedback expression can produce analogous changes in NF-κB dynamics.

Part of the success of our approach is probably due to the biological homogeneity of the clones, which derive from cells of the same type that come from a single embryo. We assume that transcriptional levels are informative of protein levels; while this is not necessarily true, every deviation from the assumption will be identical in each clone. We hypothesize that a similar transcriptional approach could be used to predict the relative difference in the dynamic response of other TFs in subpopulations within other relatively homogeneous cell populations, as for example in cells derived from the same tissue or in clones within a tumor mass (Greaves & Maley, 2012) that might respond differently to therapy (Paek *et al*, 2016).

NF-κB nuclear localization dynamics in single living cells was observed for the first time more than 15 years ago (Nelson *et al*, 2004) and since then its oscillatory nature was subject to discussion (Barken *et al*, 2005; Nelson *et al*, 2005). More recently, it has been argued that NF-κB displays damped oscillations (Zambrano *et al,* 2016) as compared to the sustained oscillations reported by others (Kellogg & Tay, 2015). This work shows that classification of NF-κB dynamics is not necessarily binary. Within a population of quasi-identical cells, we can find subpopulations that are more and less prone to oscillate. For circadian oscillators as well, it was found that clonal populations have different oscillatory features (Li *et al,* 2020). For our cells, we show that this largely depends on the expression level of genes belonging to the NF-κB regulatory circuit. It has been previously proposed that oscillations are a way to provide opportunity windows for decision (Zambrano *et al,* 2016), and this work shows such windows can be diverse across cell subpopulations, which can contribute to population robustness in response to stimuli (Paszek *et al,* 2010). Our work sheds light on the origin of the dynamic variability reported in the literature: if small transcriptional differences can affect the dynamics of NF-κB, it is not surprising that different cell types have completely different oscillatory phenotypes.

The increasing availability of single-cell data on NF-κB dynamics has shown that it is possible for cells to discriminate between stimulus type (Adelaja *et al,* 2021; Cheng *et al,* 2021; Martin *et al,* 2020), dose (Tay *et al,* 2010; Zambrano *et al*, 2014; Zhang *et al,* 2017a) and dynamic profile (Ashall *et al,* 2009; Lee *et al*, 2016; Zambrano *et al,* 2016). Here, we find that two MEF clones from the same embryo, clone G and clone B, do respond differently to two different stimuli: clone G responds strongly to IL-1β, while clone B responds strongly to both TNF-α and IL-1β. On the other hand, clone R produces a sharper and more oscillatory NF-κB response than clone B. This

indicates that stimulus specificity in NF-κB dynamics is clone-dependent and, all the more so, that it will vary among cell types within the same organism. A recent study shows that a synthetic version of the NF-κB circuit ectopically expressed in yeast (Zhang *et al*, 2017c) displays different types of dynamics and responses by manipulation of the key kinetic parameters. Furthermore, since immortalized MEFs maintain certain characteristics of primary MEFs (Beg & Baltimore, 1996; Gapuzan *et al*, 2005), our work suggests that a similar fine-tuning can take place naturally in primary mammalian cells.

We show that the dynamical differences observed between clones are robust and persist over time and cell culturing. Persistent transcriptional differences can be due to sequence variants in the control elements of the genes, especially in enhancers (Natoli & Ostuni, 2019), or in epigenetic changes in DNA methylation or chromatin accessibility of the same control elements. Our RNA-sequence based bioinformatic analysis did not detect any variant among clones in the mRNA sequence of genes involved in the NF-κB response. We inferred a substitution rate in the genome of the clones in the order of $5{\cdot}10^{-7}$ per base pair, which would translate to <100 substitutions per haploid genome. This substitution rate is consistent with somatic variability of cells from the same organism (Amand *et al*, 2016; Milholland *et al*, 2017). However, our analysis cannot detect other genetic changes, such as sequence changes in the regulatory regions or copy number variations. This genetic variability could contribute to the small (although robust) differences in gene expression reported here. The other possibility is epigenomic variation between different cells. We find that the most visible difference in the transcriptomics of the different clonal populations is related to developmental programs, which indeed involve epigenetic variations. Whether expression of different developmental programs within different cells of the same population can give rise to the difference in response dynamics of NF-κB and other TFs remains to be proved, but we speculate that this is at least likely.

We find that the NF-κB dynamic response of the cells within each clonal population is still heterogeneous. We speculate that this cell-to-cell variability can have a purely stochastic component related to the probabilistic nature of the activation of gene transcription. Indeed, it has been shown that even highly transcribed genes under the control of NF-κB like the one encoding for IκBα are transcribed stochastically (Zambrano *et al*, 2016). Thus, the same cell might be oscillatory or not at different times, depending on how recently it had a burst of IκBα transcription and translation.

Future studies will be needed to connect the transcriptional history of each single cell with its NF-κB dynamics.

In sum, our work shows that part of the NF-κB dynamic heterogeneity observed within a relatively homogenous population of cells can be due to the co-existence of cell subpopulations with distinct dynamics, which correlates with robust although small differences in the expression levels of genes belonging to the regulatory circuit. However, some heterogeneity remains between cells of the same clone, suggesting that ephemeral variations of transcript levels follow transcriptional bursts in individual cells. We speculate that analogous mechanisms might also diversify the dynamic response of other TFs to external cues.

6.2 NF-κB heterogeneous dynamics encode spatiotemporal information and is shaped by desensitization

Cell-to-cell communication plays a key role in multicellular organisms, in particular to produce different spatiotemporal behaviors in the tissues. An example is the generation of concentration gradients through morphogen secretions, which plays a crucial role to shape cellular processes (i.e., cell migration and epithelial morphogenesis) in space and time (Rogers & Schier, 2011). This spatiotemporal point of view has received less attention in the context of the immune response to pathogens or damage. However, it is already known that spatially localized danger signals in a certain part of a tissue create cytokine niches where cells are subjected to various concentration of cytokine depending on their location (Pangault *et al*, 2010). NF-κB plays a key role in the response to cytokine and in the previous part of this thesis we showed a clear example of how its dynamic behavior is fundamental to understand the response to inflammatory stimuli. In this part of our work, we studied how such cytokine niches can translate into NF-κB activation heterogeneity and what are the spatial and temporal characteristics of NF-κB activation within them.

Previously it has been reported that traditional two-dimensional (2D) cell culture models provide essential but limited insights on functions of real living tissues (Pampaloni *et al*, 2007). This is due to the conventional monolayer culturing typically used with cells on a flat surface, where they lack most of their cell to cell and cell to extracellular matrix contact, all of which takes place under a pool of cell culture medium. The study of cell-to-cell inflammatory communication using this kind of setup was thought to be challenging, since secreted cytokines were believed to be diluted and diffused in the medium above the cells in a matter of seconds. However,

here we showed that, despite the above-mentioned limiting factors, traditional 2D cell culture models can recapitulate a number of features of cell-to-cell communication, such as spatial heterogeneity in NF-κB activation. Such 2D cultures might provide insights on how cells might use NF-κB activation gradients in vivo; indeed, in the context of morphogenesis it was shown that 2D culture models can inform about the design principles of morphogenic gradients (Li *et al*, 2018).

Through generation of a novel in vitro sender-receiver model, in which cells do secrete TNF-α almost instantaneously upon biotin, we were able to characterize the spatial dynamics of NF-κB activation in a monolayer of cells. We found that the strength of NF-κB activation is defined by the distance to the cytokine source. Cells located closer to the source activated NF-κB stronger than those that are further, even though they maintain a strong dynamical heterogeneity. Of note, these features are also maintained when using the more physiological -but less controllable- RAW 264.7 cells as senders of cytokines. This suggests that sender cells generate concentration gradients to communicate location and severity of the danger signals and bystander cells decode this information into the spatially varying dynamics of NF-κB activation. In principle such niches can be modulated by factors such as concentration of secreted cytokines or the density of cytokine consuming cells (Bagnall *et al*, 2018). Testing these parameters in our sender-receiver model will be technically feasible and will allow us to reveal other potential roles of spatial dynamics of NF-κB.

Timely activation of NF-κB is crucial for cells to initiate proper gene expression regulation upon stimulation (Zambrano *et al*, 2016). We found that cells closer to the source had an earlier NF-κB activation than those that are further. This shows that the location of cells also affects timing of NF-κB activation. How receiving cells translate this signal to gene expression patterns within a tissue is still an unanswered question. However, a very recent work that combines microfluidics, live cell imaging and population level transcriptional assay reported that signal sending cells can generate gene activation zones within a responding cell population (Son *et al*, 2021a). Our sender receiver co-culture system would be able to provide additional insights on how such gene expression patterns arise at single cell level under different conditions such as different strengths of the stimulus. A potential way to do this would be by applying smRNA-FISH (Zambrano *et al*, 2020) to quantify transcripts level at single-cell level in the spatiotemporal context generated by our sender-receiver system.

By generating our in-vitro sender-receiver systems we were able to provide an additional layer of characterization to the emerging picture of a spatiotemporal complex dynamics of NF-κB activation in cytokine niches, and hence at tissue level. A striking overall finding is that contrary to what has been observed in microfluidic devices where a layer of cells is put in contact to an artificially generated gradient of cytokines (Son *et al*, 2021a), the response of the signal-receiving cells is very heterogeneous, both in terms of amplitude and timing. Our observations in immunohistochemistry indeed hints of tissue regions "enriched" for active cells but which are yet heterogeneous, where cells with a strong activation sit within the tissue side-by-side with others that are not activated. In other words, gradients of NF-κB activation are not observed in our HCC and APAP induced inflammatory context. Other works have instead reported that the intestine resident macrophages can uniformly activate neighboring epithelial cells through LPS-induced paracrine signaling (Hausmann *et al*, 2021). We speculate that the presence of cytokine niches can generate heterogeneous NF-κB response in a tissue and cell specific way. We believe that our setup could allow us to dissect further how NF-κB dynamics is regulated within cytokine niches in different tissues, by modifying the cell systems considered and even moving to 3D cultures.

Our system also led to some unexpected insights, such as a desensitization effect, that could not be observed in situations in which the senders and receiving cells are put in contact only after cytokine release upon stimulation (Son *et al*, 2021a). We first observed it when co-culturing MEFs and RAW 264.7 cells and activating paracrine secretion of the latter through low LPS doses: the resulting average activation of the bystander MEFs was always lower than the activation obtained in MEFs cultivated alone and stimulated with medium of LPS activated RAW 264.7 cells. The same effect is observed in our RUSH system of sender receivers: receivers co-cultured with senders are less responsive to TNF-α. We find that they respond in a distance-to-sender dependent way: the closer they are to a sender, the less they'll respond. However, this desensitization effect is overcome when cytokine niches are induced both by RUSH senders and RAW 264.7 cells, so in any case receivers closer to senders respond more, and faster, than cells further from a cytokine emitting cell. This shows desensitization effect is for sure shaping the NF-κB response of receivers. We believe that this effect is mediated by soluble factors, since we find that both RAW 264.7 and RUSH MEFs are leaky and secrete basally NF-κB activating cytokines. We also found that, in our side-by-side cultures of sender and receivers, cells co-cultured in the same well overnight would not respond when TNF-α secretion is induced. Recently

also for NF-κB activation it was reported that previous cytokine exposure creates a short-term memory for the activation threshold so that cells only respond to cytokine concentration differences (i.e., if continuously exposed to TNF-α, they will only respond again to higher doses, as when senders secrete TNF-α). This mechanism is controlled by negative feedbacks of NF-κB and includes resetting of receptor abundance (Son *et al*, 2021b), and could well be the molecular mechanism of the spatiotemporal desensitization that we report here.

We can also speculate about the potential role of desensitization that we observed. For example, it would allow tissue cells to adapt to the presence of immune cells surveilling their environment, putting them in an "alert" state while avoiding unnecessary additional immune response. During immune cell differentiation highly activated immune cells were shown to downregulate their receptor expression (Perona-Wright *et al*, 2010a; Skrenta *et al*, 2000) to avoid exaggerated immune responses. A slow travelling immune cell could secrete basally desensitizing cytokines to cells around it; in response to pathogens (as for example RAW 264.7 cells do in presence of LPS) they could release additional cytokines and produce a moderate activation of the neighboring cells. Of note, despite the spatiotemporal structure described above for the receiver's response when senders secrete cytokines, we find that in our sender-receivers system the average response of the population of the receivers was very similar and much lower than the activation upon TNF-α described for our pool of MEFs in the first part of this thesis work. We then suggest that the trade-off between increasing effect of cytokines and increasing desensitization effect as we get close to the sender can lead to a sort of global modulation of the average response, that is kept moderate for a wide range of ratios between senders and receivers.

Finally, our findings also provide an intriguing insight on a potential NF-κB activation due to TNF-α secretion. We find that our RUSH senders get activated when induced with biotin; but they are almost non-responsive to soluble TNF-α. It is known that the soluble form of TNF-α shows high affinity to TNF receptor 1 (TNFR1) whereas its membrane bound precursor form (mTNF-α) mostly interacts with TNF receptor 2 (TNFR2) (Qu *et al*, 2017). We speculate that continuous exposure to soluble TNF-α in the medium of sender MEFs might result in downmodulation of their TNFR1 dependent NF-κB activation by a similar desensitization mechanism as the one described above, and the strong activation could be a result of TNFR1 independent NF-κB activation via TNFR2. Further experiments will shed light on the action of this mechanism. Overall, it seems clear that this mechanism would allow cells that

continuously secrete TNF-α (and would get desensitized for this reason) to obtain additional NF-κB activation upon an increase of their own TNF-α secretion.

In sum, here we studied two models of sender-receivers of cytokines in the context of inflammatory cell-to-cell communication: co-culture of RAW 264.7 and MEFs and an inducible system of TNF-α secreting MEFs. These models allowed us to characterize spatiotemporal dynamics of NF-κB activation within a monolayer of cells. We showed how single cells use spatiotemporal NF-κB activation to encode location and strength of the danger signals, keeping in any case a strongly heterogeneous activation. We showed that the location of cells plays an important role also in basal conditions through a desensitization effect. In this way, we speculate that cells in a population will provide an average moderate yet spatially structured NF-κB response to stimulus in a wide range of situations. Overall, we showed how it is possible to produce an in vitro model allowing to dissect the key players determining how inflammation develops in space and time, that we hope might pave the way for future studies on the inflammatory response in healthy and pathological conditions.

7. MATERIALS AND METHODS

Part of the presented methods in the following chapters of this thesis (7.1-7.15) is published in BioRxiv preprint server (Kizilirmak *et al,* 2021).

7.1 Cell line and cell culture

GFP-p65 knock-in mouse embryonic fibroblasts (MEFs) were a kind gift from Manolis Pasparakis. In short, they were derived from a single embryo of homozygous knock-in GFP-p65 expressing mouse using standard protocols and immortalized by serial passaging also known as the 3T3 method and typically involves 20-30 passages (Amand *et al*, 2016). The cells were cultured in phenol-red free DMEM supplemented with 10% FCS, 50 mM b-mercaptoethanol, 1x L-glutamine, 1x pen/strep, 1x sodium pyruvate and 1x non-essential amino acids. MEFs were passaged every 2-3 days before they reached 100% confluency and kept at 37°C and 5% CO_2.

7.2 Generation of the clonal populations by single cell cloning

MEFs were harvested by 1x Trypsin solution and counted. Final concentration of 5 cells/ml was achieved by serial dilutions and 100 µl of the cell suspension per well were pipetted to a 96-well plate. The plate was screened for single colonies and selected colonies were then expanded.

7.3 Cell treatments

Where indicated the cells were stimulated with the final concentration of 10 ng/ml of recombinant human TNF-α protein (R&D Systems) or 100 ng/ml of recombinant human interleukin 1 beta (IL-1β, PeproTech).

7.4 Live-cell imaging

Live cell imaging of GFP-p65 knock-in MEFs was performed as in (Zambrano *et al*, 2016). We used a Leica TCS SP5 confocal microscope with an incubation system where cells were stably maintained at 37°C in 5% CO_2. Time-lapse images were acquired at 6 minutes intervals for up to 10 hours. We used a low magnification objective (20x, 0.5 NA) and an open pinhole (Airy 3), ensuring that the image depth (10.7 µm) contains the thickness of the whole cell so that images capture the total cell fluorescence. GFP-p65 is imaged with the 488 nm Argon laser (GFP channel) while Hoechst 33342 stained nuclei are imaged with the low energy 405 nm UV diode laser at 5% of its maximum intensity (HOE channel). The staining was performed at room temperature for 10-15 minutes using NucBlue™ Live ReadyProbes™ Reagent, ThermoFischer), 1:100 v/v and incubated 10-15 min at room temperature, which

was previously shown to not interfere with the response to TNF-α (Zambrano *et al*, 2016). Images were acquired as 16 bit, 1024×1024, TIFF files. Experiment replicates were performed on different days. In each experiment we typically imaged more than one clone in different wells of an 8-well chamber.

7.5 Automated quantification of NF-κB dynamics in single living cells

To quantify NF-κB nuclear localization dynamics in living cells, we follow previously described procedure of normalizing the average nuclear signal intensity by the average cytosolic fluorescence intensity (Zambrano *et al*, 2016) to obtain the nuclear to cytosolic intensity (NCI), also used by others (Kellogg & Tay, 2015; Paszek *et al*, 2010). The custom-made routines run on MATLAB R2015. In short, nuclei are segmented based on the intensity of the HOE channel, and nuclear masks are used to compute the nuclear average NF-κB intensity in each cell. In order to estimate the average cytoplasmic NF-κB intensity, first the background was computed by taking a square area centered on the cell nucleus, dividing it in tiles and using the one with the smallest average intensity in the GFP channel. After this, pixels belonging to the cytoplasm are those with intensity above the background on a ring around each nucleus of width 0.5 times the nuclear radius. Tracking of cells between frames is performed through an optimized algorithm based on the Hungarian linker method (Careccia, 2019). Cells are discarded upon abrupt changes of the nuclear and/or cytosolic areas, indicative of erroneous tracking or cell death or mitosis.

7.6 Stochastic clustering of the NF-κB dynamic profiles

The unsupervised clustering of NF-κB dynamic profiles from cells of the 8 clones was performed using the k-means algorithm (k=8) based on the Euclidean distance between profiles (MATLAB). In each realization, 50 profiles from each clonal population were randomly picked. The profiles are then clustered in 8 groups, and we compute the number of cells from each clonal population in each cluster. In each realization we compute p_{ik}, representing the fraction of trajectories of clone k that are present in the cluster where the clone i has a higher number of clustered profiles. For $k=i$, it represents the fraction of cells of the clone i in the cluster where it is more represented. For each realization we computed the disorder parameter defined as $S = -\sum_{i,j} p_{ij} \log p_{ij}$ and compared with the same result when the dynamic profiles are randomly assigned to the eight clonal populations and then clustered stochastically. We followed this procedure 500 times and the disorder parameter was always higher for cells randomly assigned to clonal populations, indicating further that NF-κB

dynamic profiles are clustered according to a certain pattern strongly related with the clonal population of origin.

7.7 Analysis of NF-κB dynamics

To extract the dynamic features of the NCI time series we followed the same procedure as in (Zambrano *et al*, 2014, 2016). In short, NCI series are smoothed, and peaks are detected using standard MATLAB functions (*smooth* and *pkfnd*, respectively) and those with a prominence $\theta>0.15$ are considered real peaks. This value is well beyond the prominence of noisy peaks found in this type of datasets (Zambrano *et al*, 2016) and provides a reasonably good compromise between the need to ignore noise peaks and the need to detect small peaks of valuable dynamical information (e.g., if a cell is oscillating or not). The timing of the peak was determined considering the maximum value. Instead, the area under the curve is calculated as the integral in the time interval considered of NCI(t).

7.8 Cell cycle analysis

Cell cycle analysis was done as described in (Brambilla *et al*, 2020): MEFs were harvested and fixed with cold 70% ethanol and kept overnight at -20°C. Cells were then washed once with 5% FBS/PBS and stained with PBS containing 10 µg/ml propidium iodide and 10 µg/ml RNAse A for 1 hour at room temperature. Samples were then read at a cytometer using a 488 nm laser.

7.9 Cell cycle computational correction

An artificial dataset of NCI time series of clone R was generated: the top 25% of the population was assumed to be the S-phase high responders (Ankers *et al*, 2016) and their percentage was increased to 43% by neglecting the corresponding fraction of the less responding cells. The resulting dataset has a higher value than the original but still a lower value of the AUC than clone B which makes it unlikely that cell cycle is the key driver of this inter-clonal difference, as for the differences between B and G detailed in the text.

7.10 RNA isolation and real time PCR

$1.5x10^5$ MEFs were plated on a 6-well plate a day before the extraction. Total RNA was isolated using the NucleoSpin RNA II kit (Macherey-Nagel). The amount of RNA was determined using a NanoDrop spectrophotometer (Thermo Fisher Scientific) and 1 µg was then reverse transcribed using SuperScript IV Reverse Transcriptase (Thermo Fisher Scientific).

qPCR was performed using LightCycler 480 SYBR Green I Master (Roche). The expression of *IκBa* and A20 were checked using following primers:

IκBα forward: 5′ CTTGGCTGTGATCACCAACCAG 3′

IκBα reverse: 5′ CGAAACCAGGTCAGGATTCTGC 3′

A20 forward: 5′ ACAGAGCAGGGACAAGCAAGTG 3′

A20 reverse: 5′ GTTTAGGGGGCTCTTCAGGC 3′

TNF-α forward: 5′ TCTTCTCATTCCTGCTTGTGG 3′

TNF-α reverse: 5′ CACTTGGTGGTTTGCTACGA 3′

7.11 RNA sequencing and bioinformatic analysis

Libraries for Illumina NGS were prepared as described in (Brambilla *et al*, 2020). After trimming the adapter sequences (cutadapt, https://cutadapt.readthedocs.io) reads were mapped to mouse genome (mm10) using hisat2 (http://daehwankimlab.github.io/hisat2/) using parameters "-p 20 -5 5".

Read counting was performed using featureCounts from the Subread Package and features displaying less than 10 reads were filtered out. Differential expression analysis was performed using DESeq2 (https://bioconductor.org/packages/release/bioc/html/DESeq2.html) with the following design formula "=~ 1 + clone + treatment + clone:treatment".

Principal component analysis (PCA) was performed using MATLAB, keeping only genes for which RPKM>1 in at least five samples. Additional RNA-seq samples from several mouse tissues were retrieved from the ENCODE Database (https://www.encodeproject.org). Volcano plots were generated using MATLAB and p-values derived from the t-test statistics. Gene ontology was performed using the "*clusterProfiler*" R package (https://bioconductor.org/packages/release/bioc/html/clusterProfiler.html).

Heatmap and Hierarchical clustering was performed using the "*Pheatmap*" R package. Genes annotated in the mouse TNF-signaling were retrieved from WikiPathways (https://www.wikipathways.org/index.php/Pathway:WP246).

7.12 Estimation of the genetic differences between clonal populations.

The SNP calling step was performed using the GATK 3.6 toolkit (McKenna *et al*, 2010) in order to split splice junction reads, to recalibrate quality scores and to call

variants. To minimize false positive variants the GATK Variant filtration tool was used using the following parameters:

"--filterExpression QD < 5.0 --filterExpression DP < 10 --filterExpression ReadPosRankSum < -8.0 --filterExpression MQRankSum < -12.5 --filterExpression MQ < 40.0 --filterExpression FS > 60.0". Nucleotide positions with heterozygosity scores < 0.10 were excluded as previously described (Adetunji *et al*, 2019).

We called SNPs with different levels of confidence based on three different coverage cut-offs (5x, 10x, 20x) and then we calculated the number of unique SNPs for each clone. We find that our clones differ in a range of 200-400 nucleotides (Table 1) which, once divided by the length of the genome at the specific coverage cut-off, provided us a "mutation rate" of approximately $5x10^{-7}$ per base pair.

Table 1. Length of the genome covered for different coverage thresholds (in basepairs) *using RNA-seq reads, and number of different SNPs identified between clones.*

coverage\length	genome covered R	genome covered B	genome covered G	Diff. B vs G	Diff. B vs R	Diff. G vs B
5x	560805040	614001397	576431940	351	301	338
10x	470022271	513879107	480558887	193	172	179
20x	384083108	425738181	392300809	163	108	135

7.13 Frequency of order relations for genes involved in the NF-κB pathway

We define the relative expression level of a gene in one of the clonal populations as its expression level divided by the average expression level across the clones B, R and G. By definition, for a given gene, the sum of their relative expression levels in clones R, G and B is always 3. For a given gene list we can calculate the relative expression value of each gene and then calculate the average value of the relative expression value of the gene list for each population and denote it as <R>, <G> and <B> respectively. It is easy to see that their sum has also to be equal to 3:

$$<R> + <G> + <B>=3$$

Hence, the average relative expression of two of the populations determine the value of the third. For a given gene list we can plot the average relative expression in just two dimensions, which for the sake of simplicity we take as <R> and <B> (**Figures 5.14C**, **5.15B**, **5.17C**). Hence the average relative expression levels can be projected in the <R>-<B> plane. Choosing the average relative expression allows us to have a vision of the ensemble without giving a weight according to the average expression level of each gene. This appears reasonable since the proportionality between mRNA and protein might vary between genes.

Here we calculate the average relative expression levels in three different gene lists:

TNF-α to NF-κB: *Tnfrsf1a, Tab2, Tab1, Traf2, Chuk, Tradd, Ikbkg, Ripk1, Ikbkb, Map3k7, Map3k3, Traf5, Fadd*.

IL-1β to NF-κB: *Tab2, Tab1, Myd88, Il1r1, Chuk, Ikbkg, Irak1, Ikbkb, Traf6, Map3k7, Irak4, Irak2, Il1rap, Irak3*

NF-κB negative feedback: *Nfkbia, Tnfaip3, Nfkbie, Nfkbib, Cyld.*

To assign a statistical significance to the order relations and the average relative expression values, we sampled across our RNA-seq data to find random gene sets with expression levels within the limits of those of the dataset considered (with values between the minimum and the maximum value of the gene set considered) and compute the probability of different average relative expression levels projected in the <R>-<B> plane (see Figures 5.14C for genes of the "TNF-α to NF-κB" list , 5.15B for genes of the "IL-1β to NF-κB" list and 5.17C for genes of the "NF-κB negative feedbacks" list). In each of them we also plot the average relative expression values of the dataset considered as a red dot, which of course falls in the section of the <R>-<B> plane that corresponds to the order relation obtained.

7.14 Mathematical model of NF-κB signaling

Elaborating on previous models (Zambrano *et al*, 2014, 2016) where the negative feedbacks were provided by the inhibitor IκBα and the A20 protein, we developed a more complete model in which the additional negative feedbacks specified in Figure 5.17A are taken into account.

In this new model, the amount of free nuclear NF-κB, N, depends on its continuous association-dissociation with the three IκB inhibitor proteins, whose amount we represent as I_i with $i = \{\alpha, \beta, \varepsilon\}$. They can indeed form the complex (cytosolic) forms $(N{:}\, I_i)$ for $i = \{\alpha, \beta, \varepsilon\}$. The equilibrium between forms is also dependent on the presence of the kinase IKK complex whose amount we denote as K. This means that:

$$\frac{dN}{dt} = \sum_{i=\alpha,\beta,\varepsilon} -k_{a,i}N \cdot I_i + k_{d,i} \cdot (N{:}I_i) + d_{C,i} \cdot (N{:}I_i) + d_{K,i} \cdot K \cdot (N{:}I_i)$$

Where $k_{a,i}$ and $k_{d,i}$ are the association and dissociation constants, respectively, while $d_{K,i}$ is the degradation rate of the complex due to the presence of the kinase complex and $d_{C,i}$ accounts for the spontaneous degradation of the complex. For each of the complex ($i = \{\alpha, \beta, \varepsilon\}$) we have that:

$$\frac{d(N{:}I_i)}{dt} = +k_{a,i}N \cdot I_i - k_{d,i} \cdot (N{:}I_i) - d_{C,i} \cdot (N{:}I_i) - d_{K,i} \cdot K \cdot (N{:}I_i)$$

For the inhibitors, beyond the association and dissociation processes of the complex, the evolution will depend also on the translation rate $k_{I,i}$ of the available mRNA of each of the three inhibitors, that we denote as R_i, and on the inhibitors own degradation rate $d_{I,i}$ and the kinase-dependent degradation rate $d_{IK,i}$:

$$\frac{dI_i}{dt} = -k_{a,i}N \cdot I_i + k_{d,i} \cdot (N{:}I_i) - d_{IK,i} \cdot K \cdot I_i + k_{I,i} \cdot R_i - d_{I,i} \cdot I_i$$

The amount of the kinase complex K is regulated by the amount of the protein A20, that we denote A, through a hill function of parameters A_0 and n, and will also depend on the degradation rate of the kinase complex d_K and the presence ($S = 1$) or absence ($S = 0$) of the external inflammatory signal and on the constant K_0:

$$\frac{dK}{dt} = \frac{S \cdot K_0}{(1 + \left(\frac{A}{A_0}\right)^n)} - d_K \cdot K$$

The amount of A20 depends on the translation rate $k_{t,A}$ of the available mRNA, that we denote as R_A, and on the degradation rate d_A so:

$$\frac{dA}{dt} = k_{t,A} \cdot R_A - d_{\mathrm{A}} \cdot \mathrm{A}$$

The mRNA expression level of each repressor is encoded by the following equations:

$$\frac{dR_j}{dt} = k_j G_j - \delta_j R_j$$

$$\frac{dG_j}{dt} = k_{on,j} N \cdot (2 - G_j) - k_{off,j} G_j$$

Where $j = \{\alpha, \beta, \varepsilon, A\}$; A is the index representing A20. $G_j(t)$ represents the gene activity status for each of the negative feedbacks considered (number of "on" alleles) and $R_j(t)$ the mRNA levels. Concerning the parameters, δ_j is the degradation rate of the mRNA considered, k_j is the transcription rate, and $k_{on,j}$ and $k_{off,j}$ are the gene activation-inactivation rate for each of them. The starting parameters, largely based on those provided in (Zambrano *et al*, 2016) but further constrained by our experiments (see below) are provided in Table 2.

Table 2. Parameters of the mathematical model. *For clone R. Specified for $j = \{\alpha, \beta, \varepsilon, A\}$ and $i = \{\alpha, \beta, \varepsilon\}$. Transcription rates for all the inhibitors (also from clone B) derive from the specified transcription rate k_α. Starting number of NF-κB molecules for clone R is estimated as $3 \cdot 10^3$.*

Parameter	Value	units
$k_{a,i}$	$1.9 \cdot 10^{-6}$	$molecules^{-1}\, s^{-1}$
$k_{d,i}$	$8.4 \cdot 10^{-6}$	s^{-1}
$d_{C,i}$	$1.3 \cdot 10^{-5}$	s^{-1}
$d_{K,i}$	$2.5 \cdot 10^{-9}$	$molecules^{-1}\, s^{-1}$
$k_{I,i}$	$2.5 \cdot 10^{-1}$	s^{-1}
$d_{I,i}$	$6.7 \cdot 10^{-5}$	s^{-1}
K_0	21	$molecules^{-1}\, s^{-1}$
d_K	$2.1 \cdot 10^{-4}$	s^{-1}
A_0	$3 \cdot 10^4$	molecules
n	1	-
$k_{t,A}$	$2.5 \cdot 10^{-1}$	s^{-1}
d_A	$6.7 \cdot 10^{-5}$	s^{-1}
$k_{on,j}$	$6.9 \cdot 10^{-8}$	$molecules^{-1}\, s^{-1}$
$k_{off,j}$	$4.2 \cdot 10^{-4}$	s^{-1}
δ_j	$7.5 \cdot 10^{-4}$	s^{-1}
k_α	$2 \cdot 10^{-1}$	$molecules \cdot s^{-1}$

7.15 Downmodulation of IκBα using antisense oligonucleotides

The antisense oligos to target the *Nfkbia* gene were designed by Aum Biotech, LLC (Philadelphia, PA, USA). Four custom antisense oligos in the final concentration of 5 μM were used to treat MEFs for 24 hours to reduce the expression of IκBα.

7.16 Animal studies and tissue preparation

Animal experiments were performed according to the approved guidelines of Animal Care and Use Committees (IACUC) of San Raffaele Hospital. Mice were injected intraperitoneally (i.p.) with 20 ng of human recombinant TNF-α protein (R&D Systems). After given timepoints post injection, the mice were perfused through the left ventricle with 10 ml of cold heparinized PBS, followed with 25 ml of 4% buffered formalin. Livers were removed and fixed in formalin overnight. The next day the liver was submitted for paraffin embedding in cassettes for the immunostaining.

7.17 Immunohistochemistry

Paraffin embedded liver cassettes were used for immunohistochemistry (IHC). As a primary antibody NF-κB p65 (Cell Signaling, 8242) was used. Antigens are retrieved in Citrate Buffer pH 6.0 for 30 minutes at 95°C. Primary antibodies are revealed using Rabbit Specific HRP/DAB IHC Detection Kit (Abcam, 64261). IHC is performed by OSR Mouse Clinic, Mouse Histopathology Unit.

7.18 Agarose beads preparation

Agarose beads (Sigma) were 1:1 mixed with TNF-α in the final concentration of 100 ng/ml and incubated over night at 4°C. The next day beads were washed 3 times with PBS and 4 μl of beads was given to the cells for live-cell imaging. PBS that does not contain any bead after centrifugation was used as a control.

7.19 RAW 264.7-MEF co-cultures

Same as MEFs, RAW 264.7 cells were also cultured in phenol-red free DMEM supplemented with 10% FCS, 50 mM b-mercaptoethanol, 1x L-glutamine, 1x pen/strep, 1x sodium pyruvate and 1x non-essential amino acids. RAW 264.7 cells were passaged every 3 days by a cell scraper before they reached 100% confluency and kept at 37°C and 5% CO_2. For the co-culture experiments, RAW 264.7 cells were labelled using Vybrant™ DiD Cell-Labeling Solution (Thermo Fisher Scientific, 22887) according to manufacturer's instructions.

7.20 Immunofluorescence for p65

$1.5x10^5$ RAW 264.7 cells were plated on coverslips placed in a 6-well plate a day before the staining. Next day cells were treated with either 1 ng/ml LPS or 10 ng/ml TNF-α for 15 minutes and then fixed by 4% PFA solution at room temperature for 20 minutes. We permeabilized cells in HEPES-Triton-X100 buffer (20 mM HEPES pH 7.4, 300 mM sucrose, 50 mM NaCl, 3mM $MgCl_2$, 0.2% Triton-X100) for 5 minutes at 4°C and performed blocking step using 10% goat serum in PBS for 1 hour at room temperature. NF-κB p65 (Cell Signaling, 8242) antibody is used for staining (1:500 dilution in 0.2% BSA in PBS) for 1 hour followed by secondary antibody (1:1000 dilution in 0.2% BSA in PBS) incubation and Hoechst staining (1:1000 dilution in PBS). 0.2% BSA in PBS used as a wash buffer in between each step. Coverslips were then mounted for imaging.

7.21 RUSH plasmids and the lentiviral particles for infection

The RUSH plasmids: 65283 pCDH_TNF-SBP-mCherry, 65307 pCDH_Str-KDEL_neomycin were purchased from Addgene. Lentiviral particles were prepared as described in (Brambilla *et al*, 2020). In short, particles were produced in HEK 293T cells that were cultured in DMEM supplemented with 10% FCS, 1x L-glutamine, 1x pen/strep and 1x sodium pyruvate. The calcium/phosphate method was used for transfection of the packaging plasmids. The plasmid solution that contains TNF-α and KDEL constructs were added to the cell culture media dropwise. The virus containing medium was then collected after 48 hours and used for MEF infections.

7.22 Biotin preparation

D-biotin was purchased from Novabiochem (8.51209). 800 μM of biotin stock solution was prepared directly in cell culture media and filtered through 0.22 μm membrane. For the experiments final concentration of 80 μM biotin was used.

7.23 Biophysical estimations of effective intercellular communication distances leading to NF-κB activation

In the paper by (Francis & Palsson, 1997) they use a number of simplifications and the diffusion equation to estimate the maximum range of intercellular communication in 2D cultures. In short, they use mathematical methods to show how far the cytokines sent by a spherical cell of radius ρ that secretes a certain flux F_0 (in molecules per area and per unit of time) of molecules with a diffusion coefficient D, can be sensed by neighboring cells. Using analytical methods, they

show that the concentration of cytokines around the cell tends to have a constant concentration gradient c(r) that is formed around the sending cells and scales like:

$$c(r) \propto \frac{1}{r}$$

Where r is the distance from the center of the sending cell. How long does it take this gradient to form? It will take some time, since before the secretion starts the cytokine level is zero around the cell, and then gradually increases until the value c(r). They estimate that the time it takes to establish half the maximum concentration at a distance of n cell radii scales like:

$$\tau_\infty \approx \frac{\rho^2}{D} n^2$$

Finally, how far do the signals travel? This depends on the minimum concentration under which we can consider that the cells do not respond, c_0. Hence the maximum distance at which the concentration eventually reaches a concentration value above c_0 (if we wait long enough) is given by:

$$d_{max} \approx \alpha \cdot \rho$$

Where

$$\alpha = \frac{F_0 \rho}{D c_0}$$

With all this information, we can try to provide some rough estimations of these parameters for the sender-receiver systems that we generated here.

First, the mouse embryonic fibroblasts have a typical area A_fibro≈35 μm × 65 μm when observed at the microscope so, if we assume that our cells are spherical, this means that for fibroblasts:

$$\rho \approx \sqrt{\frac{A_{fibro}}{\pi}} \approx 25\ \mu m$$

that would be our "characteristic fibroblast radius".

The diffusion coefficient for TNF-α has been estimated to be roughly $D = 3 \cdot 10^{-10}\ \mu m^2/s$ consistent with the values provided in Francis and Palsson for cytokines. This means that the characteristic timescale for the maximum concentration around the sending cells to be reached is:

$$\tau_\infty \approx \frac{\rho^2}{D} n^2 \approx 2\ n^2\ s$$

In other words, it takes few seconds to go a small number of radii away. Of note, it seems that variations of the order of minutes can lead to some variation in the response of NF-κB to cytokines, but not of the order of seconds. We can then consider that such gradients are formed almost instantaneously.

How far do signals travel? First, we need an estimation of F_0. To do it we can consider the surface secreting of the fibroblast A_{fibro} described above (we can estimate that it is roughly half the total surface of the cell, which would be the one in contact with the medium and hence through which secretion takes place). On the other hand, we find (Figure 5.28A) that fibroblasts secrete additional 6 ng/ml of TNF-α in a cell culture medium upon biotin. In such culture we plated roughly 300 thousand cells in a volume of 2 ml. All this allow us to calculate the value of F_0, using that the molecular weight of TNF-α is 17 kDa. On the other hand, we need to consider what is the minimum concentration of the stimulus to which our cells respond. As shown in (Zambrano *et al* 2014), at concentrations below 0.1 ng/ml TNF-α the response is very mild and far for uniform, so we might take it as a reasonable minimum concentration value. Taking all this into consideration, we find that:

$$d_{max} \approx 4 \cdot \rho$$

In other words, we expect that cells cannot communicate beyond 100 μm. This makes it reasonable to stratify the cells between close and far from sending cells using the threshold of 50 μm, which is right in the middle of the "gradient zone" where concentrations vary producing some response in the cells. As we will discuss later, this simplistic picture is further complicated by the presence of other effects (such as desensitization) and potentially of multiple sells sending signals to the receivers. The calculations involved a number of simplifications and rounded some numbers to obtain an appropriate final formula, which in any case do not alter the basic message: that in traditional 2D cultures, in principle, paracrine activation of through TNF-α should not travel beyond few cells.

7.24 Statistical analysis

For all the statistical analysis not detailed elsewhere: non-parametric Kruskal-Wallis (for multiple comparisons) and Student's t-test were used as described in the figure captions. The threshold of significance was set to p=0.05. In boxplots the median is shown as a line within the first and third quartiles, whiskers show 1-99 percentile.

8. REFERENCES

Adamson A, Boddington C, Downton P, Rowe W, Bagnall J, Lam C, Maya-Mendoza A, Schmidt L, Harper C, Spiller D, *et al* (2016) Signal transduction controls heterogeneous NF-κB dynamics and target gene expression through cytokine-specific refractory states. *Nat Commun* 7

Adcock IM & Caramori G (2009) Chapter 31 - Transcription Factors. In *Asthma and COPD (Second Edition)*, Barnes PJ Drazen JM Rennard SI & Thomson NC (eds) pp 373–380. Oxford: Academic Press

Adelaja A, Taylor B, Sheu K, Liu Y, Luecke S & Hoffmann A (2021) Six distinct NFκB signaling codons convey discrete information to distinguish stimuli and enable appropriate macrophage responses. *Immunity* 54: 916-930.e7

Adetunji MO, Lamont SJ, Abasht B & Schmidt CJ (2019) Variant analysis pipeline for accurate detection of genomic variants from transcriptome sequencing data. *PLoS ONE* 14: e0216838

A.Hoffmann, Levchencko A, Scott ML & Baltimore D (2002) The IkappaB-NF-kappaB signalling module: temporal control and selective gene activation. *Science* 298: 1241–1245

Amand MM, Hanover JA & Shiloach J (2016) A comparison of strategies for immortalizing mouse embryonic fibroblasts. *J Biol Methods* 3: e41–e41

Ankers JM, Awais R, Jones NA, Boyd J, Ryan S, Adamson AD, Harper CV, Bridge L, Spiller DG, Jackson DA, *et al* (2016) Dynamic NF-κB and E2F interactions control the priority and timing of inflammatory signalling and cell proliferation. *eLife* 5: e10473

Ashall L, Horton CA, Nelson DE, Paszek P, Harper CV, Sillitoe K, Ryan S, Spiller DG, Unitt JF, Broomhead DS, *et al* (2009) Pulsatile Stimulation Determines Timing and Specificity of NF- B-Dependent Transcription. *Science* 324: 242–246

Bagnall J, Boddington C, England H, Brignall R, Downton P, Alsoufi Z, Boyd J, Rowe W, Bennett A, Walker C, *et al* (2018) Quantitative analysis of competitive cytokine signaling predicts tissue thresholds for the propagation of macrophage activation. *Sci Signal* 11: eaaf3998–eaaf3998

Barken D, Wang CJ, Kearns J, Cheong R, Hoffmann A & Levchenko A (2005) Comment on 'Oscillations in NF-κB Signaling Control the Dynamics of Gene Expression'. *Science* 308: 52–52

Bartfeld S, Hess S, Bauer B, Machuy N, Ogilvie LA, Schuchhardt J & Meyer TF (2010) High-throughput and single-cell imaging of NF-kappaB oscillations using monoclonal cell lines. *BMC Cell Biol* 11: 21

Beg AA, Sha WC, Bronson RT, Ghosh S & Baltimore D (1995) Embryonic lethality and liver degeneration in mice lacking the RelA component of NF-κB. *Nature* 376: 167–170

Beg AA & Baltimore D (1996) An Essential Role for NF-κB in Preventing TNF-α-Induced Cell Death. *Science* 274: 782–784

Ben-Neriah Y & Karin M (2011) Inflammation meets cancer, with NF-κB as the matchmaker. *Nat Immunol* 12: 715–723

Bonanomi D, Chivatakarn O, Bai G, Abdesselem H, Lettieri K, Marquardt T, Pierchala BA & Pfaff SL (2012) Ret Is a Multifunctional Coreceptor that Integrates Diffusible- and Contact-Axon Guidance Signals. *Cell* 148: 568–582

Boncompain G, Divoux S, Gareil N, de Forges H, Lescure A, Latreche L, Mercanti V, Jollivet F, Raposo G & Perez F (2012) Synchronization of secretory protein traffic in populations of cells. *Nat Methods* 9: 493–498

Brambilla F, Garcia-Manteiga JM, Monteleone E, Hoelzen L, Zocchi A, Agresti A & Bianchi ME (2020) Nucleosomes effectively shield DNA from radiation damage in living cells. *Nucleic Acids Res* 48: 8993–9006

Bushdid PB, Brantley DM, Yull FE, Blaeuer GL, Hoffman LH, Niswander L & Kerr LD (1998) Inhibition of NF-kappaB activity results in disruption of the apical ectodermal ridge and aberrant limb morphogenesis. *Nature* 392: 615–618

Careccia G Colombo, F, Tirone, M, Agresti,A, Bianchi, ME, Zambrano, S, Vénéreau, E (2019) Exploiting Live Imaging to Track Nuclei During Myoblast Differentiation and Fusion. *J Vis Exp JoVE* In press

Carlotti F, Chapman R, Dower SK & Qwarnstrom EE (1999) Activation of Nuclear Factor κB in Single Living Cells: DEPENDENCE OF NUCLEAR TRANSLOCATION AND ANTI-APOPTOTIC FUNCTION ON EGFPRELA CONCENTRATION *. *J Biol Chem* 274: 37941–37949

Chen CL, Singh N, Yull FE, Strayhorn D, Van Kaer L & Kerr LD (2000) Lymphocytes lacking I kappa B-alpha develop normally, but have selective defects in proliferation and function. *J Immunol Baltim Md 1950* 165: 5418–5427

Cheng QJ, Ohta S, Sheu KM, Spreafico R, Adelaja A, Taylor B & Hoffmann A (2021) NF-κB dynamics determine the stimulus specificity of epigenomic reprogramming in macrophages. *Science* 372: 1349–1353

Covert MW, Leung TH, Gaston JE & Baltimore D (2005) Achieving Stability of Lipopolysaccharide-Induced NF-kB Activation. *Science* 309: 1854–1857

Cruz JA, Mokashi CS, Kowalczyk GJ, Guo Y, Zhang Q, Gupta S, Schipper DL, Smeal SW & Lee REC (2021) A variable-gain stochastic pooling motif mediates information transfer from receptor assemblies into NF-κB. *Sci Adv* 7: eabi9410

De Lorenzi R, Gareus R, Fengler S & Pasparakis M (2009) GFP-p65 knock-in mice as a tool to study NF-κB dynamics in vivo. *genesis* 47: 323–329

DeFelice MM, Clark HR, Hughey JJ, Maayan I, Kudo T, Gutschow MV, Covert MW & Regot S (2019) NF-κB signaling dynamics is controlled by a dose-sensing autoregulatory loop. *Sci Signal* 12

Ferrara M, Chialli G, Ferreira LM, Ruggieri E, Careccia G, Preti A, Piccirillo R, Bianchi ME, Sitia G & Venereau E (2020) Oxidation of HMGB1 Is a Dynamically Regulated Process in Physiological and Pathological Conditions. *Front Immunol* 11: 1122

Francis K & Palsson BO (1997) Effective intercellular communication distances are determined by the relative time constants for cyto/chemokine secretion and diffusion. *Proc Natl Acad Sci U S A* 94: 12258–62

Frank T & Tay S (2015) Automated co-culture system for spatiotemporal analysis of cell-to-cell communication. *Lab Chip* 15: 2192–200

Franklin JM, Ghosh RP, Shi Q, Reddick MP & Liphardt JT (2020) Concerted localization-resets precede YAP-dependent transcription. *Nat Commun* 11: 4581

Gangstad SW, Feldager CW, Juul J & Trusina A (2013) Noisy transcription factor NF-κB oscillations stabilize and sensitize cytokine signaling in space. *Phys Rev E - Stat Nonlinear Soft Matter Phys* 87: 1–5

Gapuzan M-ER, Schmah O, Pollock AD, Hoffmann A & Gilmore TD (2005) Immortalized fibroblasts from NF-kappaB RelA knockout mice show phenotypic heterogeneity and maintain increased sensitivity to tumor necrosis factor alpha after transformation by v-Ras. *Oncogene* 24: 6574–6583

Greaves M & Maley CC (2012) Clonal evolution in cancer. *Nature* 481: 306–313

Hagai T, Chen X, Miragaia RJ, Rostom R, Gomes T, Kunowska N, Henriksson J, Park J-E, Proserpio V, Donati G, *et al* (2018) Gene expression variability across cells and species shapes innate immunity. *Nature* 563: 197–202

Hausmann A, Felmy B, Kunz L, Kroon S, Berthold DL, Ganz G, Sandu I, Nakamura T, Zangger NS, Zhang Y, *et al* (2021) Intercrypt sentinel macrophages tune antibacterial NF-κB responses in gut epithelial cells via TNF. *J Exp Med* 218

Hayden MS & Ghosh S (2008) Shared Principles in NF-kappaB Signaling. *Cell* 132: 344–344

Hu Y, Baud V, Delhase M, Zhang P, Deerinck T, Ellisman M, Johnson R & Karin M (1999) Abnormal morphogenesis but intact IKK activation in mice lacking the IKKalpha subunit of IkappaB kinase. *Science* 284: 316–320

Hughey JJ, Gutschow MV, Bajar BT & Covert MW (2015) Single-cell variation leads to population invariance in NF-κB signaling dynamics. *Mol Biol Cell* 26: 583–590

Hutti JE, Turk BE, Asara JM, Ma A, Cantley LC & Abbott DW (2007) IkappaB kinase beta phosphorylates the K63 deubiquitinase A20 to cause feedback inhibition of the NF-kappaB pathway. *Mol Cell Biol* 27: 7451–7461

Junkin M, Kaestli AJ, Cheng Z, Jordi C, Albayrak C, Hoffmann A & Tay S (2016) High-Content Quantification of Single-Cell Immune Dynamics. *Cell Rep* 15: 411–422

Kasper CA, Sorg I, Schmutz C, Tschon T, Wischnewski H, Kim ML & Arrieumerlou C (2010) Cell-cell propagation of NF-κB transcription factor and MAP kinase activation amplifies innate immunity against bacterial infection. *Immunity* 33: 804–816

Kellogg R & Tay S (2015) Noise facilitates transcriptional control under dynamic inputs. *Cell* 160: 381–392

Kellogg RA, Tian C, Lipniacki T, Quake S & Tay S (2015) Digital signaling decouples activation probability and population heterogeneity. *eLife*

Kizilirmak C, Monteleone E, García-Manteiga JM, Brambilla F, Agresti A, Bianchi ME & Zambrano S (2021) Small transcriptional differences lead to distinct NF-κB dynamics in quasi-identical cells

Klement JF, Rice NR, Car BD, Abbondanzo SJ, Powers GD, Bhatt PH, Chen CH, Rosen CA & Stewart CL (1996) IkappaBalpha deficiency results in a sustained NF-kappaB response and severe widespread dermatitis in mice. *Mol Cell Biol* 16: 2341–2349

Lane K, Van Valen D, DeFelice MM, Macklin DN, Kudo T, Jaimovich A, Carr A, Meyer T, Pe'er D, Boutet SC, *et al* (2017) Measuring Signaling and RNA-Seq in the Same Cell Links Gene Expression to Dynamic Patterns of NF-κB Activation. *Cell Syst* 4: 458-469.e5

Lawrence T (2009) The nuclear factor NF-kappaB pathway in inflammation. *Cold Spring Harb Perspect Biol* 1: a001651

Lee RE, Walker SR, Savery K, Frank DA & Gaudet S (2014) Fold change of nuclear NF-kappaB determines TNF-induced transcription in single cells. *Mol Cell* 53: 867–879

Lee REC, Qasaimeh MA, Xia X, Juncker D & Gaudet S (2016) NF-κB signalling and cell fate decisions in response to a short pulse of tumour necrosis factor. *Sci Rep*

Lee TK, Denny EM, Sanghvi JC, Gaston JE, Maynard ND, Hughey JJ & Covert MW (2009) A Noisy Paracrine Signal Determines the Cellular NF-kappaB response to Lipopolysaccharide. *Sci Signal* 2: 1–9

Levine JH, Lin Y & Elowitz MB (2013) Functional Roles of Pulsing in Genetic Circuits. *Science* 342: 1193–1193

Li P, Markson JS, Wang S, Chen S, Vachharajani V & Elowitz MB (2018) Morphogen gradient reconstitution reveals Hedgehog pathway design principles. *Science* 360: 543–548

Li Q, Lu Q, Hwang JY, Büscher D, Lee KF, Izpisua-Belmonte JC & Verma IM (1999) IKK1-deficient mice exhibit abnormal development of skin and skeleton. *Genes Dev* 13: 1322–1328

Li Y, Shan Y, Desai RV, Cox KH, Weinberger LS & Takahashi JS (2020) Noise-driven cellular heterogeneity in circadian periodicity. *Proc Natl Acad Sci* 117: 10350–10356

Lipniacki T, Puszynski K, Paszek P, Brasier A & Kimmel M (2004) Mathematical model of NF-kappaB regulatory module. *J Theor Biol* 228: 195–215

Liu T, Zhang L, Joo D & Sun S-C (2017) NF-κB signaling in inflammation. *Signal Transduct Target Ther* 2: 17023–17023

Lowrey PL & Takahashi JS (2004) Mammalian circadian biology: elucidating genome-wide levels of temporal organization. *Annu Rev Genomics Hum Genet* 5: 407–441

Martin EW, Pacholewska A, Patel H, Dashora H & Sung M-H (2020) Integrative analysis suggests cell type–specific decoding of NF-κB dynamics. *Sci Signal* 13

Matsuda M, Hayashi H, Garcia-Ojalvo J, Yoshioka-Kobayashi K, Kageyama R, Yamanaka Y, Ikeya M, Toguchida J, Alev C & Ebisuya M (2020) Species-specific segmentation clock periods are due to differential biochemical reaction speeds. *Science* 369: 1450–1455

McKenna A, Hanna M, Banks E, Sivachenko A, Cibulskis K, Kernytsky A, Garimella K, Altshuler D, Gabriel S, Daly M, *et al* (2010) The Genome Analysis Toolkit: a MapReduce framework for analyzing next-generation DNA sequencing data. *Genome Res* 20: 1297–1303

Meyer-Ficca ML, Meyer RG, Kaiser H, Brack AR, Kandolf R & Küpper J-H (2004) Comparative analysis of inducible expression systems in transient transfection studies. *Anal Biochem* 334: 9–19

Milholland B, Dong X, Zhang L, Hao X, Suh Y & Vijg J (2017) Differences between germline and somatic mutation rates in humans and mice. *Nat Commun* 8: 15183

Milo R & Phillips R (2016) Cell Biology by the numbers New York: Garland Science

Natoli G & Ostuni R (2019) Adaptation and memory in immune responses. *Nat Immunol* 20: 783–792

Nelson DE, Ihekwaba AE, Elliott M, Johnson JR, Gibney CA, Foreman BE, Nelson G, See V, Horton CA, Spiller DG, *et al* (2004) Oscillations in NF-kappaB signaling control the dynamics of gene expression. *Science* 306: 704–708

Nelson DE, Horton CA, See V, Johnson JR, Nelson G, Spiller DG, Kell DB & White MRH (2005) Response to Comment on 'Oscillations in NF-κB Signaling Control the Dynamics of Gene Expression'. *Science* 308: 52–52

Netea MG, Balkwill F, Chonchol M, Cominelli F, Donath MY, Giamarellos-Bourboulis EJ, Golenbock D, Gresnigt MS, Heneka MT, Hoffman HM, *et al* (2017) A guiding map for inflammation. *Nat Immunol* 18: 826–831

Newton K & Dixit VM (2012) Signaling in innate immunity and inflammation. *Cold Spring Harb Perspect Biol* 4: a006049

Nourshargh S & Alon R (2014) Leukocyte Migration into Inflamed Tissues. *Immunity* 41: 694–707

Oh H & Ghosh S (2013) NF-κB: roles and regulation in different CD4(+) T-cell subsets. *Immunol Rev* 252: 41–51

Oyler-Yaniv A, Oyler-Yaniv J, Whitlock BM, Liu Z, Germain RN, Huse M, Altan-Bonnet G & Krichevsky O (2017) A Tunable Diffusion-Consumption Mechanism of Cytokine Propagation Enables Plasticity in Cell-to-Cell Communication in the Immune System. *Immunity* 46: 609–620

Paek AL, Liu JC, Loewer A, Forrester WC & Lahav G (2016) Cell-to-Cell Variation in p53 Dynamics Leads to Fractional Killing. *Cell* 165: 631–642

Pampaloni F, Reynaud EG & Stelzer EHK (2007) The third dimension bridges the gap between cell culture and live tissue. *Nat Rev Mol Cell Biol* 8: 839–845

Pangault C, Amé-Thomas P, Ruminy P, Rossille D, Caron G, Baia M, De Vos J, Roussel M, Monvoisin C, Lamy T, *et al* (2010) Follicular lymphoma cell niche: identification of a preeminent IL-4-dependent T(FH)-B cell axis. *Leukemia* 24: 2080–2089

Paszek P, Ryan S, Ashall L, Sillitoe K, Harper CV, Spiller DG, Rand DA & White MRH (2009) Pulsatile stimulation determines timing and specificity of NF-kappaB-dependent transcription. *Science* 324: 242–246

Paszek P, Ryan S, Ashall L, Sillitoe K, Harper CV, Spiller DG, Rand DA & White MRH (2010) Population robustness arising from cellular heterogeneity. *Proc Natl Acad Sci USA* 107: 11644–11649

Patel P, Drayman N, Liu P, Bilgic M & Tay S (2021) Computer vision reveals hidden variables underlying NF-κB activation in single cells. *Sci Adv* 7 43: eabg4135

Perona-Wright G, Mohrs K, Mayer KD & Mohrs M (2010a) Differential Regulation of IL-4Rα Expression by Antigen versus Cytokine Stimulation Characterizes Th2 Progression In Vivo. *J Immunol* 184: 615–623

Perona-Wright G, Mohrs K & Mohrs M (2010b) Sustained signaling by canonical helper T cell cytokines throughout the reactive lymph node. *Nat Immunol* 11: 520–526

Pikarsky E, Porat RM, Stein I, Abramovitch R, Amit S, Kasem S, Gutkovich-Pyest E, Urieli-Shoval S, Galun E & Ben-Neriah Y (2004) NF-κB functions as a tumour promoter in inflammation-associated cancer. *Nature* 431: 461–466

Purvis JE & Lahav G (2013) Encoding and decoding cellular information through signaling dynamics. *Cell* 152: 945–956

Purvis JE, Mock KWKC, Batchelor E, Loewer A & Lahav G (2012) p53 Dynamics Control Cell Fate. *Science* 336: 1440–1444

Qu Y, Zhao G & Li H (2017) Forward and Reverse Signaling Mediated by Transmembrane Tumor Necrosis Factor-Alpha and TNF Receptor 2: Potential Roles in an Immunosuppressive Tumor Microenvironment. *Front Immunol* 8: 1675

Rescigno M, Martino M, Sutherland CL, Gold MR & Ricciardi-Castagnoli P (1998) Dendritic Cell Survival and Maturation Are Regulated by Different Signaling Pathways. *J Exp Med* 188: 2175–2180

Rogers KW & Schier AF (2011) Morphogen gradients: from generation to interpretation. *Annu Rev Cell Dev Biol* 27: 377–407

Rudolph D, Yeh WC, Wakeham A, Rudolph B, Nallainathan D, Potter J, Elia AJ & Mak TW (2000) Severe liver degeneration and lack of NF-kappaB activation in NEMO/IKKgamma-deficient mice. *Genes Dev* 14: 854–862

Schmitz ML & Baeuerle PA (1991) The p65 subunit is responsible for the strong transcription activating potential of NF-kappa B. *EMBO J* 10: 3805–17

Schwanhäusser B, Busse D, Li N, Dittmar G, Schuchhardt J, Wolf J, Chen W & Selbach M (2011) Global quantification of mammalian gene expression control. *Nature* 473: 337–342

Selimkhanov J, Taylor B, Yao J, Pilko A, Albeck J, Hoffmann A, Tsimring L & Wollman R (2014) Accurate information transmission through dynamic biochemical signaling networks. *Science* 346: 1370–1373

Sen R & Baltimore D (1986) Multiple nuclear factors interact with the immunoglobulin enhancer sequences. *Cell* 46: 705–716

Seshasayee AS, Bertone P, Fraser GM & Luscombe NM (2006) Transcriptional regulatory networks in bacteria: from input signals to output responses. *Curr Opin Microbiol* 9: 511–519

Shankaran H, Ippolito DL, Chrisler WB, Resat H, Bollinger N, Opresko LK & Wiley HS (2009) Rapid and sustained nuclear-cytoplasmic ERK oscillations induced by epidermal growth factor. *Mol Syst Biol* 5: 332–332

Singer M, Deutschman CS, Seymour CW, Shankar-Hari M, Annane D, Bauer M, Bellomo R, Bernard GR, Chiche J-D, Coopersmith CM, *et al* (2016) The Third International Consensus Definitions for Sepsis and Septic Shock (Sepsis-3). *JAMA* 315: 801–10

Skrenta H, Yang Y, Pestka S & Fathman CG (2000) Ligand-Independent Down-Regulation of IFN-γ Receptor 1 Following TCR Engagement. *J Immunol* 164: 3506–3511

Son M, Frank T, Holst-Hansen T, Wang A, Junkin M, Kashaf SS, Trusina A & Tay S (2021a) Spatiotemporal NF-κB dynamics encodes the position, amplitude and duration of local immune inputs. 2021.11.30.470463 doi:10.1101/2021.11.30.470463 [PREPRINT]

Son M, Wang AG, Tu H-L, Metzig MO, Patel P, Husain K, Lin J, Murugan A, Hoffmann A & Tay S (2021b) NF-κB responds to absolute differences in cytokine concentrations. *Sci Signal* 14: eaaz4382

Sun S-C (2017) The non-canonical NF-κB pathway in immunity and inflammation. *Nat Rev Immunol* 17: 545–558

Sung M-H, Li N, Lao Q, Gottschalk RA, Hager GL & Fraser IDC (2014) Switching of the Relative Dominance Between Feedback Mechanisms in Lipopolysaccharide-Induced NF-κB Signaling. *Sci Signal* 7: ra6–ra6

Sung MH, Salvatore L, Lorenzi RD, Indrawan A, Pasparakis M, Hager GL, Bianchi ME & Agresti A (2009) Sustained Oscillations of NF-kappaB Produce Distinct Genome Scanning and Gene Expression Profiles. *PLoS ONE* 5: e7163–e7163

Szekanecz Z & Koch AE (2017) Chapter 25 - Cell Recruitment and Angiogenesis. In *Kelley and Firestein's Textbook of Rheumatology (Tenth Edition)*, Firestein GS Budd RC Gabriel SE McInnes IB & O'Dell JR (eds) pp 384-395.e5. Elsevier

Takahashi K & Yamanaka S (2006) Induction of Pluripotent Stem Cells from Mouse Embryonic and Adult Fibroblast Cultures by Defined Factors. *Cell* 126: 663–676

Tay S, Hughey JJ, Lee TK, Lipniacki T, Quake SR & Covert MW (2010) Single-cell NF-kappaB dynamics reveal digital activation and analogue information processing. *Nature* 466: 267–271

Turner DA, Paszek P, Woodcock DJ, Nelson DE, Horton CA, Wang Y, Spiller DG, Rand DA, White MR & Harper CV (2010) Physiological levels of TNF-alpha stimulation induce stochastic dynamics of NF-kappaB responses in single living cells. *J Cell Sci* 123: 2834–2843

Wang N, Liang H & Zen K (2014) Molecular mechanisms that influence the macrophage m1-m2 polarization balance. *Front Immunol* 5: 614

Whiteside ST & Goodbourn S (1993) Signal transduction and nuclear targeting: regulation of transcription factor activity by subcellular localisation. *J Cell Sci* 104: 949–955

Wong VC, Bass VL, Bullock ME, Chavali AK, Lee REC, Mothes W, Gaudet S & Miller-Jensen K (2018) NF-κB-Chromatin Interactions Drive Diverse Phenotypes by Modulating Transcriptional Noise. *Cell Rep* 22: 585–599

Yde P, Mengel B, Jensen MH, Krishna S & Trusina A (2011) Modeling the NF-kB mediated inflammatory response predicts cytokine waves in tissue. *BMC Syst Biol* 5: 115–115

Yissachar N, Sharar Fischler T, Cohen AA, Reich-Zeliger S, Russ D, Shifrut E, Porat Z & Friedman N (2013) Dynamic Response Diversity of NFAT Isoforms in Individual Living Cells. *Mol Cell* 49: 322–330

Yizhak K, Aguet F, Kim J, Hess JM, Kübler K, Grimsby J, Frazer R, Zhang H, Haradhvala NJ, Rosebrock D, *et al* (2019) RNA sequence analysis reveals macroscopic somatic clonal expansion across normal tissues. *Science* 364

Zambrano S, Bianchi ME & Agresti A (2014) High-throughput analysis of NF-κB dynamics in single cells reveals basal nuclear localization of NF-κB and spontaneous activation of oscillations. *PLoS ONE* 9

Zambrano S, Loffreda A, Carelli E, Stefanelli G, Colombo F, Bertrand E, Tacchetti C, Agresti A, Bianchi ME, Molina N, *et al* (2020) First Responders Shape a Prompt and Sharp NF-κB-Mediated Transcriptional Response to TNF-α. *iScience* 23: 101529

Zambrano S, de Toma I, Piffer A, Bianchi ME & Agresti A (2016) NF-kappaB oscillations translate into functionally related patterns of gene expression. *eLife* 5: e09100–e09100

Zhang Q, Gupta S, Schipper DL, Kowalczyk GJ, Mancini AE, Faeder JR & Lee REC (2017a) NF-κB Dynamics Discriminate between TNF Doses in Single Cells. *Cell Syst* 5: 638-645.e5

Zhang Q, Leonardo MJ & Baltimore D (2017b) 30 Years of NFkappaB: A Blossoming of Relevance to Human Pathobiology. *Cell* 168: 37–57

Zhang Z-B, Wang Q-Y, Ke Y-X, Liu S-Y, Ju J-Q, Lim WA, Tang C & Wei P (2017c) Design of Tunable Oscillatory Dynamics in a Synthetic NF-κB Signaling Circuit. *Cell Syst* 5: 460-470.e5